Modelling the inhibitory components of the Interleukin-1β network

Johnny Kelsey

CoMPLEX
University College London

A thesis submitted to the University of London in the
Department of Mathematics for the degree of Doctor of Philosophy

June 2010

Abstract

The inhibitory influences present in the interleukin-1β network are considered, and their effect on the network elucidated. IL-1β is a pro-inflammatory cytokine essential to the functioning of the immune system.

The IL-1 network exhibits a complexity which has been noted by many researchers. It exists in two forms, α and β, which afforded a natural way of drawing a boundary around which part of the network was to be modelled: a choice between the α or β forms. The β form was chosen for investigation since it is known to have a higher potency than the α form.

IL-1β requires the formation of a signalling ternary complex in order to trigger signalling transduction; it needs to bind with the signalling (Type-I) receptor, and for this binary complex in turn to be bound by a receptor accessory protein, before signalling transduction can proceed. A variety of control mechanisms which inhibit the formation of this signalling ternary process have evolved. These have been modelled using a variety of techniques.

This work was generously supported by the Engineering and Physical Sciences Research Council.

Acknowledgements

My enormous thanks go to Professor Rob Seymour and Professor Brian Henderson, most especially: to the former, for patience shown over mistakes with long division, and to the latter, for much debate about the structure of syntax.

I am sure I will be back in Rob's office again soon, as he explains to me with infinite patience what he has told me for the $n + 1$th time, for arbitrary n.

Contents

List of Tables

List of Figures

Chapter 1

Introduction

1.1 Interleukin-1: a short history

Endotoxin, a combination of Gram-negative lipopolysaccharide (LPS) plus associated outer cell membrane proteins, is one of the most potent inflammatory moieties. Endotoxin shock still kills millions each year worldwide. Thus there has been a long-term interest in how endotoxin induces the severe, often lethal, inflammatory state in individuals with Gram-negative bacterial infections. It is the study of this problem that led to the discovery of interleukin-1 (IL-1) and, indeed, to the concept of the local homeostatic mediators known as cytokines.

In 1939, Paul Beeson, working in the United States, showed that leukocytes exposed to endotoxin produced a pyrogenic (fever producing) molecule that was not endotoxin. This was called granulocyte pyrogen (GP), because of the preponderance of these cells in the rabbit exudates he was using. Later this activity was called leukocyte pyrogen (LP) or endogenous pyrogen (EP).

A large amount of work during the 1950s added to our knowledge of this potential activity, but also introduced the problem of ensuring that the activity being measured was not due to tiny amounts of endotoxin contamination. However, it was not until the 1970s that the attempts at purifying EP (as it was then called) started to show some degree of success. Studies by Bodel (10) and Murphy (68) using rabbit material demonstrated that EP would survive gel filtration techniques; a molecule with molecular mass of 14-15kDa was identified as containing the EP bioactivity. Charles Dinarello, working on human EP, found evidence for two isolectric forms of the protein (Dinarello et al, 1974). Using these materials, Dinarello raised antibodies to the two presumptive forms of EP.

Contemporaneously, other workers were identifying a wide range of biological activities which would later be shown to be due to EP/IL-1. These factors had a weird variety of names (Table 1.1). The 1970s and 1980s are a period of increasing interest in EP as more and more important biological actions are ascribed to this protein (Table 1.2); for example, it was claimed that EP was equivalent to a potent T cell mitogenic factor called lymphocyte-activating factor (LAF). The suggestion that so many different functions could be caused by a single mediator was still considered to be controversial, however (13).

What brought all this confusion and controversy to an end (or nearly so)

The many names of IL-1
Endogenous pyrogen
Leukocytic endogenous mediator
Lymphocyte activating factor
Hemopoietin-1
Mononuclear cell factor
Proteolysis inducing factor
Catabolin
Osteoclast activating factor

Table 1.1: Before its discovery, many different names were used to refer to IL-1(21).

Pleiotropism of IL-1
Causes fever
Stimulates acute-phase proteins
Augment lymphocyte responses
Induce degenerative changes in joints
Increase bone marrow cells

Table 1.2: Some of the effects of IL-1, originally attributed to many different factors(21).

was the cloning of the genes for what turned out to be two distinct proteins with almost identical activities. Surprisingly, the homology between the two IL-1 sequences was found to be low (26%). Moreover, both proteins lacked a classical leader sequence typical of secreted proteins. The cloned proteins were of 31kDa. This was the mature protein, which was later shown to be cleaved to a lower molecular mass (17kDa) form which expressed the biological activity (particularly with IL-1β). The terms IL-1α and IL-1β were introduced after both of these genes had been cloned and the recombinant proteins shown to have EP activity.

These discoveries raised a number of questions. What was the relationship between the two cDNA sequences? Why were there heterogeneous protein sizes? How were the precursor forms processed into an active form?

A human form of the cDNA already discovered in the mouse was reported in 1985 (60). It took several more years until the discovery of the mechanism which converted IL-1 from its precursor form to its active, soluble form (13).

With these discoveries, the uncertainty surrounding IL-1 gradually diminished. It was known that IL-1 had two forms. The acidic form of IL-1 was now known to be IL-1α, and the neutrally charged form IL-1β. Both forms of IL-1 were known to occur in a precursor form, which required further processing before becoming biologically active. The heterogeneity in size was accounted for by the precursor and mature forms of IL-1. A major question was whether or not so many diverse and apparently unrelated biological roles could be fulfilled by a single protein; the discovery of IL-1α and IL-1β answered this question (21).

Biological activities of IL-1
Affects bone formation
Promotes acute phase response
Modulates endocrine function
Induces production of multiple cytokines
Upregulates cell-surface cytokine expression
Stimulates hematopoietic progenitor proliferation
Influences immune regulation (T- and B-cell responses)

Table 1.3: Selected biological activities of IL-1.

1.2 IL-1 as a key pro-inflammatory mediator

IL-1 is a primary mediator of an essential biological process known as inflammation. Inflammation is a vascular process by which leukocytes, present in the blood vessels, are directed to leave these blood vessels and enter into the extravascular tissues. Inflammation and immunity are jointly linked systems that have evolved to enable animals to kill pathogens. Pathogens come in many forms, from the tiny non-living virus up to huge intestinal worms metres long. The diversity of the cellular elements of inflammation/immunity is to cope with the diversity of our pathogens. The complexity of the processes of vascular activation, leukocyte activation, leukocyte movement (extravasation and chemotaxis) and leukocyte apoptosis requires exquisite control. Interleukin-1 and the IL-1 family are now recognised as central regulators of inflammation. Before describing in detail the biological roles of the IL-1 family members (Table 1.3) a brief description of the central elements of the inflammatory process will be provided.

As defined by John Hunter, inflammation is a salutary process; in other words, it is an essential process for our survival, and one that we only recognise if either: (i) it functions too vigorously or (ii) it functions aberrantly. For most of our lives, and without our being aware of it, the inflammatory process is constantly engaging and consuming infective agents.

Inflammation is a vascular phenomenon that takes place only within the post-capillary venule. The main processes involved in the acute inflammatory response are vasodilation, an increase of vascular permeability, and an influx of phagocytes into the affected tissue.

Vasodilation, the increase in the diameter of blood vessels, occurs as those vessels which carry blood away from the site constrict, causing engorgement of the capillary network. The engorged capillaries cause two of the symptoms of inflammation, reddening of the tissue and a localised increase in temperature.

The increase in capillary permeability effects an influx of fluid and cells from the capillary network into the affected tissue. The fluid accumulation contributes to another symptom of inflammation, swelling of the tissue, otherwise known as edema. Increased tissue permeability also permits an influx of phagocytes into the affected site, which is in itself a complex process involving the expression of adhesion molecules on the endothelial wall, migration of the cells out of the capillary and into the tissue, and their migration towards the affected site, as guided by chemokines. This process will be summarised below.

Type	Cell type
E-selectin	Endothelial
L-selectin	Leukoctyes
P-selectin	Platelets / endothelial cells

Table 1.4: Types of the selectin cell adhesion molecule, and the cell types which express it.

Name	Distribution	Ligand
$\alpha_1\beta_1$	Various	Collagens, laminins
$\alpha_2\beta_1$	Various	Collagens, laminins
$\alpha_4\beta_1$	Haematopoietic cells	Fibronectin, VCAM-1
$\alpha_5\beta_1$	Fibroblasts	Fibronectin, proteinases
$\alpha_L\beta_2$	T-lymphocytes	ICAM-1, ICAM2
$\alpha_M\beta_2$	Monocytes	Serum proteins, ICAM-1
$\alpha_{IIb}\beta_3$	Platelets	Serum proteins, fibronectin
$\alpha_V\beta_3$	Platelets	Vitronectin
$\alpha_V\beta_5$	Platelets	Matrix macromolecules, proteinases
$\alpha_6\beta_4$	Epithelial cells	Laminin

Table 1.5: Integrins expressed in mammals: integrins are heterodimers which contain two distinct chains, the α and β subunits.

Macrophages at the affected site release pro-inflammatory cytokines, IL-1 and TNF-α, and chemokines. The cytokines cause the endothelial cells to express cell adhesion molecules (CAM) called selectins on their surface. A list of selectin types is given in Table (1.4). Leukocytes are attracted to the site of injury or infection by the chemokines.

The selectins on the endothelial wall bind to ligands on the leukocytes. The distal lectin-like domain of the selectin binds to carbohydrate groups on leukocyte surface proteins such as P-selectin glycoprotein ligand-1 (PSGL-1). Since there is only a mild affinity between the adhesion molecules and the leukocyte ligands, the bonds are relatively easy to form and break, causing the cells to begin rolling along the inner surface of the vessel wall.

The leukocytes become activated by the presence of chemokines, which causes them to release integrins from cellular stores. A list of integrin types is given in Table (1.5). The integrins have a higher affinity for CAM, causing the leukocyte to adhere tightly to the endothelial wall, arresting its movement.

The transmigration of leukocytes from the venule into the tissue requires the reorganisation of their cytoskeletons. After the reorganisation, the leukocytes are spread over the endothelial wall. Platelet/endothelial cell adhesion molecule (PECAM) proteins, expressed on both the leukocyte and the endothelial cells, interact to pull the leukocyte through the endothelium, a process known as diapedesis. Leukocytes then follow the chemotactic gradient to the affected site.

Macrophages which have migrated to the site of injury or infection release mediators such as pro-inflammatory cytokines and chemokines, primarily IL-1 and TNF-α. These cytokines induce many of the localised and systemic changes

Figure 1.1: Extravasation of a leukocyte. ©Brown University

observed in the acute inflammatory response, as given in Table (1.6). As an example of cytokine redundancy and pleiotropism, the overlapped, multiple functionality between IL-1 and TNF-α is striking. Both cytokines act locally, promoting further migration of neutrophils, macrophages and monocytes to the affected site by their pro-inflammatory action, inducing further vascular permeability, expression of adhesion molecules and production of chemokines. Also, both cytokines increase phagocytic activity by activating macrophages and neutrophils.

Accompanying the local inflammatory response is the systemic acute-phase response. Among other processes initiated in the acute-phase response are an increased production of leukocytes, fever, and production by the liver of acute-phase proteins. The raised body temperature inhibits growth of several microorganisms. IL-1 (and TNF-α) acts on the hypothalamus to trigger the fever response. Acute-phase proteins, such as the components of the complement system, play many roles in attacking pathogens, including opsonisation and cell lysis.

1.3 IL-1β as the target of this thesis

The complexity of the IL-1 network has been noted by many researchers (23), (7). IL-1 has two forms, IL-1α and IL-1β. There are two receptors which bind IL-1 (see section (1.4) for details of components of the IL-1 network). A receptor accessory protein is necessary to form a signalling complex; many inhibitory factors are part of the network.

Assuming complexity of the network as a given, experimental work involving its components would most likely be arduous and time-consuming. However, a model of such a complex system would, according to Klipp, " ... assist experimentation. With an adequate model one may test different scenarios that are not accessible by experiment [...] One may impose perturbations that are not feasible in the real system. One may cause precise perturbations without

Effect	IL-1	TNF-α
Endogenous pyrogen fever	+	+
Synthesis of acute phase proteins by liver	+	+
Increased vascular permeability	+	+
Increased adhesion molecules on vascular endothelium	+	+
Fibroblast proliferation	+	+
Platelet production	+	-
Chemokine induction (e.g. IL-8)	+	+
Induction of IL-6	+	+
T-cell activation	+	+
B-cell activation	+	+

Table 1.6: Redundant and pleiotropic effects of IL-1 and TNF-α: derived from Kuby Immunology 4th Ed.(35)

directly changing other system components, which is usually impossible in real systems. Model simulations can be repeated often and for many different conditions" (53). Furthermore, a model would allow us to find the equilibrium (or equilibria) of the system, if such exists. It would enable us to analyse the effects of different combinations of the inhibitory factors on the signalling of IL-1, and the qualitative or quantitative changes on the system equilibrium. The purpose of such a modelling process would be to *clarify* a system which has the complexity of IL-1; such clarification may also lead to hypotheses on system behaviour which can then be confirmed by experimentation.

A necessary first step of the modelling process is to decide which parts of a system to model; in terms of systems theory, this is to establish the system boundary. The IL-1 network has two ligands, IL-1α and -β. It would be possible to model both, or to treat both types as a generalised ligand, but for clarification of the model, it would be simpler to choose one or the other.

How then should we make a choice between them? Both are subject to (largely) the same inhibitory factors (see section (2.A) for details of these), both have roughly the same association and dissociation rates, both require the same accessory protein to initiate a signalling event, and both use the same receptors. One significant difference between the two types of IL-1 concerns their secretion from the cell: IL-1β has been found to be secreted earlier than IL-1α in response to an immunogenic stimulus (40). Working on human peripheral blood monocytes (HPBM), Hazuka and colleagues stimulated them with LPS and found that IL-1β is secreted at a much earlier phase that IL-1α, an observation matched by the respective half-lives of their mRNA. IL-1β, but not IL-1α, has been found to be necessary for regulating T-cell-dependent antibody production (69). Another way of choosing which of the two forms of IL-1 to model is their respective potency. In the context of the production of adrenocorticotropin (ACTH), a hormone that stimulates the adrenal cortex, IL-1β was found to be eight times more potent than IL-1α (62). In a study of the pyrogenic efficacy of IL-1, the β type was found to be five times more potent than the α form (19). With these factors in mind, we will choose IL-1β.

1.4 Components of the IL-1β network

This section will examine the major components of the IL-1β network: IL-1β, the two receptors, the accessory protein, and the receptor antagonist. These relationships between these components will form the main basis of the models to developed later in the thesis.

1.4.1 IL-1β

IL-1β is found at 2q14 and forms 269 amino acids. Both forms of IL-1 are initially synthesised as 31 kDa precursors (pro-IL-1) (20). A unique feature of IL-1 is that neither of the precursor forms contain a signal peptide sequence indicating a natural cleavage site for the N-terminus (3). Cleavage of pro-IL-1 by proteases results in a carboxyl terminal 17-kDa peptide known as mature IL-1, which is the biologically active form.

Both forms of IL-1 appear to be under different forms of transcriptional control. When stimulated by LPS, IL-1β mRNA synthesis is rapid: in some cell lines (e.g. macrophages) RNA transcription is observed under fifteen minutes from LPS exposure. There have been suggestions of rapid synthesis of a transcriptional repressor, and an increase in half-life of the mRNA.

Transcription of IL-1 mRNA without translation can be observed after exposure of blood monocytes to, for example, recombinant C5a. Schindler et al investigated the effects of recombinant C5a (rC5a) on gene expression and synthesis of IL-1β in human peripheral blood mononuclear cells (PBMC) (83). They found that rC5a provides primarily a transcriptional but not translational signal for IL-1 beta and TNF; the half-life of the untranslated mRNA is the same as that of the translated message; rC5a-induced transcription upregulates PBMC for enhanced synthesis of these cytokines; and a translational signal can be provided by LPS or IL-1 itself. The half-life of mRNA was found to be unchanged using this stimulus, and unlike the case when using LPS, there was found to be no translation of IL-1 mRNA into the protein form.

IL-1β mRNA levels in human monocytes have been found to rise rapidly after fifteen minutes and, depending on the stimulant, decrease after four hours. The decrease is attributed to either a transcriptional repressor and/or a decrease in mRNA half-life (47), (48); however, the effect of the stimulus is important, since using IL-1 itself as a stimulant IL-1β mRNA levels can be maintained for over twenty-four hours (82), (87). Increasing cAMP levels via histamine exposure has been found to similarly raise IL-1β gene expression and subsequent protein synthesis (101).

Inhibition of mRNA translation by cycloheximide has been reported as resulting in enhanced splicing of exons, excision of introns and increased levels of mature mRNA; synthesis of mature IL-1β mRNA appears to implicate an intrinsic inhibition to process precursor mRNA. A dissociation between the transcription and translation phases of IL-1β has been noted (81). Most of the IL-1β is degraded, despite the presence of excitatory signals such as C5a, and little significant translation into pro-IL-1β is undertaken. Stimulus by IL-1 or endotoxin to cells with a high level of steady-state IL-1β mRNA results, contrastingly, in the activation of high levels of translation (88), (82): one possible explanation for this phenomenon is that stabilisation of the 3' untranslated region occurs in those cells stimulated with LPS. The stabilisation of mRNA by LPS induce

large-scale translation and eventual expression of IL-1β (64); another is that IL-1 may stabilise its own mRNA by preventing deadenylation, as it has been shown to do for the chemokine gro-α (98).

Pro-IL-1β remains largely cytosolic after synthesis until cleavage and transport out of the cell; pro-IL-1β has, as yet, no known membrane form and is minimally biologically active (50). There are several sites in pro-IL-1β available for cleavage by enzymes, each of which produces a biologically active, mature form of IL-1β.

1.4.2 Cleavage of the full length protein

Pro-IL-1β, as intimated above, requires cleavage by a suitable protease to metamorphose into its biologically active, mature form. The protagonist in this interaction is the IL-1β converting enzyme (ICE), also known as caspase-1. ICE is composed of a enzymatically active heterodimer comprising a 10- and 20-kDA chain, with the active site cysteine located on the 20-kDa chain. The precursor of ICE requires two cleavage events before it is active itself, and is involved in its own processing; ICE assists processing of the precursor form by undergoing oligomerisation with itself or other ICE homologues (106), (39). ICE is classified as a member of the caspase family, a group of intracellular cysteine proteases; cleavage by caspases occurs after an aspartic acid residue on the target protein precursor.

A tetramer is formed from two molecules of the ICE heterodimer and two molecules of pro-IL-1β: the aspartic acid, position 116 of the precursor, is the target site for ICE cleavage, and enzymes such as elastase and granzyme A (46) cleave the precursor at, respectively, amino acid 112 and 120 (106), (103); this results in biologically active IL-1β.

The primary nature of ICE in the production of mature IL-1β is attested to by the accumulation of pro-IL-1β, but minimal extracellular presence of mature IL-1β, in ICE-deficient mice. A novel caspase-1-independent pathway involving matrix metalloproteinases which results in mature IL-1β has also been identified (84).

1.4.3 IL-1 receptor superfamily

The IL-1 receptors are part of a superfamily of structurally homologous proteins. A large number of mammalian homologues of IL-1RI contain a highly conserved region in their cytosolic domains, also found in a receptor protein of the *Drosophila* fruit fly called Toll. The conserved region is accordingly known as a Toll/IL-1R (TIR) domain, and the homology has defined a superfamily of receptors known as the IL-1R/Toll-like receptor (TLR) superfamily (32). Figure 1.2 shows the structure of the TIR domain, and figure 1.3 shows members of the superfamily, along with the consensus sequence of the TIR domain.

The superfamily divides into two subfamilies, those with leucine-rich repeats, and those with three immunoglobulin (Ig) domains. This latter group includes the receptors and receptor accessory protein of the IL-1 network, and other receptors in the interleukin cytokine group, such as IL-18R (the receptor for interleukin-18), and the orphan receptors T1/ST-2, SIGIRR and IL-1Rrp2. The superfamily is diverse, but the degree of homology in the TIR domain and its

Figure 1.2: Structure of the Toll/IL-1R (TIR) domain, a highly conserved region common to receptors in many mammalian, and other, species .©Berkeley University

Figure 1.3: Members of the IL-1R/TLR superfamily. The family is defined by a homologous TIR (Toll/IL-1R) domain. Most of the receptors have unknown ligands, otherwise known as orphan receptors; the exceptions are IL-1RI, IL-18R, TLR-2 and TLR-4. The concensus motif for the superfamily is also shown, consisting of some 200 amino acids. Particularly conserved regions, those present in all member of the family, are underlined ©(73)

Figure 1.4: IL-1β/IL-1RI complex ©(41): The complex is displayed as a ribbon diagram with the carboxy terminus of the receptor located at the bottom. The type-I receptor is composed of three Ig-like domains, designated 1, 2, and 3, all of which interact with IL-1β. Receptor binding sites have been classified into two regions on IL-1β, sites A and B. The secondary structural elements for the β-strands are represented as arrowed ribbons with the IL-1R1 receptor depicted in blue, and IL-1β in grey. The IL-1β residues that comprise binding site A are shown in red, with the binding site B residues displayed in yellow. Histidine 30, which makes critical interactions at site A, is highlighted in green for clarity.

presence across so many different species suggests that the superfamily is an ancient part of host defense (33).

1.4.4 The type-I receptor: IL-1RI

IL-1RI is coded for at the locus 2q12, and consists of 4909 base pairs. It is composed of 569 amino acids (92), and has a molecular weight of 65402 Da. The type-I receptor effects IL-1β signal transduction by forming a ternary signalling complex, binding to both IL-1β and the IL-1 receptor accessory protein, IL-1RAcP.

IL-1RI is not an abundant receptor, but evokes a powerful response without a high level of receptor occupancy (6), as the receptor activates many pathways which operate in parallel. It is thought that as few as ten occupied receptors are sufficient to evoke a strong response (93). IL-1RI binds both forms, IL-1α and IL-1β, and a receptor antagonist, IL-1Ra. The human form of the type-I receptor contains seven glycosylation sites; glycosylation is necessary for binding (28).

Crystallographic studies of the IL-1β/IL-1RI binary complex reveal that the first and second Ig-like domains are held rigidly in place by disulphide bonds; the third domain has a more flexible alignment (see figure (1.4)). Once a ternary signalling complex has been formed, after the further binding of the IL-1 receptor accessory protein, it is internalised by receptor mediated endocytosis (92).

1.4.5   The type-II receptor: IL-1RII

The DNA sequence for IL-1RII is found at the locus 2q12-q22, and consists
of 1484 base pairs, which yield 398 amino acids. It has a molecular weight of
45421Da. It was originally cloned from human and murine B-cells (63), and
is expressed on many cells, including monocytes, neutrophils, dendritic cells,
macrophages, B-cells, T-cells and epithelial cells. It binds both IL-1α and IL-
1β.

The IL-1RII receptor binds both IL-1α and IL-1β, and so competes with
the type-I receptor for ligand (71). The receptor has an extracellular region,
containing three Ig-like domains with a high homology to the type-I receptor.
However, it also has a short intracellular domain, some 29 amino acids in length
and lacking the TIR domain, which means that it is unable to initiate signal
transduction (15). Since it binds IL-1β and lacks the mechanisms to induce a
signal, it acts as a decoy target, or sink, for IL-1β (74) by sequestering it, and
therefore acts as an inhibitor on the IL-1β network.

It has also been noted that IL-1RII interacts with the IL-1 receptor accessory
protein (IL-1RAcP) (59), and so both types of receptor are in effect in compe-
tition for both IL-1 and IL-1RAcP (54). In order for a signal transduction
event to occur, IL-1RI and IL-1β requires the receptor accessory protein, and
an inhibitory factor on IL-1RAcP will also be inhibitory on signal transduction.

Similarly, IL-1RII has a low affinity for the IL-1 receptor antagonist (IL-1Ra,
see below) (99), and so does not act as a sink for this antagonist protein. This
is consistent with its apparent role of inhibitory factor of the IL-1β network.

1.4.6   Soluble IL-1RII (sIL-1RII)

A soluble form of the type-II receptor IL-1RII has also been discovered (99). It
has been shown that increased IL-1RII shedding attenuates the biological activ-
ity of IL-1β (16). Soluble IL-1RII lacks both cytoplasmic and transmembrane
regions. Two of the three Ig-like domains have been shown to be sufficient to
bind with IL-1β (55), and so sIL-1RII also acts as a sink for mature IL-1β.

1.4.7   Receptor accessory protein (IL-1RAcP)

The IL-1 receptor accessory protein (IL-1RAcP) can be found at human chromo-
some location 3q28. It consists of 4726 base pairs, which yield 570 amino acids,
with a molecular weight of 65418 Da. There is a significant homology with the
type-I and type-II receptors, with the protein sharing some 25% identity with
the two receptors (36).

It is clear that IL-1RAcP is an essential component in the IL-1 signal trans-
duction pathway (17). IL-1RAcP does not bind directly to IL-1β, but rather
to the binary complex formed by either of the receptors and the ligand. This can
cause inhibition of signal transduction when IL-1RAcP binds to the nonsignalling
binary complex formed by the type-II and the IL-1β ligand (104).

The binary complex is formed when IL-1β binds to one of the two types of
receptors. IL-1β binds the receptor through the Ig-like domains 1 and 2, which
results in a conformational change in the receptor such that domain 3 wraps
around the ligand. The ternary complex is formed when the conformational
change allows the interaction between IL-1RAcP and the binary complex (102).

1.4.8   Soluble IL-1RAcP (sIL-1RAcP)

Human and murine soluble forms of IL-1RAcP have been identified (49). sIL-1RAcP binds to IL-1RI, and so forms another inhibitory control mechanism of the IL-1β network, by binding with and blocking type-I receptors, thereby preventing them from binding with IL-1β and forming a binary signalling complex.

1.4.9   Receptor antagonist (IL-1Ra)

The IL-1 receptor antagonist is coded for on human chromosome 2q14, consisting of 1612 base pairs. It has a molecular weight of 20055 Da, and is comprised of 177 amino acids. There are a number of different forms, encoded by the same genes but generated by alternative splicing of different first exons, only one of which is secreted; the secreted isoform has a mass of 17 kDa (see (5) for more information on the intracellular forms of IL-1Ra). IL-1Ra shows a high degree of homology to IL-1RI and IL-1RII (29).

IL-1Ra has been described as a pure receptor antagonist (5), which binds to IL-1RI receptors but does not activate the signalling cascade. Furthermore, it appears that the complex formed does not undergo endocytosis, and so blocks receptor recycling, thus presumably blocking the receptor on the membrane until the receptor is internalised. The receptor antagonist has lower affinity for the type-II decoy receptor than the type-I signalling receptor. IL-1Ra represents another control mechanism, inhibiting the IL-1β signalling pathway.

1.5   Inhibitory/antagonistic elements in the IL-1β network

There are many different control mechanisms evident in the IL-1β network; several of the major components have an inhibitory effect on the network. It is a matter of speculation as to why these different mechanisms have evolved, but it is appropriate to emphasise the complexity and redundancy of the network's control mechanisms, and to summarise them here.

- IL-1RII $\mapsto$ IL-1β: The type-II receptor acts as a decoy receptor on the cell membrane, capturing IL-1β and preventing it from binding to the type-I receptor.

- IL-1RII+IL-1β $\mapsto$ IL-1RAcP: The type-II/IL-1β binary nonsignalling complex can sequester the receptor accessory protein, necessary for the bound type-I complex to initiate the signalling cascade, to form a ternary nonsignalling complex, thus preventing a ternary signalling complex if insufficient IL-1RAcP exists on the cell membrane.

- IL-1Ra $\mapsto$ IL-1IR: The receptor antagonist IL-1Ra can bind with the type-I receptor, thus blocking IL-1β from binding to IL-1RI.

- sIL-1RII $\mapsto$ IL-1β: The soluble form of the type-II receptor, sIL-1RII, acts as a sink for extracellular IL-1β, thus preventing it from reaching type-I receptors on the cell membrane.

- sIL-1RII+IL-1β $\mapsto$ sIL-1RAcP : The soluble form of the receptor accessory protein binds to IL-1RI, blocking the receptor binding to IL-1β.

As will be appreciated, this represents a considerable number of inhibitory mechanisms at work in the IL-1β network.

In the following chapters, models of the inhibitory components of the IL-1β network will be presented. A number of modelling techniques will be applied to explore the action of these components on the cytokine. We aim to identify the major inhibitory components of the network, and discover by which mechanisms they inhibit IL-1β.

Chapter 2

Ordinary differential equation model

2.1 Derivation of the four-dimensional model

A four-dimensional ordinary differential equation model is developed by applying Michaelis-Menten and Briggs-Haldane modelling methods (see the appendix (2.A)) for more details on these methods). We are investigating the formation of the binary complexes from the receptors IL-1RI and IL-1RII, and the IL-1β cytokine, and the further formation of the ternary signalling and nonsignalling complexes, formed from the binary complexes with an IL-1RAcP accessory protein. The assumption is that the system will rapidly approach a steady state, so that it is more akin to the Briggs-Haldane model of protein kinetics.

There are a number of assumptions made by the Michaelis-Menten framework which may influence how applicable it is to the task of modelling the IL-1β network. The assumptions are (86):

- The enzyme is a catalyst.

- The enzyme and substrate react rapidly to form an enzyme-substrate complex.

- Only a single substrate and a single enzyme-substrate complex are involved and the enzyme-substrate complex breaks down to form free enzyme and product.

- The substrate concentration is much larger than the enzyme concentration.

- The overall rate of the reaction is limited by the breakdown of the complex to form free enzyme and product.

- Enzyme, substrate, and enzyme-substrate complex are at equilibrium - the rate at which the complex dissociates to component parts is much faster than the rate at which the product and free enzyme are produced. This is the quasi-equilibrium or rapid equilibrium assumption.

It would be useful to examine these assumptions and consider their applicability to the IL-1β network and the modelling process.

- The enzyme is a catalyst: This should not pose any conceptual problems for IL-1β; the ligand acts much like an enzyme, with the formation of binary and ternary complexes analogous to the chemical reactions enzymes initiate.

- Complex is formed rapidly: Binding between IL-β and its receptors is not likely to be any more rapid than other cytokines and their receptors.

- Single substrate/single enzyme-substrate complex: In applying the equilibrium assumption, we are considering the receptors IL-1R1, IL-1R2 and IL-1RAcP as analogous to substrates in a chemical reaction. This assumption does apply, since the model has been extended to accommodate multiple substrates and enzymes, and so need not concern us.

- Substrate concentration is greater than enzyme concentration: This assumption may be of concern if the amount of IL-1β is much greater than the number of IL-RI receptors available, and would be an interesting case for further analysis.

- Rate of reaction limited by complex breakdown: This assumption need not be a problem for a model of the network.

- Rapid equilibrium: This will be borne out by the results below (see section(3.1)).

If we let RI, RII be the type-I and type-II receptors, respectively, and L the IL-1β, then the chemical rate equations governing the formation of binary complexes are:

$$RI + L \xrightarrow{k_{RIL}^+} RIL \tag{2.1}$$

$$RII + L \xrightarrow{k_{RIIL}^+} RIIL \tag{2.2}$$

Note that this gives only the *forward* reaction rate. To represent the association of ternary complexes, let C represent the amount of IL-1RAcP, we have:

$$RIL + C \xrightarrow{k_{RILC}^+} RILC \tag{2.3}$$

$$RIIL + C \xrightarrow{k_{RIILC}^+} RIILC \tag{2.4}$$

where once again we are showing only the forward reaction rate. We must now turn these chemical rate equations into a system of differential equations. In order to begin building the model we would use the Law of Mass Action, which

states the rate of a chemical reaction is proportional to the concentrations of the reacting substances.

Let C_{R1} and C_{R2} be the type-I and type-II receptors, and let each type of receptor be conserved; then the number of unbound type-I receptors is given by C_{R1} minus the binary and ternary signalling complexes, and similarly, the unbound type-II receptors by C_{R2} minus binary and ternary nonsignalling complexes. If we let w symbolise the number of binary signalling complexes, x the binary nonsignalling complexes, y the ternary signalling complexes, and z the ternary nonsignalling complexes, then the number of unbound type-I and type-II receptors are given respectively by the conservation laws:

$$\text{Unbound type I} \quad = \quad [R1] = C_{R1} - w - y \tag{2.5}$$
$$\text{Unbound type II} \quad = \quad [R2] = C_{R2} - x - z \tag{2.6}$$

We assume that the IL-1β, L, in the system is conserved. The unbound ligand is therefore given by:

$$\text{Unbound ligand} = L - w - x - y - z \tag{2.7}$$

Similarly, the IL-1RAcP, C_{AP}, is assumed to be conserved. Accessory protein is consumed by both the signalling and nonsignalling complexes, and so a conservation law is given by:

$$\text{Unbound accessory} = C_{AP} - y - z \tag{2.8}$$

Following on from these conservation laws, as a first approximation to the equations governing the change in binary signalling and nonsignalling complexes, we obtain:

$$\frac{dw}{dt} \quad = \quad k_w^+ \left(C_{R1} - w - y\right)\left(L - w - x - y - z\right) \tag{2.9}$$

$$\frac{dx}{dt} \quad = \quad k_x^+ \left(C_{R2} - x - z\right)\left(L - w - x - y - z\right) \tag{2.10}$$

where k_w^+ is the association rate of binary signalling complex, and k_x^+ is the association rate of the binary nonsignalling complex. Similarly, the corresponding ternary complex rate equations are given by:

$$\frac{dy}{dt} \quad = \quad k_y^+ w \left(C_{AP} - y - z\right) \tag{2.11}$$

$$\frac{dz}{dt} \quad = \quad k_z^+ x \left(C_{AP} - y - z\right) \tag{2.12}$$

where k_y^+ and k_z^+ are the association rates for the ternary complexes.

However, these equations so far represent only association events, and we need to take dissociation events into account. The binary signalling complex has a rate of dissociation given by k_w^-; it will be decreased by the formation of the ternary signalling complex, and increased by its dissociation. With this in mind, the rate of change of binary signalling complexes is given by:

$$\frac{dw}{dt} = k_w^+ (C_{R1} - w - y)(L - w - x - y - z) \tag{2.13}$$
$$-k_w^- w + k_y^- y - k_y^+ w (C_{AP} - y - z)$$

where k_w^- is the dissociation rate of the binary signalling complex, and $k_y^\pm$ are the association/dissociation rates of the ternary signalling complex.

A similar argument yields the following equation for the rate of change of signalling ternary complexes:

$$\frac{dy}{dt} = k_y^+ w (C_{AP} - y - z) - k_y^- y \tag{2.14}$$

where, once again, the dissociation rate of the ternary complex is given by k_y^-.

Collecting the results together, the system of equations for the formation of binary and ternary signalling and nonsignalling complexes is given by:

$$\frac{dw}{dt} = k_w^+ (C_{R1} - w - y)(L - w - x - y - z) \tag{2.15}$$
$$-k_w^- w + k_y^- y - k_y^+ w (C_{AP} - y - z)$$
$$\frac{dx}{dt} = k_x^+ (C_{R2} - x - z)(L - w - x - y - z) \tag{2.16}$$
$$-k_x^- x + k_z^- z - k_z^+ x (C_{AP} - y - z)$$
$$\frac{dy}{dt} = k_y^+ w (C_{AP} - y - z) - k_y^- y \tag{2.17}$$
$$\frac{dz}{dt} = k_z^+ x (C_{AP} - y - z) - k_z^- z \tag{2.18}$$

The above equations (2.15) - (2.18) is the reaction-kinetic ordinary differential equation model for the IL-1β system. We will analyse the model in subsequent sections.

2.2 Analysis of the ODE model

We shall simplify the system given by equations (2.15) - (2.18) above [1] . We wish to reduce the four equations to two, and find where $\dot{w} - \dot{y} = 0 = \dot{x} - \dot{z}$; we are looking for the conditions where two hyperplanes intersect. To effect this, we introduce some substitutions. Let $w = C_{R1}\theta$, $x = C_{R2}\theta$, $y = C_{R1}\phi$, and $z = C_{R2}\phi$, where we have $\theta < 1$, $\phi < 1$, and $\theta + \phi < 1$:

---

[1]I am especially indebted to Professor Seymour for his advice on the analysis in this section

$$\frac{dC_{R1}\theta}{dt} = k_w^+(C_{R1}(1-\theta-\phi))(L-(C_{R1}+C_{R2})(\theta+\phi)) \qquad (2.19)$$
$$-k_w^-C_{R1}\theta + k_y^-C_{R1}\phi - k_y^+C_{R1}\theta(C_{AP}-(C_{R1}+C_{R2})\phi)$$

$$\frac{dC_{R2}\theta}{dt} = k_x^+(C_{R2}(1-\theta-\phi))(L-(C_{R1}+C_{R2})(\theta+\phi)) \qquad (2.20)$$
$$-k_x^-C_{R2}\theta + k_z^-C_{R2}\phi - k_z^+C_{R2}\theta(C_{AP}-(C_{R1}+C_{R2})\phi)$$

$$\frac{dC_{R1}\phi}{dt} = k_y^+C_{R1}\theta(C_{AP}-(C_{R1}+C_{R2})\phi) - k_y^-C_{R1}\phi \qquad (2.21)$$

$$\frac{dC_{R2}\phi}{dt} = k_z^+C_{R2}\theta(C_{AP}-(C_{R1}+C_{R2})\phi) - k_z^-C_{R2}\phi \qquad (2.22)$$

A considerable simplification to these equations occurs if we assume $k_w^\pm = k_x^\pm$, $k_y^\pm = k_z^\pm$. Biologically, this is not the case; however, it does allow us to get some idea of the behaviour of the system, and so might be mathematically justified. From (2.19) and (2.20) we have

$$\frac{1}{C_{R1}}\frac{d(C_{R1}\theta)}{dt} = k_w^+(1-\theta-\phi)(L-C_R(\theta+\phi)) \qquad (2.23)$$
$$-k_w^-\theta + k_y^-\phi - k_y^+\theta(C_{AP}-C_R\phi)$$

$$\frac{1}{C_{R2}}\frac{d(C_{R2}\theta)}{dt} = k_x^+(1-\theta-\phi)(L-C_R(\theta+\phi)) \qquad (2.24)$$
$$-k_x^-\theta + k_z^-\phi - k_z^+\theta(C_{AP}-C_R\phi)$$

where the total receptor density is given by $C_R = C_{R1} + C_{R2}$. Since C_{R1} and C_{R2} are assumed to be constant, these two equations must be identical.

Similarly, we have, from (2.17) and (2.18)

$$\frac{1}{C_{R1}}\frac{d(C_{R1}\phi)}{dt} = k_y^+\theta(C_{AP}-C_R\phi) - k_y^-\phi \qquad (2.25)$$

$$\frac{1}{C_{R2}}\frac{d(C_{R2}\phi)}{dt} = k_z^+\theta(C_{AP}-C_R\phi) - k_z^-\phi \qquad (2.26)$$

and once again we have two identical equations if $k_y^\pm = k_z^\pm$.

We have reduced the 4-dimensional system (2.15) - (2.18) to the 2-dimensional system

$$\dot{\theta} = k_w^+(1-\theta-\phi)(L-C_R(\theta+\phi)) \qquad (2.27)$$
$$-k_w^-\theta + k_y^-\phi - k_y^+\theta(C_{AP}-C_R\phi)$$

$$\dot{\phi} = k_y^+\theta(C_{AP}-C_R\phi) - k_y^-\phi \qquad (2.28)$$

We nondimensionalise the system of equations by letting $\tau = k_y^+t$; we assume $r = \frac{k_w^+}{k_y^+} = 1$, and we let $\rho_w = \frac{k_w^-}{k_y^+}$, $\rho_y = \frac{k_y^-}{k_y^+}$. Finally, we let $S = C_{R1} + C_{R2}$. With some simplifications and substitutions we have:

Table 2.1: Association/dissociation rates: the association and dissociation rates of the signalling and nonsignalling complexes of the IL-1β network, where S is the signalling binary and NS the nonsignalling binary.(51)

Agent	Binds	Assoc. $(M^{-1}s^{-1})$	Dissoc. (s^{-1})
IL-1RI[1]	IL-1β	4.67×10^7	1.6×10^{-11}
S [1]	IL-1RAcP	4.03×10^7	0.32×10^{-11}
IL-1RII [2]	IL-1β	8.85×10^6	6.92×10^{-10}
NS [2]	IL-1RAcP	9.5×10^6	6.82×10^{-10}

[1] Source: (4), (24)   [2] Source: (4), (25)

$$\dot{\theta} = (1 - (\theta + \phi))(L - S(\theta + \phi)) \tag{2.29}$$
$$-\rho_w\theta + \rho_y\phi - \theta(C_{AP} - S\phi)$$
$$\dot{\phi} = \theta(C_{AP} - S\phi) - \rho_y\phi \tag{2.30}$$

where $\dot{\theta}, \dot{\phi}$ refers to differentiation w.r.t. τ. Adding these equations, we obtain:

$$\dot{\theta} + \dot{\phi} = (1 - (\theta + \phi))(L - S(\theta + \phi)) - \rho_w\theta \tag{2.31}$$

Referring again to Table 2.1, we note the extremely small magnitude of both ρ_w and ρ_y, that is, that the association rates in this cytokine network are orders of magnitude larger than the dissociation rates, making these ratios extremely small. Since $\rho_w \ll 1$, we set $\rho_w = 0$, and let $\sigma = \theta + \phi$, yielding:

$$\dot{\sigma} = (1 - \sigma)(L - S\sigma) \tag{2.32}$$

We can use this approximation to solve exactly for σ; since σ must be less than or equal to one. Therefore, steady states exist at $\sigma^* = 1, \frac{L}{S}$. Let $\dot{\sigma} = f(\sigma)$:

$$f\prime(\sigma) = -(L + S) + 2S\sigma \tag{2.33}$$
$$f\prime(1) = S - L \tag{2.34}$$
$$f\prime(\frac{L}{S}) = L - S \tag{2.35}$$

Clearly, the steady states depend on the relative sizes of L and S, the ligand and the type-I and type-II receptors.

We continue the analysis by setting ρ_y to zero, yielding:

$$\dot{\phi} = (\sigma - \phi)(C_{AP} - S\phi) \tag{2.36}$$
$$\dot{\sigma} = (1 - \sigma)(L - S\sigma) \tag{2.37}$$

The fixed points are $(1, 1)$, $(1, \frac{C_{AP}}{S})$, $(\frac{L}{S}, \frac{C_{AP}}{S})$, $(\frac{L}{S}, \frac{L}{S})$. The Jacobian is given by

$$J = \begin{pmatrix} -S\sigma + 2S\phi - C_{AP} & C_{AP} - S\phi \\ 0 & -(L + S - 2S\sigma) \end{pmatrix} \tag{2.38}$$

We will perform linear stability analysis of the approximation. At $(1,1)$ the determinant of the Jacobian evaluated at the steady state J^* is

$$J^*_{(1,1)} = \begin{pmatrix} S - C_{AP} & C_{AP} - S \\ 0 & -(L - S) \end{pmatrix} \tag{2.39}$$

For reasons of biological realism, we assume from hereon that $S \geq C_{AP}$. We can determine the behaviour of the system near the fixed point by evaluating the trace and determinant of the Jacobian.

The eigenvalues are $(\lambda_1, \lambda_2) = (S - L, S - C_{AP})$; the determinant $\text{Det}(J^*_{(1,1)}) = -(L - S)(S - C_{AP})$, and the trace is $\text{Tr}(J^*_{(1,1)}) = -L + S + S - C_{AP}$. Recall that we have simplified by setting $r = 1$.

We have the following conditions on the parameters at this steady state:

$$\text{Det}(J^*_{(1,1)}) < 0 \quad \text{and} \quad \text{Tr}(J^*_{(1,1)}) < 0 \tag{2.40}$$
$$\Leftarrow \quad S > 0 \text{ and } L > 2S \text{ and } 0 \leq C_{AP} < S \tag{2.41}$$
$$\text{or} \quad L = 2S \text{ and } 0 < C_{AP} < S \tag{2.42}$$
$$\text{or} \quad L > S \text{ and } L < 2S, L + C_{AP} > 2S \tag{2.43}$$
$$\text{and } S > C_{AP} \tag{2.44}$$

Furthermore, examining the eigenvalues, we obtain

$$\lambda_1 \lambda_2 \quad = \quad S - L \times S - C_{AP} = S^2 + LC_{AP} - LS - SC_{AP} \tag{2.45}$$
$$\lambda_1 \lambda_2 < 0 \quad \Leftarrow \quad S < L \text{ and } C_{AP} < S \tag{2.46}$$
$$\lambda_1 \lambda_2 > 0 \quad \Leftarrow \quad L < S \text{ and } C_{AP} < S \tag{2.47}$$

Biologically, equation (2.46) would mean that the amount of free accessories is fewer than the unbound receptors, which in turn is fewer than the free ligand. This could be the case if the cell has already formed complexes, and so many of its receptors and accessories are already consumed. If the conditions here are met, the fixed point would be a saddle point.

If the conditions in equation (2.47) are met, the fixed point is either a node or a spiral, in which case we examine the conditions on both the eigenvalues and $\text{Tr}(J^*_{(1,1)})$; the node requires the following conditions:

$$\text{Tr}(J^*_{(1,1)})^2 \quad - \quad 4\text{Det}(J^*_{(1,1)}) > 0 \text{ and } \lambda_1 \lambda_2 > 0 \tag{2.48}$$
$$\Leftarrow \quad L = 0 \text{ and } S \leq 1 \text{ and } C_{AP} < S \tag{2.49}$$
$$\text{or} \quad L < S \leq 1 \text{ and } (0 \leq C_{AP} < L \text{ or } L < C_{AP} < S) \tag{2.50}$$

In the first case, we would have no ligand and most or all of the receptors unbound, with fewer receptor accessory proteins than receptors; in the second, the ligand are fewer than the unbound receptors and either the accessory proteins are fewer than the ligand or the ligand is fewer than the receptor accessories.

The stability of the fixed point depends on the trace; in this case, if the receptor accessories are fewer than available ligand, the equilibrium is stable.

For a spiral, we would require $\text{Tr}(J^*_{(1,1)})^2 - 4\text{Det}(J^*_{(1,1)}) < 0$; however, this cannot be the case, since $\text{Tr}(J^*_{(1,1)})^2 - 4\text{Det}(J^*_{(1,1)}) = (Lr + S - rS - C_{AP})^2$, and so we can rule out the spiral as an equilibrium.

At the fixed point $(\theta^*, \phi^*) = (1, \frac{C_{AP}}{S})$ the Jacobian $J^* = J^*_{(1, \frac{C_{AP}}{S})}$ is

$$J^* = \begin{pmatrix} C_{AP} - S & 0 \\ 0 & r(S - L) \end{pmatrix} \tag{2.51}$$

The eigenvalues $(\lambda_1, \lambda_2) = (S - L, C_{AP} - S)$; the determinant $\text{Det}(J^*) = LS - S^2 - LC_{AP} + SC_{AP}$ and the trace $\text{Tr}(J^*) = C_{AP} - L$. The conditions for a saddle point are

$$\lambda_1\lambda_2 < 0 \quad \Leftarrow \quad 0 \leq L < 1 \tag{2.52}$$
$$\text{and} \quad L < S \leq 1 \tag{2.53}$$
$$\text{and} \quad 0 \leq C_{AP} < S \tag{2.54}$$

Biologically, this would mean that both the ligand and the available receptor accessories are fewer than the unbound receptors.

The conditions for a node are as follows:

$$\text{Tr}(J^*_{(1,1)})^2 \quad - \quad 4\text{Det}(J^*_{(1,1)}) > 0 \text{ and } \lambda_1\lambda_2 > 0 \tag{2.55}$$
$$\Leftarrow \quad 0 < L \leq 1 \tag{2.56}$$
$$\text{and} \quad 0 < S < L \tag{2.57}$$
$$\text{and} \quad 0 \leq C_{AP} < S \tag{2.58}$$

The amount of receptor accessories are fewer than the unbound receptors, which in turn are fewer than the ligand. This might imply, for example, that some of the receptors and accessories have already formed complexes, or simply that a high number of ligand has been released. The stability of this steady state is determined by $\text{Tr}(J^*) = C_{AP} - L$, and since from above we have $C_{AP} < S$ and $S < L$, the fixed point is stable. None of the constraints on the variables allow the formation of a spiral or centre.

For the fixed point at $(\theta^*, \phi^*) = (\frac{L}{S}, \frac{C_{AP}}{S})$ the Jacobian $J^* = J^*_{(\frac{L}{S}, \frac{C_{AP}}{S})}$ is

$$J^* = \begin{pmatrix} C_{AP} - L & 0 \\ 0 & L - S \end{pmatrix} \tag{2.59}$$

The eigenvalues $(\lambda_1, \lambda_2) = (L - S, C_{AP} - L)$, the trace $\text{Tr}(J^*) = C_{AP} - S$, and the determinant $\text{Det}(J^*) = -(L - S)(L - C_{AP})$. The conditions for a saddle point are

$$\lambda_1\lambda_2 \quad < \quad 0 \tag{2.60}$$
$$\Leftarrow \quad L = 0 \text{ and } S \leq 1 \text{ and } C_{AP} < S \tag{2.61}$$
$$\text{or} \quad L \leq 1 \text{ and } S = 0 \text{ and } C_{AP} = 0 \tag{2.62}$$
$$\text{or} \quad L \leq 1 \text{ and } S < L \text{ and } C_{AP} \leq S \tag{2.63}$$
$$\text{or} \quad L < S \leq 1 \text{ and } L < C_{AP} \leq S \tag{2.64}$$

The (fairly complicated) conditions for a stable node are as follows:

$$\lambda_1 \lambda_2 > 0 \quad \text{and} \quad \text{Tr}(J^*)^2 - 4\text{Det}(J^*) > 0 \text{ and } \text{Tr}(J^*) < 0$$

$$\Leftarrow \quad L \leq \frac{1}{2} \text{ and } L < S < 2L \text{ and } 0 \leq C_{AP} < 2L - S$$

$$\text{or} \quad L \leq \frac{1}{2} \text{ and } L < S < 2L \text{ and } 2L - S < C_{AP} < L$$

$$\text{or} \quad L \leq \frac{1}{2} \text{ and } 2L == S \text{ and } C_{AP} < L$$

$$\text{or} \quad L \leq \frac{1}{2} \text{ and } 2L < S \leq 1 \text{ and } C_{AP} < L$$

$$\text{or} \quad \frac{1}{2} < L < 1 \text{ and } L < S \leq 1 \text{ and } 0 \leq C_{AP} < 2L - S$$

$$\text{or} \quad \frac{1}{2} < L < 1 \text{ and } L < S \leq 1 \text{ and } 2L - S < C_{AP} < L$$

The constraints on the variables means that this fixed point cannot be an unstable node, and similarly for a stable or unstable spiral.

For the steady state $(\theta^*, \phi^*) = (\frac{L}{S}, \frac{L}{S})$ we obtain the Jacobian

$$J^* = \begin{pmatrix} L - C_{AP} & C_{AP} - L \\ 0 & L - S \end{pmatrix} \tag{2.65}$$

The eigenvalues are $(\lambda_1, \lambda_2) = (L - S, L - C_{AP})$, the determinant $\text{Det}(J^*) = (L - S)(L - C_{AP})$, and the trace $\text{Tr}(J^*) = 2L - S - C_{AP}$. For the steady state to be a saddlepoint we require

$$\lambda_1 \lambda_2 \quad < \quad 0 \tag{2.66}$$

$$\Leftarrow \quad L < 1 \text{ and } L < S \leq 1 \text{ and } 0 \leq C_{AP} < L \tag{2.67}$$

Biologically, the receptor accessories should be fewer than the ligand and the ligand fewer than free receptors.

For the steady state to be a stable node, we require the following conditions:

$$\lambda_1 \lambda_2 > 0 \quad \text{and} \quad \text{Tr}(J^*)^2 - 4\text{Det}(J^*) > 0 \text{ and } \text{Tr}(J^*) < 0$$

$$\Leftarrow \quad 0 \leq L < 1 \text{ and } L < S \leq 1 \text{ and } L < C_{AP} < S$$

Biologically, we would have fewer ligand than available accessories, which in turn are fewer than unbound receptors.

For an unstable node, we require the following conditions to be met:

$$\lambda_1 \lambda_2 > 0 \quad \text{and} \quad \text{Tr}(J^*)^2 - 4\text{Det}(J^*) < 0 \text{ and } \text{Tr}(J^*) > 0$$

$$\Leftarrow \quad 0 < L \leq 1 \text{ and } 0 < S < L \text{ and } 0 \leq C_{AP} < S$$

In this case, there would be fewer accessories than receptors, and fewer receptors than ligand; so in this case, an unstable node is possible. The constraints on the receptors mean that neither a stable or unstable spiral can occur.

Linear stability analysis can give insights into the behaviour of a system, and is often sufficient to provide a general picture of system dynamics; however, a more robust analysis follows.
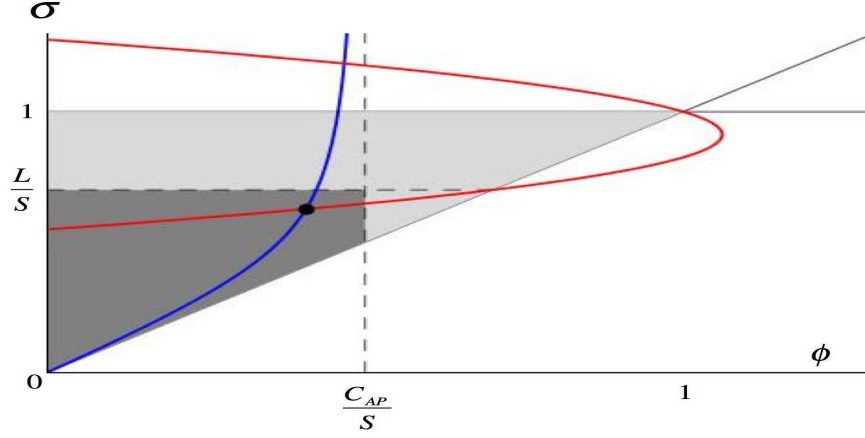
Figure 2.1: The biological domain given in equation (2.70) in the (θ, ϕ) plane is the light grey shaded region. The invariant domain $0 \leq \phi \leq \min\left\{\frac{C_{AP}}{S}, \frac{L}{S}, 1\right\}$, $0 \leq \sigma \leq \min\left\{\frac{L}{S}, 1\right\}$ is the dark grey shaded region. The blue curve is the isocline $\dot{\phi} = 0$, and the red curve the isocline $\dot{\sigma} = 0$. We have a unique equilibrium in the biological domain, inside the invariant domain, given by the point. This figure illustrates the case $\frac{C_{AP}}{S} < \frac{L}{S} < 1$.

2.3 Biological equilibria of the 2-dimensional system

We have established that the system can be written as

$$\dot{\phi} = (\sigma - \phi)(C_{AP} - S\phi) - \rho_y \phi \qquad (2.68)$$

$$\dot{\sigma} = r(1 - \sigma)(L - S\sigma) - \rho_w(\sigma - \phi) \qquad (2.69)$$

We have the following biological constraints:

$$0 \leq \phi \leq \sigma \leq 1 \qquad (2.70)$$

This is a simplex in the (ϕ, σ) plane, which we show in figure (2.1). We consider whether this domain is invariant under the dynamics given by equations (2.68), (2.69). We consider the boundary of the simplex.

The edge $\phi = 0$: From (2.69) we have $\dot{\phi} = \sigma C_{AP}$. Thus, $\dot{\phi} \geq 0$ along the edge $\phi = 0$, with equality only when $\sigma = 0$. Note that, when $\sigma = \phi = 0$, we have $\dot{\sigma} = rL > 0$. It follows that the vector field defined by equations (2.68), (2.69) is inward pointing along this edge.

The edge $\sigma = 1$: From (2.68), we have $\dot{\sigma} = -\rho_w(1 - \phi)$. In this case, $\dot{\sigma} \leq 0$ along the edge $\sigma = 1$, with equality only when $\phi = 1$. Note that, when $\sigma = \phi = 1$, we have $\dot{\phi} = -\rho_y < 0$. It follows that the vector field is inward pointing along this edge.

The edge $\sigma = \phi$: Here we have $\dot{\sigma} - \dot{\phi} = r(1 - \sigma)(L - S\sigma) + \rho_y \sigma$. This is always positive if $0 \leq \sigma \leq \min\left\{\frac{L}{S}, 1\right\}$. If $\frac{L}{S} \geq 1$, this covers the full biological range $0 \leq \sigma \leq 1$.

We have therefore shown that, if $\frac{L}{S} \geq 1$, the whole biological domain (2.70) is forward invariant under the vector field given by equations (2.68), (2.69). The vector field is, in fact, inward pointing along the boundary of this domain. From standard theorems, it follows that there is at least one equilibrium in the interior of the biological domain.

If $\frac{L}{S} < 1$, then we consider the subdomain of the biological domain given by

$$0 \leq \phi \leq \sigma \leq \frac{L}{S}, 0 \leq \phi \leq \min\left\{\frac{C_{AP}}{S}, \frac{L}{S}\right\} \tag{2.71}$$

This is illustrated in figure (2.1), given as the dark grey region, for $\frac{C_{AP}}{S} < \frac{L}{S} < 1$. We show that this region is forward invariant under the vector flow.

$\boxed{\text{The edge } \sigma = \frac{L}{S}:}$ We have $\dot{\sigma} = -\rho_w\left(\frac{L}{S} - \phi\right)$ along this edge, so $\dot{\sigma} \leq 0$ along this edge, with equality only when $\phi = \frac{L}{S}$.

$\boxed{\text{The edge } \phi = \frac{C_{AP}}{S}:}$ Along this edge we have $\dot{\phi} = -\frac{\rho_y C_{AP}}{S}$. Thus, $\dot{\phi} < 0$ along this edge.

We already know that $\dot{\phi} > 0$ along the edge $\phi = 0$, except at $\sigma = 0$, where $\dot{\phi} = 0$; we also have $\dot{\sigma} - \dot{\phi} > 0$ along the section of the edge $\sigma = \phi$ with $0 \leq \sigma \leq \frac{L}{S}$.

It now follows that the domain (2.70) is forward invariant under the flow of the vector field, and that the field is inward pointing on the boundary of this domain. From standard theorems, it now follows that there is at least one equilibrium in the interior of the biological domain. This does not, however, rule out the possibility of other equilibria within the biological domain (2.70) but outside the invariant domain (2.71), but we can see that this is not the case.

We suppose first that $\phi > \frac{C_{AP}}{S}$. It follows from (2.68) that $\dot{\phi} < 0$. Next we suppose that $\sigma > \frac{L}{S}$. It then follows from (2.69) that $\dot{\sigma} < 0$. Hence there can be no solution of $\dot{\sigma} = \dot{\phi} = 0$ in the biological domain (2.70) but outside the invariant domain defined by (2.69), (2.70). Therefore, all biologically acceptable equilibria lie in the invariant domain.

2.3.1   Uniqueness of the equilibrium

We will now show that in fact there is only one equilibrium in the interior of the invariant domain (2.71). We have shown that the vector field (2.68), (2.69) is inward pointing on the boundary of the domain (2.71), and hence any equilibria must lie in the interior of this domain. It follows from the Brower Fixed Point Theorem for flows ((97), Theorem 7, p. 197) that there is least one equilibrium in the domain (2.71). To show that there is exactly one equilibrium in the domain, we use the Poincaré-Hopf index theorem (this theorem is explored in appendix 2.C). According to this theorem, it suffices to show that the Jacobian matrix has constant sign on the invariant domain. From (2.68), (2.69) we have

$$\begin{vmatrix} \frac{\partial \dot{\phi}}{\partial \phi} & \frac{\partial \dot{\phi}}{\partial \sigma} \\ \frac{\partial \dot{\sigma}}{\partial \phi} & \frac{\partial \dot{\sigma}}{\partial \sigma} \end{vmatrix} \tag{2.72}$$

$$= \begin{vmatrix} -(C_{AP} - S\phi) + S(\sigma - \phi) - \rho_y & (C_{AP} - S\phi) \\ \rho_w & -(r(L - S\sigma) + rS(1 - \sigma) + \rho_w) \end{vmatrix}$$

and hence we have

$$
\begin{aligned}
J(\phi, \sigma) &= r(L + S - 2S\sigma)((C_{AP} + S(\sigma - 2\phi) + \rho_y) \\
&+ \rho_w(S(\sigma - \phi) + \rho_y) \geq \rho_w \rho_y
\end{aligned}
\tag{2.73}
$$

for (ϕ, σ) in the domain. Thus, $J(\phi, \sigma) < 0$ for all (ϕ, σ) in the domain. It follows from this that all equilibria in the domain are regular and isolated, and that there can be only one of them. This proves the uniqueness of the biological equilibrium.

2.3.2 Stability of the equilibrium

It follows from (2.68), (2.69) that the divergence of the vector field is

$$
\begin{aligned}
D(\phi, \sigma) &= \frac{\partial \dot{\phi}}{\partial \phi} + \frac{\partial \dot{\sigma}}{\partial \sigma} \tag{2.74} \\
&= -C_{AP} - rS(1 - \sigma) - r(L - S\sigma) \tag{2.75} \\
&\quad -S(\sigma - \phi) + S\phi - \rho_w - \rho_y \\
&\leq -(\rho_y + \rho_w)
\end{aligned}
$$

for (σ, ϕ) in the domain. Thus, $D(\phi, \sigma) < 0$ for all (σ, ϕ) in the domain (2.71). It now follows from the Poincaré-Bendixon theorem (see appendix 2.C) that there are no limit cycles of the vector field in the domain, and so we can say that the unique equilibrium is *globally asympototically stable* on this domain.

Finally, we note that the two isoclines within the biological domain are as follows:

$$
\dot{\sigma} = 0 \text{ isocline:} \tag{2.76}
$$
$$
\sigma = \sigma = \frac{1}{2}\left(\left(1 + \frac{L}{S} + \frac{\rho_w}{rS}\right) - \sqrt{\left(1 + \frac{L}{S} + \frac{\rho_w}{rS}\right)^2 - 4\left(\frac{\rho_w}{rS}\phi + \frac{L}{S}\right)}\right)
$$

$$
\dot{\phi} = 0 \text{ isocline:} \tag{2.77}
$$
$$
\sigma = \phi\left(1 + \frac{\rho_y}{(C_{AP} - S\phi)}\right)
$$

2.3.3 Biological consequences

From equations (2.76) and (2.77) the unique equilibrium in the biological domain is the solution of

$$
\begin{aligned}
&\frac{1}{2}\left(\left(1 + \frac{L}{S} + \frac{\rho_w}{rS}\right) - \sqrt{\left(1 + \frac{L}{S} + \frac{\rho_w}{rS}\right)^2 - 4\left(\frac{\rho_w}{rS}\phi + \frac{L}{S}\right)}\right) \tag{2.78} \\
&= \phi\left(1 + \frac{\rho_y}{(C_{AP} - S\phi)}\right)
\end{aligned}
$$
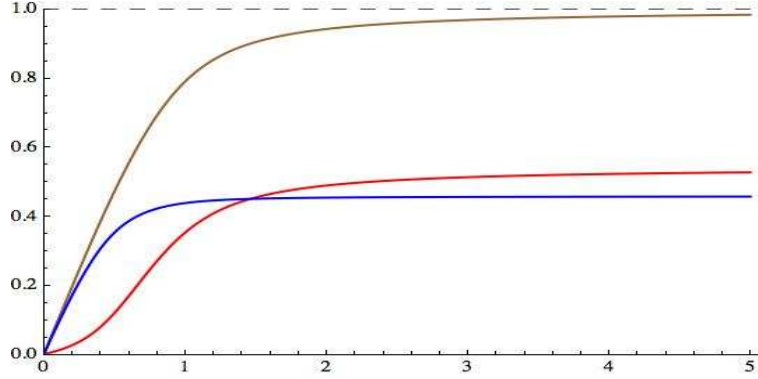
Figure 2.2: Graphs of equilibrium values of σ (shown in brown), ϕ (shown in blue), and $\theta = \sigma - \phi$ (shown in red) as functions of free ligand density $\frac{L}{S}$. The parameter values are: $\frac{C_{AP}}{S} = 0.5$, $\frac{\rho_w}{rS} = 0.125$, $\frac{\rho_y}{S} = 0.05$.

This equation defines the equilibrium solution ϕ^* as a function of $\frac{L}{S}$ (with C_{AP} fixed). Given values for the parameters $\frac{C_{AP}}{S}$, $\frac{\rho_w}{rS}$ and $\frac{\rho_y}{S}$, this equation can be solved numerically to obtain ϕ^* as a function of $\frac{L}{S}$. From the biological constraints (2.70) and (2.71) we know that $\phi^* < \min\left\{\frac{C_{AP}}{S}, 1\right\}$. We therefore have two distinct cases.

Case 1: $\frac{C_{AP}}{S} < 1$: This case is illustrated in (2.1). In this case the availability of the receptor accessory protein (C_{AP}) is less than the total availability of receptors ($S = C_{R1} + C_{R2}$). So the accessory protein is the limiting resource. This is illustrated in figure (2.1).

From section (2.2), we know that the density of binary complexes is $w + x = S\theta$, with the density of ternary complexes given by $y + z = S\phi$. It follows from the figure that for low values of $\frac{L}{S}$, the equilibrium value of θ is less than that of ϕ. The density of ternary complexes is therefore limited by the availability of ligand, rather than receptors or receptor accessory protein.

For larger values of $\frac{L}{S}$, the equilibrium value of θ is greater than that of ϕ. We therefore have more binary complexes than ternary complexes. Ternary complexes are limited by the unavailability of receptor accessory. For very large values of $\frac{L}{S}$, the equilibrium values of θ and ϕ become saturated. This occurs when there is enough unbound ligand to exploit all the binding opportunities available.

Even for low levels of ligand stimulus ($\frac{L}{S}$ small), the formation of ternary complexes in equilibrium increases rapidly with stimulus (the blue curve in figure (2.2)). Whether this results in the induction of cell signalling depends on the proportion of type-I and type-II receptors.

Case 2: $\frac{C_{AP}}{S} > 1$: In this case, the availability of receptors S is the dominant or limiting resource. We plot some equilibrium values in figure (2.3).

The equilibrium density of binary complex density θ, represented by the red curve in the figure, remains below the equilibrium density of ternary complexes (ϕ), represented by the blue curve in the figure, over the whole range of unbound ligand stimulus density $\frac{L}{S}$.
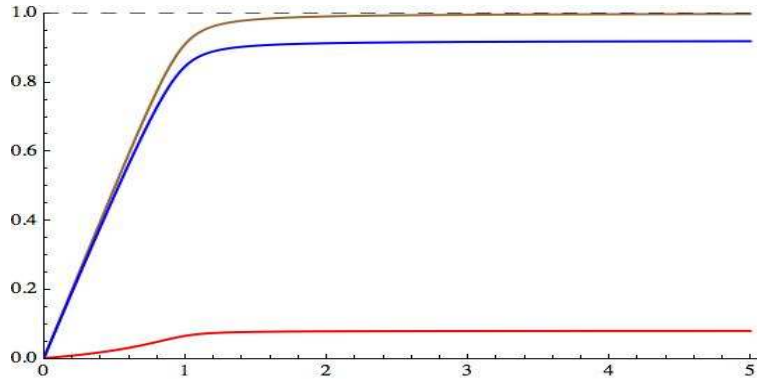
Figure 2.3: Graphs of equilibrium values of σ (shown in brown), ϕ (shown in blue), and $\theta = \sigma - \phi$ (shown in red) as functions of free ligand density $\frac{L}{S}$. The parameter values are: $\frac{C_{AP}}{S} = 1.5$, $\frac{\rho_w}{rS} = 0.125$, $\frac{\rho_y}{S} = 0.05$.

Both curves saturate rapidly as $\frac{L}{S}$ increases. The large saturated value for the ϕ curve relative to the comparatively low saturated value for the θ curve is a consequence of the relative abundance of receptor accessory protein in comparison with that of the receptors.

2.4 Results

The ordinary differential equation model derived above is resistant to a straightforward analysis; however, the approximations and perturbation analysis we developed have shown us that steady states exist which depend on the relative size ligand and the total number of receptors in the system.

The applicability of a Michaelis-Menten modelling approach to the IL-1β system was considered in section 2.1. After consideration of the assumptions underlying this modelling approach, a steady state model of the IL-1β network was developed, based on conservation laws.

A first approximation was developed in section (2.2) which reduced the four-dimensional system into a two-dimensional system. Although this approximation is not very precise, it emphasised the role played by the ratio of the IL-1 receptor accessory protein to the signalling and nonsignalling receptors, and the ratio of the ligand to the receptors; that is, $\frac{C_{AP}}{S}$ and $\frac{L}{S}$.

A more comprehensive analysis was given in Section 2.3. The biological domain, those values for which the variables representing the complexes hold, was shown to be forward invariant and inward pointing under the vector field given by equations (2.76) and (2.77). By use of the Poincaré-Hopf index theorem, it was found that within the biological domain a unique equilibrium existed.

The central role of the ratios $\frac{C_{AP}}{S}$ and $\frac{L}{S}$ was further accentuated. It was found that, if $\frac{C_{AP}}{S} < 1$, the availability of the receptor accessory protein is less than the availability of both Type-I and Type-II receptors. In this case the receptor accessory is the limiting resource. For low values of $\frac{L}{S}$, it was found that the density of ternary complexes is limited by availability of ligand.

For larger values of $\frac{L}{S}$, we find that there are more binary complexes than ternary complexes, so that ternary formation is affected by the scarcity of the receptor accessory.

In the case where $\frac{C_{AP}}{S} > 1$, the availability of the unbound receptors is the limiting resource.

2.A   Appendix: Michaelis-Menten model

The modelling of receptor-ligand models has often been based on two methods, known as the Michaelis-Menten and Briggs-Haldane models; it may be beneficial to analyse how each model is derived [2]. Study of the impact made by changes in experimental conditions on the rate of an enzyme-catalysed reaction is known as *enzyme kinetics*. The effect on the initial rate of substrate concentration of an enzyme-catalysed reaction is a concept central to enzyme kinetics: when plotted, experiments of initial rate of reaction versus substrate concentration characterises a hyperbolic curve. The Michaelis-Menten equations is based on a generalised scheme for the enzyme-catalysed synthesis of a product P from substrate S, that is, E binds S to form an enzyme-substrate complex. The biochemical reaction is given by

$$E + S \underset{k_{-1}}{\overset{k_1}{\rightleftharpoons}} ES \overset{k_2}{\longrightarrow} E + P \tag{2.79}$$
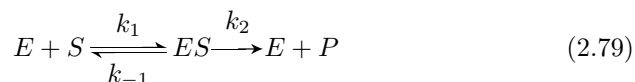
where k_1, k_{-1} and k_2 are rate constants describing, respectively, the association of substrate and enzyme, the dissociation of unaltered substrate from the enzyme, and the dissociation of product (or altered substrate) from the enzyme. A reverse reaction can take place, with the ES complex dissociating to form enzyme and substrate, but this effect can largely be disregarded when considering initial rates of reaction; when the enzyme is initially introduced to the substrate, there should not be any product available to combine with the enzyme.

It is necessary to highlight two assumptions which have been made in designing the model; the first of these is that the amount of available substrate is much larger than the concentration of enzyme, that is, $[S] \gg [E]$; furthermore, it is assumed that the system is in steady-state, in other words that the ES complex is being formed and broken down at a constant rate, implying that $[ES]$ concentration is constant. The rate, or velocity, of the reaction, given by v, is governed by the processing from ES to $E + P$, in turn mediated by the rate k_2 and the concentration of the enzyme bound with the substrate, $[ES]$:

$$v = k_2[ES] \tag{2.80}$$

The formation of $[ES]$, then, is dependent on the rate constant k_1 and the amount of enzyme and substrate available; the breakdown of $[ES]$ occurs either by the conversion of substrate to product or the dissociation of substrate from the complex. The Law of Mass Action, which states that the rate of a chemical reaction is proportional to the concentrations of the reacting substances, is applicable here, so that at steady-state we have:

---

[2]Much of this appendix, and the following appendix, synopsises Chapter 3 of Segel's "Enzyme Kinetics" (86), to which it is indebted

$$k_1[E][S] = k_{-1}[ES] + k_2[ES] \tag{2.81}$$

yielding:

$$\frac{k_1[E][S]}{k_{-1} + k_2} = [ES] \tag{2.82}$$

Since all the rate constants are on the L.H.S., we can introduce a constant :

$$K_M = \frac{k_{-1} + k_2}{k_1} \tag{2.83}$$

where K_M is known as the Michaelis constant. The total amount of enzyme in the system must, obviously, remain the same, whether it is bound or free, and so the total amount of enzyme $[E_0]$ is given by

$$[E_0] = [E] + [ES] \tag{2.84}$$

With some algebraic manipulation we arrive at an expression for v

$$v = k_2 \frac{[E_0][S]}{[S] + K_M} \tag{2.85}$$

The maximum rate would be reached when all the enzyme molecules have bound to substrate, and, where we have $[S] \gg [E]$, we could assume that all E will be in the form ES, so that $[E_0] = [ES]$; thinking again about equation (2.80) we could substitute V_{max} for v and $[E_0]$ for $[ES]$, yielding the Michaelis-Menten equation:

$$v = \frac{V_{max}[S]}{K_M + [S]} \tag{2.86}$$

There are a number of assumptions made by the Michaelis-Menten framework which may influence how applicable it is to the task of modelling the IL-1β network. The assumptions are (86):

- The enzyme is a catalyst.

- The enzyme and substrate react rapidly to form an enzyme-substrate complex.

- Only a single substrate and a single enzyme-substrate complex are involved and the enzyme-substrate complex breaks down to form free enzyme and product.

- The substrate concentration is much larger than the enzyme concentration.

- The overall rate of the reaction is limited by the breakdown of the complex to form free enzyme and product.

- Enzyme, substrate, and enzyme-substrate complex are at equilibrium - the rate at which the complex dissociates to component parts is much faster than the rate at which the product and free enzyme are produced. This is the quasi-equilibrium or rapid equilibrium assumption.

It would be useful to examine these assumptions and consider their applicability to the IL-1β network and the modelling process.

- The enzyme is a catalyst: This should not pose any conceptual problems for IL-1β.

- Complex is formed rapidly: This should also not pose any problems.

- Single substrate/single enzyme-substrate complex: This no longer applies, since the model has been extended to accommodate multiple substrates and enzymes, and so need not concern us.

- Substrate concentration greater than enzyme concentration: This assumption may be of concern if the amount of IL-1β is much greater than the number of IL-RI receptors available, and would be an interesting case for further analysis.

- Rate of reaction limited by complex breakdown: This assumption need not be a problem for a model of the network.

- Rapid equilibrium: This could pose a problem for the model, and will be dealt with below.

The rapid equilibrium framework allows us to express the enzyme-substrate complex concentration, but the derivation yields an equilibrium expression for the binding of the substrate to the enzyme; the velocity equation is obtained when the term [ES] is inserted into the velocity dependence equation, or when we derive an equation expressed in terms of $\frac{v}{V_{max}}$. However, it is not necessarily the case that the concentration of the complex is solely determined by the concentration of E and S, and in many cases this is unlikely to be the case (86). How can this problem be dealt with?

The quasi-equilibrium problem can be ameliorated by using instead a steady-state model, which will be detailed below. It should, however, be noted that surprisingly often use of either the steady-state or the rapid equilibrium theories will result in the same model; that is, the form of the equation yielded will be the same. It is also noteworthy that there is an extensive literature which applies the Michaelis-Menten theory to many different models, not all of which could be considered as near equilibrium, with good match to experimental results; as such the assumption could be considered as having been operationally relaxed.

2.B Appendix: Briggs-Haldane model

Briggs and Haldane (11) developed a general rate equation which did not require the restriction of equilibrium. They proposed instead that the system would rapidly approach a steady state level of production: that is, complex formation would form at the same rate at which it decomposed. This assumption would certainly be more realistic for our purposes. The derivation is as follows.

The enzyme-substrate complex is formed:

$$E + S \xrightarrow{k_1} ES \tag{2.87}$$

Note that the reverse reaction can initially be ignored, since during the early stages of the reaction there will be little product. The complex can decompose via two processes:

$$ES \xrightarrow{k_{-1}} E + S \tag{2.88}$$

$$ES \xrightarrow{k_2} E + P \tag{2.89}$$

so that the rate of formation can be given by (f and g here are dummy functions)

$$\frac{df}{dt} = k_1[E][S] \tag{2.90}$$

and the rate of decomposition

$$\frac{dg}{dt} = k_{-1}[ES] + k_2[ES] = (k_{-1} + k_2)[ES] \tag{2.91}$$

so, at steady state we obtain

$$\frac{df}{dt} = \frac{dg}{dt} = \frac{d[ES]}{dt} \tag{2.92}$$

and

$$k_1[E][S] = (k_{-1} + k_2)[ES] \tag{2.93}$$

Rearranging we obtain

$$[ES] = \frac{k_1[S]}{(k_{-1} + k_2)}[E] \tag{2.94}$$

If we divide by the total amount of enzyme $[E]_{tot}$

$$\frac{v}{[E]_{tot}} = \frac{k_2[ES]}{[E] + [ES]} \tag{2.95}$$

Substituting for $[ES]$:

$$\frac{v}{k_2[E]_{tot}} = \frac{\frac{k_1[S]}{(k_{-1}+k_2)}[E]}{[E] + \frac{k_1[S]}{(k_{-1}+k_2)}[E]} \tag{2.96}$$

Letting V_{max} equal $k_2[E]_{tot}$ yields

$$\frac{v}{V_{max}} = \frac{\frac{k_1[S]}{(k_{-1}+k_2)}}{1 + \frac{k_1[S]}{(k_{-1}+k_2)}} \tag{2.97}$$

If we group the rate constants as the Michaelis constant K_m we obtain

$$\frac{v}{V_{max}} = \frac{\frac{[S]}{K_m}}{1 + \frac{[S]}{K_m}} \tag{2.98}$$

$$= \frac{[S]}{K_m + [S]} \tag{2.99}$$

Notice also that

$$\frac{[E][S]}{[ES]} = \frac{k_{-1} + k_2}{k_1} = K_m \tag{2.100}$$

K_m can thus be considered a *pseudo-constant* which expresses the relationship between the steady-state concentrations. The model can also be described by a system of four differential equations:

$$\begin{align}
\frac{d[E]}{dt} &= (k_{-1} + k_2)[ES] - k_1[E][S] \tag{2.101} \\
\frac{d[ES]}{dt} &= k_1[E][S] - (k_{-1} + k_2)[ES] \tag{2.102} \\
\frac{d[S]}{dt} &= k_{-1}[ES] - k_1[E][S] \tag{2.103} \\
\frac{d[P]}{dt} &= k_2[ES] \tag{2.104}
\end{align}$$

This system of differential equations, together with the mass balance equation $[E]_{tot} = [E] + [ES]$, gives us a steady-state description of the system. Such a system of equations depends on the assumption of steady-state dynamics, and could not be derived given the assumption of equilibrium.

The system can be solved if the steady-state assumption holds and the value of certain parameters ($[E]_{tot}, k_1$, etc.) are known.

2.C   Appendix: Theorems

We give details of the theorems used in the previous chapter.

2.C.1   The Poincaré-Hopf index theorem

The 2-dimensional system defines a vector field $f : \mathcal{R}^2 \to \mathcal{R}^2$. That is, $f(\phi, \sigma) = (f_1(\phi, \sigma), f_1(\phi, \sigma))$ where

$$\begin{align}
\dot{\phi} &= (\sigma - \phi)(C_{AP} - S\phi) - \rho_y\phi \tag{2.105} \\
\dot{\sigma} &= r(1 - \sigma)(L - S\sigma) - \rho_w(\sigma - \phi) \tag{2.106}
\end{align}$$

We wish to restrict the vector field f to the biological domain (2.70), which is a simplex $\triangle \subset \mathcal{R}^2$. Specifically, we consider restricting f to the subdomain $\Omega \subset \triangle$ defined by (2.70), which is shown in (2.1).

 Preliminaries: To state the Poincaré-Hopf Theorem, we need the notion of the Euler characteristic of a polyhedral domain D, which we denote by $\chi(D)$. In two dimensions, this is defined as:

$$\begin{align}
\chi(D) = &\ \text{Number of } 0D \text{ vertices} - \text{Number of } 1D \text{ edges} \tag{2.107} \\
&+ \ \text{Number of } 2D \text{ faces}
\end{align}$$
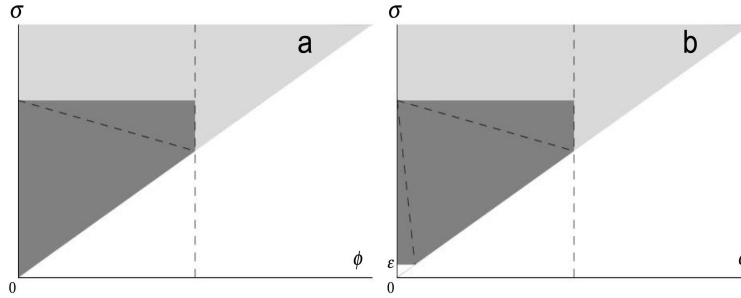
Figure 2.4: a) The biological region (2.70), shaded light grey, is the region $\triangle$. The biological region (2.71) is the subregion Ω, shaded dark grey. The dashed line is the edge we have added to calculate the Euler characteristic. b) The subregion Ω_ϵ obtained from Ω by cutting off a small corner containing the origin, given by the white triangle. f is inward pointing on the boundary of this region.

A vertex is a point, an edge is a straight line joining two vertices, and a face is the area enclosed by a triangle formed by three vertices and three connecting edges. For the simplex $\triangle$ (see figure (2.1)), we have

$$\chi(\triangle) = 3 - 3 + 1 = 1 \tag{2.108}$$

We wish to calculate the Euler characteristic for the subdomain Ω. To do this, we first need to split the region into the union of two simplices by adding an edge. We show this in figure (2.4 a). We then have

$$\text{Number of} \quad 0D \text{ vertices } = 4 \tag{2.109}$$
$$\text{Number of} \quad 1D \text{ edges } = 5 \tag{2.110}$$
$$\text{Number of} \quad 2D \text{ faces } = 2 \tag{2.111}$$
$$\Rightarrow \quad \chi(\Omega) = 4 - 5 + 2 = 1 \tag{2.112}$$

We are also interested in a subdomain $\Omega_\epsilon \subset \Omega$, which we obtain by cutting off a sufficiently small area containing the origin $(0,0)$, by the horizontal line $\sigma = \epsilon$ with $\epsilon > 0$ sufficiently small. We also add an additional edge, as shown in figure (2.4 b). This yields

$$\text{Number of} \quad 0D \text{ vertices } = 5 \tag{2.113}$$
$$\text{Number of} \quad 1D \text{ edges } = 7 \tag{2.114}$$
$$\text{Number of} \quad 2D \text{ faces } = 3 \tag{2.115}$$
$$\Rightarrow \quad \chi(\Omega) = 5 - 7 + 3 = 1 \tag{2.116}$$

This shows that the domains in which we are interested have Euler characteristic 1. According to Spanier, the Euler characteristic is a *topological invariant* ((97), chapter 4): if two polyhedra K and $K\prime$ are topologically homeomorphic, then we have $\chi(K\prime) = \chi(K)$. Clearly, $\triangle$, Ω and Ω_ϵ are all homeomorphic to each other, and so have the same Euler characteristic.

We have shown in the main text that the vector field f restricted to Ω is inward pointing on the boundary of Ω, except at the point $(0,0)$, where we have

$$
\begin{aligned}
\dot{\phi} &= f_1(0,0) = 0 & (2.117)\\
\dot{\sigma} &= f_2(0,0) = rL > 0 & (2.118)
\end{aligned}
$$

The vector field is non-zero at this point, but points along the boundary edge $\phi = 0$. If, however, we consider the domain Ω_ϵ, then along the additional edge $\sigma = \epsilon$, $\phi = \epsilon\xi$ with $0 \le \xi \le 1$, we have

$$
\begin{aligned}
\dot{\phi} &= f_1(\epsilon\xi, \epsilon) = \epsilon\left((1-\xi)\,C_{AP} - \rho_y\xi\right) + \mathcal{O}(\epsilon^2) & (2.119)\\
\dot{\sigma} &= f_2(\epsilon\xi, \epsilon) = r(1-\epsilon)(L - S\epsilon) - \epsilon\rho_w(1-\xi) & (2.120)\\
&= rL + \mathcal{O}(\epsilon^2)
\end{aligned}
$$

Clearly, $\hat{\sigma} > 0$ along this edge for sufficiently small ϵ. Also

$$
\dot{\phi} = f_1(0, \epsilon) = \epsilon C_{AP} + \mathcal{O}(\epsilon^2) > 0 \tag{2.121}
$$

at $\xi = 0$, and

$$
\dot{\phi} = f_1(\epsilon, \epsilon) = -\epsilon\rho_y + \mathcal{O}(\epsilon^2) < 0 \tag{2.122}
$$

at $\xi = 1$. Therefore, the vector field f is inward pointing into the domain Ω_ϵ at all points on the boundary of Ω_ϵ.

We further note that, with $\epsilon > 0$ chosen sufficiently small, then we have $\dot{\sigma} > 0$ at all points in the excluded region $0 \le \sigma < \epsilon$, $0 \le \phi < \epsilon$, given by the small white triangle in (2.4 b).We have already shown that there are no further equilibria of the vector field f in $\triangle - \Omega$; it follows that any biologically allowable equilibria must be in the interior of Ω_ϵ.

$\boxed{\text{Regular equilibria and the index:}}$ Let $x^8 = (\phi^*, \sigma^*)$ be an equilibrium of the system in Ω_ϵ. Such an equilibrium is said to be *regular* if the Jacobian $J(\phi^*, \sigma^*)$ is non-zero. It follows from equation (2.73) that all equilibria in Ω_ϵ are regular.

We now define the *index* of the equilibrium x^* of the vector field f restricted to Ω_ϵ by

$$
\operatorname{ind}_f(x^*) = \operatorname{sign} J(x^*) \tag{2.123}
$$

We can now state the Poincaré-Hopf Index Theorem [3]:

Theorem 2.C.1. Poincaré-Hopf Index Theorem *Let $\Gamma \subset \mathbf{R}^n$ be a compact domain with non-empty interior and piecewise boundary $\partial\Gamma$. Let $g : \mathbf{R}^n \mapsto \mathbf{R}^n$ be a differentiable vector field that is non-zero and outward-pointing on $\partial\Gamma$. Suppose that g has only finitely many, regular equilibria in Γ. Then*

$$
\sum_{\text{equilibria } x^*} \operatorname{ind}_g(x^*) = \chi(\Gamma) \tag{2.124}
$$

---

[3]A more general statement of :Poincaré-Hopf Index Theorem can be found in Milnor (65)

We can apply this to the vector field $g = -f$ in the figure (2.4 b) on $\mathbf{R}^2$ with $\Gamma = \Omega_\epsilon$. We have shown that f is inward pointing on $\partial\Omega_\epsilon$, and so g is outward pointing. Clearly, f and g have the same, regular, equilibria in ω_ϵ. It therefore follows from Theorem (2.C.1) and the already-established $\chi(\Omega_\epsilon) = 1$ that

$$\sum_{\text{equilibria } x^*} \text{ind}_{-f}(x^*) = 1 \tag{2.125}$$

It follows from the definition that

$$J_{-f} = \text{Det} \begin{pmatrix} -\frac{\partial f_1}{\partial \phi} & -\frac{\partial f_1}{\partial \sigma} \\ -\frac{\partial f_2}{\partial \phi} & -\frac{\partial f_2}{\partial \sigma} \end{pmatrix}(x^*) \tag{2.126}$$

$$= \frac{\partial f_1}{\partial \phi}\frac{\partial f_2}{\partial \sigma} - \frac{\partial f_1}{\partial \sigma}\frac{\partial f_2}{\partial \phi} \tag{2.127}$$

$$= \text{Det} \begin{pmatrix} \frac{\partial f_1}{\partial \phi} & \frac{\partial f_1}{\partial \sigma} \\ \frac{\partial f_2}{\partial \phi} & \frac{\partial f_2}{\partial \sigma} \end{pmatrix}(x^*) = J_f(x^*) \tag{2.128}$$

and hence from equation (2.122) that $\text{ind}_{-f}(x^*) = \text{ind}_f(x^*)$, so we have from equation (2.125)

$$\sum_{\text{equilibria } x^*} \text{ind}_f(x^*) = 1 \tag{2.129}$$

We now note from (2.124) that $J(x^*) > 0$ for *any* equilibrium x^*; in fact, this holds for any point in Γ_ϵ. Then it follows that $\text{ind}_f(x^*) = 1$ for all equilibria $x^* \in \Gamma_\epsilon$. We let m be the number of such equilibria; then it follows from (2.129) that $m = 1$. We have exactly one equilibrium of the vector field f in Γ_ϵ. We have therefore proven the uniqueness-of-equilibrium asserted in the main text.

$\boxed{\text{The Poincaré-Bendixson Theorem:}}$ The necessary version of the theorem is the following[4]:

Theorem 2.C.2. Poincaré-Bendixon Theorem *Let $\Gamma \subset \mathbf{R}^2$ be a compact subset that is forward invariant under the flow of a differentiable vector field $f : \mathbf{R}^2 \mapsto \mathbf{R}^2$. Then Γ contains a rest point or a periodic orbit.*

We take $\Gamma = \Omega_\epsilon$. We have shown that the vector field f, as plotted in (2.4 a), is inward pointing on the boundary of Γ_ϵ. Therefore, Γ_ϵ is forward invariant under the flow of f. We have also shown in equation (2.74) that

$$\text{div } f(\phi, \sigma) = D(\phi, \sigma) < 0 \tag{2.130}$$

for $(\phi, \sigma) \in \Gamma_\epsilon$. This implies that areas in Ω_ϵ are contracting, and so cannot contain a periodic orbit, and the interior of Γ_ϵ is an open set which contracts in time to the only possible limit set, which is the unique equilibrium in the interior of Γ_ϵ. Thus we have proven what we asserted in the main text, that the unique equilibrium is globally asymptotically stable on Γ_ϵ.

---

[4]Hofbauer and Sigmund (42), chapter 4, have a more general analysis.

Chapter 3

The unconstrained receptor model

IL-1β binds to two receptors on the cell membrane, the type-I and type-II receptor: the type-I receptor can cause a signal transduction event; the type-II receptor is commonly considered to be a *decoy receptor*, lacking the transmembrane apparatus to initiate a signalling event (15). We will model the interaction of IL-1β at the level of the cell membrane with type-I signalling and type-II nonsignalling receptors, in order to discover the effect of the type-II receptor on the dynamics of the system.

The IL-1β network contains many putative inhibitory elements, one of which is the receptor antagonist IL-1Ra. This ligand binds with both the type-I and type-II receptors, sequestering the receptor accessory IL-1RAcP, forming binary and ternary complexes in much the same way as IL-1β; however, it does not initiate signalling transduction. Since it consumes both receptors and receptor accessory proteins, it may be considered an inhibitory influence on the network. We will construct a model which investigates its efficacy as an IL-1β inhibitor.

The IL-1β network is composed of elements which occur at very low physiological quantities. The type-I receptor is not abundant, but evokes a powerful response without a high level of receptor occupancy (6), as the receptor activates many pathways which operate in parallel. Unlike most other cytokines, it is thought that as few as ten occupied receptors are sufficient to evoke a strong response (93). Since IL-1β typically acts at very low concentrations, the population sizes of signalling and nonsignalling complexes will be small, and random fluctuations will have a disproportionate effect. The use of stochastic methods is indicated to model such a system.

3.1   The IL-1β network

This section explores the effect of the type-II receptor on the IL-1β network. The interactions we model are as follows:

- IL-1β + type-I receptor: IL-1β associates with the signalling receptor to form a signalling binary complex

- signalling binary complex + receptor accessory protein: promotion of the receptor accessory forms a signalling ternary complex, and signalling occurs

- IL-1β + type-II receptor: IL-1β associates with the nonsignalling receptor to form a nonsignalling binary complex

- nonsignalling binary complex + receptor accessory protein: promotion of the receptor accessory forms a nonsignalling ternary complex

As in any reaction, the binding event is reversible; the complexes can both associate and dissociate. The association and dissociation rates for the binary and ternary signalling and nonsignalling complexes are given in Table (3.1). [1]

We use the following notation: L is free (unbound) IL-1β, $R1$ is the type-I signalling receptor, $R2$ is the type-II nonsignalling receptor, S is the signalling binary complex, NS is the nonsignalling binary complex, R is the receptor accessory protein, T is the signalling ternary complex, NT is the nonsignalling ternary complex. Association rates are given as k_u^+ for a component u, and dissociation rates are k_u^-. In the notation of chemical reactions, the interactions are:

$$L + R1 \quad \underset{k_S^-}{\overset{k_S^+}{\rightleftharpoons}} \quad S \tag{3.1}$$

$$L + R2 \quad \underset{k_{NS}^-}{\overset{k_{NS}^+}{\rightleftharpoons}} \quad NS \tag{3.2}$$

$$S + R \quad \underset{k_T^-}{\overset{k_T^+}{\rightleftharpoons}} \quad T \tag{3.3}$$

$$NS + R \quad \underset{k_{NT}^-}{\overset{k_{NT}^+}{\rightleftharpoons}} \quad NT \tag{3.4}$$
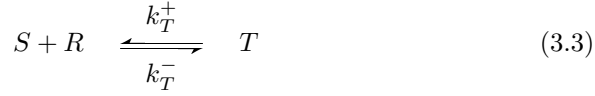
Units for dissociation rates k_u^- are s^{-1}, and these rates can be construed as probabilities per unit time (= 1s). However, the units for association rates, k_u^+, are M^{-1}s^{-1}, and these cannot be interpreted as probabilities without a transformation, $\hat{k}_u^+ = ck_u^+$, where c is a suitable conversion factor having dimension M (concentration).

We choose c to be a concentration based on one international unit of specific activity of IL-1β. A standard international unit (IU) of IL-1β activity is defined as a preparation (NISBC code: 86/632) which contains 0.75mg per ampoule with assigned potency of 75000 units per ampoule (76). We can use this as a basis for a conversion factor between association/dissociation constants and probabilities. According to the standard, a 0.75mg ampoule has a defined potency of 0.75×10^5 international units (IUs). So one unit of IL-1β can be expressed as

---

[1]The first source for the association and dissociation rates are from the Journal of Immunology, authored by Arend et al (4). One of Arend's team who worked on the paper, Professor Steven Dower, kindly sent the author unpublished data with more accurate figures which he had obtained using Biacore surface plasmon resonance technology (24), (25).

Table 3.1: Association/dissociation rates: the association and dissociation rates of the signalling and nonsignalling complexes of the IL-1β network, where S is the signalling binary and NS the nonsignalling binary.(51)

Agent	Binds	Assoc. $(M^{-1}s^{-1})$	Dissoc. (s^{-1})
IL-1RI[1]	IL-1β	4.67×10^7	1.6×10^{-11}
S [1]	IL-1RAcP	4.03×10^7	0.32×10^{-11}
IL-1RII [2]	IL-1β	8.85×10^6	6.92×10^{-10}
NS [2]	IL-1RAcP	9.5×10^6	6.82×10^{-10}

[1] Source: (4), (24)   [2] Source: (4), (25)

$$1 \text{ U} = 10 \text{ pg} = 10^{-8} \text{ mg}$$

IL-1β therefore has an activity of $\frac{10^8 \text{ U}}{\text{mg}}$. Also, recall that $M = \frac{\text{mol}}{\text{litre}}$ and that $1 \text{ mol} = 1.7 \times 10^4 \text{g}$, so that a single unit of IL-1β can be expressed as follows:

$$1 \text{ U} = 10^{-8} \text{ mg} = 10^{-11} \text{ g}$$

Thus

$$1 \text{ U} = \frac{10^{-11}}{1.7 \times 10^4} \text{ mol} = 5.9 \times 10^{-16} \text{ mol}$$

This can be expressed as a standardised concentration in terms of M:

$$\frac{\text{Unit}}{\text{ml}} = 5.9 \times 10^{-13} \text{ M}$$

We use this as our conversion factor c to express association rates as probabilities.

We also need to express dissociation rates as probabilities; clearly, the dissociation rates will need to be multiplied by a number which will result in a probability which is proportional to the association probabilities. We can do this by simply using c and dropping the associated units, so that we have

$$c^* = 5.9 \times 10^{-13}$$

This will result in dissociation probabilities which are of a proportional order of magnitude to the association probabilities, and can be used as a probability in a simulation.

The derived probabilities are given in Table (3.2).

3.1.1 Markov chain model

The theory of discrete-time Markov chains provides powerful techniques for modelling random processes which are generally straightforward to implement computationally (38).

A Markov chain can be described by a diagram showing the transitions between the various states of a system. Figure (3.1) shows the transition graph

Table 3.2: Probabilities $\mathbb{P}(X)$ such that $\hat{k}_u^{\pm} \in [0, 1]$ derived from association and dissociation rates $k_u^{\pm}$.

Association probabilities		
Complex	Symbol	$\mathbb{P}(X)$
Signalling binary	$\hat{k}_S^+$	2.75×10^{-5}
Nonsignalling binary	$\hat{k}_{NS}^+$	5.22×10^{-6}
Signalling ternary	$\hat{k}_T^+$	2.37×10^{-5}
Nonsignalling ternary	$\hat{k}_{NT}^+$	5.6×10^{-6}
Dissociation probabilities		
Complex	Symbol	$\mathbb{P}(X)$
Signalling binary	$\hat{k}_S^-$	1.6×10^{-11}
Nonsignalling binary	$\hat{k}_{NS}^-$	6.92×10^{-10}
Signalling ternary	$\hat{k}_T^-$	0.32×10^{-11}
Nonsignalling ternary	$\hat{k}_{NT}^-$	6.82×10^{-10}
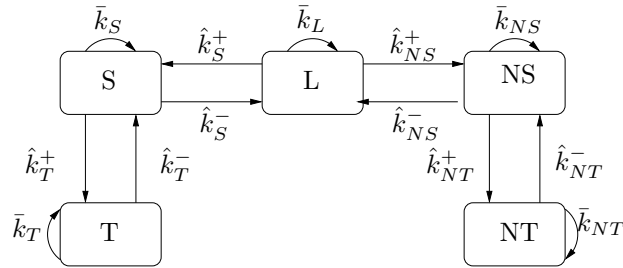
Figure 3.1: State transition diagram for IL-1β network, where L is IL-1β, S is the signalling binary complex, NS is the nonsignalling binary complex, T is the signalling ternary complex, and NT the nonsignalling ternary complex. Probabilities are derived from the association and dissociation rates $\hat{k}_u^{\pm}$.

for the subset of the IL-1β network directly associated with receptor binding, both signalling and nonsignalling.

The vertices of the diagram represent possible states which a unit of IL-1β can occupy. The arrows represent directed state transitions, with their associated (non-zero) probabilities. A self-loop at a vertex represents the probability that the current state does not change in a given time step.

Notice that the diagram has excluded both the receptors and the receptor accessory protein; we will assume that sufficient resources of these components exist to form signalling and nonsignalling complexes, since the components we wish to model are the unbound IL-1β and the complexes themselves. Estimates of the number of type-I and type-II receptors R on human and murine cells yield a range of $200 \leq R \leq 2000$ (61), (8), (9), (43), (85); in comparison with the potency of IL-1β, and the low level of occupied receptors required to effect a cellular response, this simplification seems justified. It is, of course, possible to include receptor dynamics explicitly in a stochastic model, and such a model would be needed to investigate the case given a large concentration of IL-1β (supersaturation) and a low number of receptors expressed on the cell surface.

The matrix of transition probabilities defining the Markov process illustrated in Figure (3.1) is given in equation (3.5); note that the diagonal entries in the matrix are one minus the sum of the others in the row.

$$
\mathbf{P} =
\begin{bmatrix}
 & \text{IL}-1\beta & \text{S} & \text{NS} & \text{T} & \text{NT} \\
\text{IL}-1\beta & \bar{k}_L & \hat{k}_S^+ & \hat{k}_{NS}^+ & 0 & 0 \\
\text{S} & \hat{k}_S^- & \bar{k}_S & 0 & \hat{k}_T^+ & 0 \\
\text{NS} & \hat{k}_{NS}^- & 0 & \bar{k}_{NS} & 0 & \hat{k}_{NT}^+ \\
\text{T} & 0 & \hat{k}_T^- & 0 & \bar{k}_T & 0 \\
\text{NT} & 0 & 0 & \hat{k}_{NT}^- & 0 & \bar{k}_{NT}
\end{bmatrix}
\tag{3.5}
$$

Computational experiments were performed to investigate the time spent in each state, and to find any stationary distributions to which the Markov process is attracted in the long run.

Table (3.3) shows the results of repeating the experiment and averaging it over the number of iterations n and the number of trials N. Each trial iterates over the stochastic matrix for n iterations, where $100 \leq n \leq 5 \times 10^8$; each experiment was repeated $N = 500$ times. The initial state is selected randomly, from among the states L, S, NS, T, NT, and then evolves according to the probabilities based on association and dissociation rates. After the experiments have run, we calculate the average of how long the system spent in any particular state.

As can be seen from the table, with a low number of iterations the Markov chain is evenly distributed between its states. However, as the number of iterations increases, the stochastic matrix is rapidly attracted to the signalling ternary state, and spends an increasing number of iterations in this state. It would seem that the signalling ternary state is, in dynamical systems terms, a robust attractor for the stochastic matrix.

Table 3.3: The results of iterating over the stochastic matrix P. The labels are: L, unbound ligand; S, signalling binary; NS, nonsignalling binary; T, signalling ternary; NT, nonsignalling ternary. The experiments consisted of n iterations as given in the rightmost column, and each experiment ran $N = 500$ trials. The number of times the systems is in a state S is recorded for each experiment and then averaged by the number of iterations n and repetitions of the experiment N. As can be seen, the time the system spent in the signalling ternary state increases with the number of iterations.

L	S	NS	T	NT	Iterations
0.18756	0.18788	0.20154	0.23902	0.18400	100
0.13538	0.20607	0.20800	0.26855	0.18200	200
0.11487	0.17557	0.18178	0.32176	0.20600	500
0.07669	0.11322	0.20676	0.39731	0.20600	1000
0.03934	0.08522	0.17392	0.52157	0.17993	2000
0.01902	0.03195	0.15765	0.58935	0.20200	5000
0.00954	0.01809	0.14662	0.63773	0.18800	10000
0.00608	0.01085	0.10482	0.66330	0.21493	20000
0.00258	0.00464	0.05216	0.73181	0.20878	50000
0.00168	0.00215	0.02924	0.75901	0.20790	100000
0.00069	0.00111	0.01497	0.77371	0.20949	200000
0.00033	0.00047	0.00775	0.80312	0.18831	500000
0.00018	0.00028	0.00432	0.87185	0.12335	1000000
0.00008	0.00014	0.00276	0.89592	0.10108	2000000
0.00003	0.00005	0.00116	0.95572	0.04301	5000000
0.00002	0.00003	0.00061	0.96736	0.03196	1×10^7
0.00001	0.00001	0.00031	0.98529	0.01437	2×10^7
4.08×10^{-6}	6.10×10^{-6}	0.00012	0.99430	0.00555	5×10^7
2.65×10^{-6}	2.99×10^{-6}	0.00006	0.99757	0.00236	1×10^8
1.13×10^{-6}	1.59×10^{-6}	0.00002	0.99824	0.00172	2×10^8
4.37×10^{-7}	6.67×10^{-7}	9.94×10^{-6}	0.99942	0.00056	5×10^8
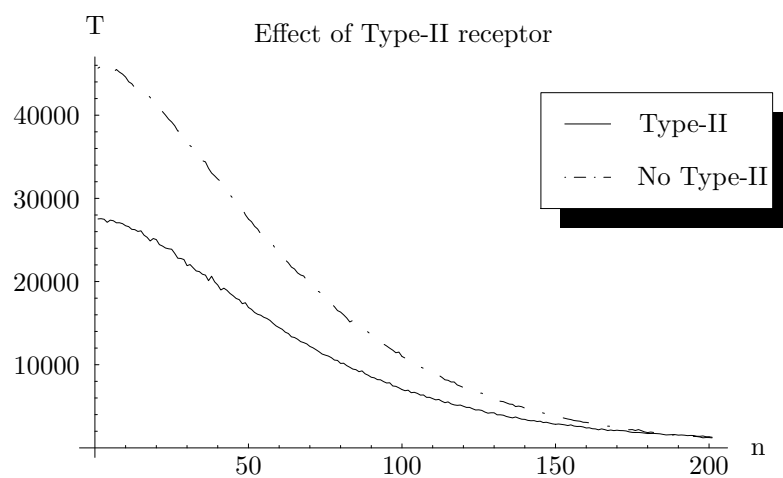
Figure 3.2: Sample paths: n is the number of iterations taken to reach the signalling ternary state, T the number of experimental trials. Each experiment consisted of $N = 5 \times 10^6$ trials. The type-II receptor slows the formation of signalling ternary complexes. Results up to $n = 200$ iterations (the majority of trials) are shown.

3.1.2   The effect of inhibitory receptor

We would like to know how long it takes before the probability distribution arrives at the signalling ternary state T, starting from the ligand state L. Note that it is not necessarily the case that the system will end up at the signalling ternary state, and we have yet to analyse the system to see if there is a stationary distribution, which we will pursue later (see section (3.1.3)).

The protocol for the experiment is as follows: we suppose that the system is currently in state i, and we wish to consider which state it goes to next. The probability distribution which determines this is

$$\mathbf{p}_i = \{p_{i1}, p_{i2}, \mathbf{K}, p_{im}\} \tag{3.6}$$

where m is the number of possible states and p_{ij} is the transition probability from state i to state j. Then $\sum_{j=1}^{m-1} p_{ij} = 1$ for each i.

To find the subsequent state, a uniformly distributed random number x is generated between zero and one. The following rules are then applied:

- If $x < p_{i1}$, then the subsequent system state is 1.

- If $\sum_{j=1}^{k} p_{ij} \leq x < \sum_{j=1}^{k+1} p_{ij}$, then the subsequent system state is $k + 1$, for $1 \leq k < m - 2$.

- If $x \geq \sum_{j=1}^{m-1} p_{ij}$, then the subsequent system state is m.

Each experimental trial is a sample path of the Markov chain. The number of iterations required to reach a state T is recorded as the result of the trial. There is a maximum number of iterations for each trial, after which the trial terminates. The experiment was run for a large number of trials.

We can observe the behaviour of the system when there is no inhibitory, type-II nonsignalling receptor. Repeating the experiment without the nonsignalling binary (NS) and ternary (NT) states shows what would happen if the network consisted only of the type-I signalling receptor. Thus we can directly compare the behaviour of the sample paths in the presence or absence of the inhibitory receptor, in order to illustrate its effect.

The results from both experiments are in Figure (3.2). The experiment consisted of N trials. The maximum possible number of iterations over the system was set to $n = 50000$; if the system arrived at the signalling ternary complex before n, the program terminated and the number of iterations recorded. The figure shows the trials up to $n = 200$ iterations, which are most of the results; outlying results, which show those trials which run up to the maximum number of iterations without a ternary complex forming, are omitted . From the figure, we can see that the effect of type-II receptors is to slow the formation of signalling ternary complexes; without the type-II receptor, the complexes form much more quickly.

The means and standard deviations for both experiments are given in Table (3.4). Notice that the mean Markov chain length of the experiment with type-II receptors is an order of magnitude higher than the mean of the experiment without type-II receptors. The sample paths take on average an order of magnitude longer to reach the signalling ternary complex state with the type-II receptor present. Also, note that the standard deviations are very large indeed, in comparison with the means. This can be explained by noting that the experiment

Table 3.4: Mean path length and standard deviation from experiments: effect of type-II receptor. The means are quite large, in comparison with figure (3.2), as are the standard deviations; however, the experimental trials continue until either a ternary complex is formed or until the maximum number of iterations has been reached.

Experiment	Mean	Standard deviation
Type-II receptor present	3713.96	8154.79
Type-II receptor absent	363.96	468.49

is designed to start with initial state L, and terminate either after it reaches the state T or reaches a maximum number of iterations. If the system remains in any other state without transitioning to T and therefore terminating, this will increase the standard deviation considerably, since it will (infrequently) reach the maximum number of iterations.

From these experiments, we can observe that the type-II nonsignalling receptor slows the formation of signalling ternary complexes, thus indirectly slowing the response of the cell to IL-1β.

3.1.3 Long-term behaviour of the system

The transition matrix $\mathbf{P}$ given in equation (3.5) depends on only eight parameters, namely $\hat{k}_S^{\pm}, \hat{k}_{NS}^{\pm}, \hat{k}_T^{\pm}, \hat{k}_{NT}^{\pm}$, because the diagonal entries are determined in terms of these parameters by the requirement that the sum of the entries in each row must be 1 (since P is a stochastic matrix). From Figure (3.1), we see that it is possible to move from any state to any other along a path having positive probability. That is, the process defined by $\mathbf{P}$ is ergodic. Standard theorems (see, for example, Grimmett and Stirzaker (38)) tell us that, for an ergodic process, a stationary distribution π exists and also satisfies $\pi_j > 0$.

Let

$$
\begin{aligned}
D = {} & \hat{k}_{NS}^+ \hat{k}_{NT}^+ \hat{k}_S^- \hat{k}_T^- + \hat{k}_S^+ \hat{k}_T^+ \hat{k}_{NS}^- \hat{k}_{NT}^- + \hat{k}_{NS}^+ \hat{k}_S^- \hat{k}_T^- \hat{k}_{NT}^- + \\
& \hat{k}_S^+ \hat{k}_{NS}^- \hat{k}_T^- \hat{k}_{NT}^- + \hat{k}_S^- \hat{k}_{NS}^- \hat{k}_T^- \hat{k}_{NT}^-
\end{aligned}
\tag{3.7}
$$

Solving the equation $\pi\mathbf{P} = \pi$ algebraically, we find:

$$
\pi_1 = \frac{\hat{k}_S^- \hat{k}_{NS}^- \hat{k}_T^- \hat{k}_{NT}^-}{D}
\tag{3.8}
$$

$$
\pi_2 = \frac{\hat{k}_S^+ \hat{k}_{NS}^- \hat{k}_T^- \hat{k}_{NT}^-}{D}
\tag{3.9}
$$

$$
\pi_3 = \frac{\hat{k}_{NS}^+ \hat{k}_S^- \hat{k}_T^- \hat{k}_{NT}^-}{D}
\tag{3.10}
$$

$$
\pi_4 = \frac{\hat{k}_S^+ \hat{k}_T^+ \hat{k}_{NS}^- \hat{k}_{NT}^-}{D}
\tag{3.11}
$$

$$\pi_5 = \frac{\hat{k}_{NS}^+ \hat{k}_{NT}^+ \hat{k}_S^- \hat{k}_T^-}{D} \tag{3.12}$$

Substituting and solving numerically, the stationary distribution is given as:

$$
\begin{align}
\pi_1 &\approx 7.85 \times 10^{-14} \tag{3.13} \\
\pi_2 &\approx 1.35 \times 10^{-7} \tag{3.14} \\
\pi_3 &\approx 5.92 \times 10^{-10} \tag{3.15} \\
\pi_4 &\approx 0.999995 \tag{3.16} \\
\pi_5 &\approx 4.86 \times 10^{-6} \tag{3.17} \\
& \tag{3.18}
\end{align}
$$

Clearly, the values of π_1, π_2, π_3 and π_5 are many orders of magnitude smaller than π_4, which is extremely close to 1. Hence, to all intents and purposes, the system ends up in the signalling ternary state (with probability 1), irrespective of the initial distribution.

Given that the probabilities which represent the dissociation of the complexes, namely $\hat{k}_S^-, \hat{k}_{NS}^-, \hat{k}_T^-, \hat{k}_{NT}^-$, are so small, it may be instructive to consider the limiting case when all of these parameters are set to zero. In that case, the transition diagram for the Markov chain can be represented schematically by

$$T \longleftarrow S \longleftarrow L \longrightarrow NS \longrightarrow NT, \tag{3.19}$$
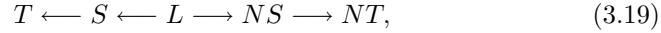
from which it is clear that the chain is reducible in this special case. Indeed, if the system leaves any state other than one of the ternary complexes (T or NT) then it can never return there. The transition matrix for this special case has the upper triangular form

$$\mathbf{P} = \begin{pmatrix} 1 - \hat{k}_S^+ - \hat{k}_{NS}^+ & \hat{k}_S^+ & \hat{k}_{NS}^+ & 0 & 0 \\ 0 & 1 - \hat{k}_T^+ & 0 & \hat{k}_T^+ & 0 \\ 0 & 0 & 1 - \hat{k}_{NT}^+ & 0 & \hat{k}_{NT}^+ \\ 0 & 0 & 0 & 1 & 0 \\ 0 & 0 & 0 & 0 & 1 \end{pmatrix}. \tag{3.20}$$

We can again solve the vector equation $\pi\mathbf{P} = \pi$ for the reduced matrix (3.20), which results in a family of stationary distributions

$$
\begin{align}
\pi_1 &= 0 \tag{3.21} \\
\pi_2 &= 0 \\
\pi_3 &= 0 \\
\pi_4 &= q \\
\pi_5 &= 1 - q
\end{align}
$$

Compare this with the stationary distribution we found where the dissociation probabilities are non-zero; there, all states would tend toward the signalling

ternary complex state T with a probability $\pi_4 \approx 1$. In this case, with the dissociation probabilities set to zero, we have a one-parameter family of stationary distributions, with the parameter q such that $0 \leq q \leq 1$. There are therefore two possible outcomes for the system, the signalling and nonsignalling ternary states. The non-uniqueness of the stationary distribution means that the limiting state of the chain is highly dependent on the initial distribution.

What are the probabilities of reaching either state? Firstly, we can see that if the system has the initial state $X_0 = S$, then it can only remain in state S and then (after a finite number of steps, m say) transit to state T, where it will then remain, and so $P(X_\infty = T \,|\, X_0 = S) = \sum_{m=0}^{\infty} \hat{k}_T^+ (1 - \hat{k}_T^+)^m = 1$. Similarly $P(X_\infty = NT \,|\, X_0 = NS) = 1$.

On the other hand, for the initial state $X_0 = L$, at each step the system can stay in that state with probability $(1 - \hat{k}_S^+ - \hat{k}_{NS}^+)$, or transit to S with probability $\hat{k}_S^+$ (in which case it will ultimately reach T with probability 1), or transit to NS with probability $\hat{k}_{NS}^+$ (in which case it will ultimately reach NT).

Summing over transitions to S after m steps, for each m, gives $P(X_\infty = T \,|\, X_0 = L) = \sum_{m=0}^{\infty} \hat{k}_S^+ (1 - \hat{k}_S^+ - \hat{k}_{NS}^+)^m$, and an analogous formula holds for $P(X_\infty = NT \,|\, X_0 = L)$. Hence we see that if the system starts off with an unbound ligand, so $X_0 = L$, then it can end up in either of the ternary states, with the limiting probabilities being

$$
P(X_\infty = T \,|\, X_0 = L) \;\;=\;\; \frac{\hat{k}_S^+}{(\hat{k}_S^+ + \hat{k}_{NS}^+)} = q \approx 0.840465, \qquad (3.22)
$$

$$
P(X_\infty = NT \,|\, X_0 = L) \;\;=\;\; \frac{\hat{k}_{NS}^+}{(\hat{k}_S^+ + \hat{k}_{NS}^+)} = 1 - q \approx 0.159535. \quad (3.23)
$$

What observations can we make from this analysis? It seems that the dissociation probabilities, despite their insignificant size relative to the association probabilities, play an essential role in the dynamics of the IL-1β network. Without the dissociation probabilities, we have two possible final outcomes for the system, the signalling and nonsignalling ternary complexes T and NT; however, with the dissociation probabilities greater than zero, the probability of the Markov process arriving at the signalling ternary complex T is $\pi_4 \approx 1$.

3.2 Stochastic model of IL-1 network including receptor antagonist

We examine the effects of the interleukin-1 receptor antagonist (IL-1Ra) on the dynamics of the IL-1β network. The receptor antagonist, the properties of which have been discussed in the introductory chapter (see chapter 1), is capable of binding to both the type-I and type-II receptors, and therefore blocking IL-1β from binding to the signalling receptor. This sections examines IL-1Ra inhibition of the signalling process.

3.2.1 Description of the system

As in section 3.1 we will exclude both the receptor types and receptor accessory proteins from explicit analysis, assuming that there are resources available to
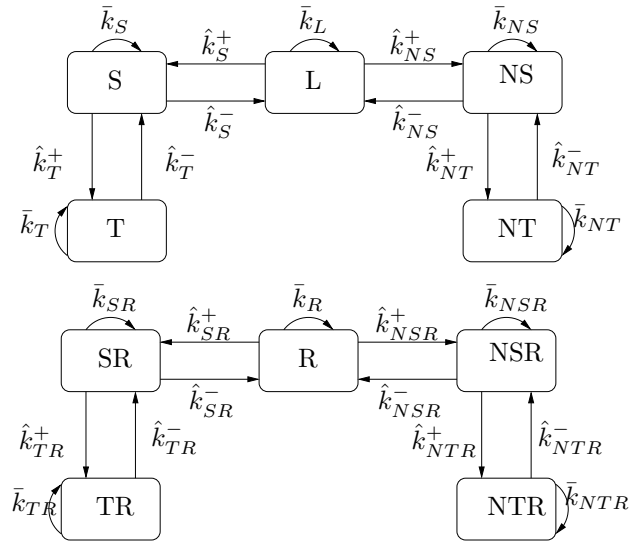
Figure 3.3: State transition diagram for IL-1β network including the receptor antagonist, where L is IL-1β, R is IL-1Ra, S is the signalling binary complex, SR is the complex formed by IL-1Ra and the type-I receptor, NS is the nonsignalling binary complex, NSR the binary complex formed by IL-1Ra and the type-II receptor, T is the signalling ternary complex, TR is the equivalent ternary complex containing the receptor antagonist, NT the nonsignalling ternary complex, and NTR its IL-1Ra counterpart. Note that the state transition diagram consists of two separate systems; this is the case since we are considering an unconstrained supply of receptors and receptor accessory proteins. Probabilities are derived from the association and dissociation rates $\hat{k}_u^{\pm}$..

form complexes. This is a not unreasonable assumption, as we have seen, and allows us to reduce the complexity of the stochastic matrix.

We will use the following notation. $R, SR.NSR, TR, NTR$ are, respectively: the receptor antagonist (R), the binary complex formed by the type-I receptor and IL-1Ra (SR), the binary complex formed by the type-II receptor and IL-1Ra (NSR), the ternary complex formed by the complex SR and the receptor accessory (TR), and the ternary complex formed by the complex NSR and the receptor accessory (NTR). All other entries are as given in Section 3.1 Table 3.3, but are given here for completeness: L, unbound ligand (IL-1β); S, signalling binary; NS, nonsignalling binary; T, signalling ternary; NT, nonsignalling ternary.

The association and dissociation probabilities are represented, for example, by $\hat{k}_R^+$, which is the association probability between IL-1Ra and the type-I receptor, and $\bar{k}_S$ the probability of the signalling binary complex remaining in the same state. $\hat{k}_R^+, \hat{k}_{NR}^+, \cdots$ are as given in Table 3.6.

The system we wish to represent, equation (3.25), is shown in the state transition diagram given in Figure (3.3). Notice from the figure that the transition diagram appears to consist of two separate systems. If a ligand is in state L (a unit of IL-1β) then it subsequently stays in the upper part of this diagram. If a ligand is in state R (a unit of IL-1Ra), then it subsequently stays in the lower part of the diagram. However, an arbitrary free ligand may be of type L or type R with some probability q, depending on how the system is stimulated.

The diagonal entries $\bar{k}_U$ in equation (3.25) give the probability that the system remains in that state; for example, the probability $\bar{k}_R$ is the probability that the receptor antagonist does not bind to one of the receptors. This is made explicit in the matrix of transition probabilities given in equation (3.26). We know that, for example, the probability of IL-1Ra remaining in the same state is $\bar{k}_L = 1 - (\hat{k}_S^+ + \hat{k}_{NS}^+)$, and in general it can be seen that the sum of the entries of each row is 1, and so $\mathbf{P}$ is a stochastic matrix.

The association and dissociation constants are transformed to probabilities, as before, using:

$$\frac{\text{Unit}}{\text{ml}} = 5.9 \times 10^{-13} \, \text{M} \tag{3.24}$$

with further amplification of the probabilities to make processing of the stochastic matrix computationally tractable. Note that this uses the same conversion as used previously, based on the international unit for IL-1β. Since IL-1Ra is of a similar size to IL-1β, both approximately 17 kDa, and there is no agreed international unit, we use the conversion factor as a basis for comparison. Association and dissociation rates are as given in the literature (51), (95).

$$\bar{\mathbf{P}} = \begin{array}{c} \\ L \\ S \\ NS \\ T \\ NT \\ R \\ SR \\ NSR \\ TR \\ NTR \end{array}
\begin{bmatrix}
L & S & NS & T & NT & R & SR & NSR & TR & NTR \\
\bar{k}_L & \hat{k}_S^+ & \hat{k}_{NS}^+ & 0 & 0 & 0 & 0 & 0 & 0 & 0 \\
\hat{k}_S^- & \bar{k}_S & 0 & \hat{k}_T^+ & 0 & 0 & 0 & 0 & 0 & 0 \\
\hat{k}_{NS}^- & 0 & \bar{k}_{NS} & 0 & \hat{k}_{NT}^+ & 0 & 0 & 0 & 0 & 0 \\
0 & \hat{k}_T^- & 0 & \bar{k}_T & 0 & 0 & 0 & 0 & 0 & 0 \\
0 & 0 & \hat{k}_{NT}^- & 0 & \bar{k}_{NT} & 0 & 0 & 0 & 0 & 0 \\
0 & 0 & 0 & 0 & 0 & \bar{k}_R & \hat{k}_{SR}^+ & \hat{k}_{NSR}^+ & 0 & 0 \\
0 & 0 & 0 & 0 & 0 & \hat{k}_{SR}^- & \bar{k}_{SR} & 0 & \hat{k}_{TR}^+ & 0 \\
0 & 0 & 0 & 0 & 0 & \hat{k}_{NSR}^- & 0 & \bar{k}_{NSR} & 0 & \hat{k}_{NTR}^+ \\
0 & 0 & 0 & 0 & 0 & 0 & \hat{k}_{TR}^- & 0 & \bar{k}_{TR} & 0 \\
0 & 0 & 0 & 0 & 0 & 0 & 0 & \hat{k}_{NTR}^- & 0 & \bar{k}_{NTR}
\end{bmatrix} \tag{3.25}$$

$$\bar{\mathbf{P}} = \begin{bmatrix}
1-(\hat{k}_S^+ + \hat{k}_{NS}^+) & \hat{k}_S^+ & \hat{k}_{NS}^+ & 0 & 0 & 0 & 0 & 0 & 0 & 0 \\
\hat{k}_S^- & 1-(\hat{k}_S^- + \hat{k}_T^+) & 0 & \hat{k}_T^+ & 0 & 0 & 0 & 0 & 0 & 0 \\
\hat{k}_{NS}^- & 0 & 1-(\hat{k}_{NS}^- + \hat{k}_{NT}^+) & 0 & \hat{k}_{NT}^+ & 0 & 0 & 0 & 0 & 0 \\
0 & \hat{k}_T^- & 0 & 1-\hat{k}_T^- & 0 & 0 & 0 & 0 & 0 & 0 \\
0 & 0 & \hat{k}_{NT}^- & 0 & 1-\hat{k}_{NT}^- & 0 & 0 & 0 & 0 & 0 \\
0 & 0 & 0 & 0 & 0 & 1-(\hat{k}_{SR}^+ + \hat{k}_{NSR}^+) & \hat{k}_{SR}^+ & \hat{k}_{NSR}^+ & 0 & 0 \\
0 & 0 & 0 & 0 & 0 & \hat{k}_{SR}^- & 1-(\hat{k}_{SR}^- + \hat{k}_{TR}^+) & 0 & \hat{k}_{TR}^+ & 0 \\
0 & 0 & 0 & 0 & 0 & \hat{k}_{NSR}^- & 0 & 1-(\hat{k}_{NSR}^- + \hat{k}_{NTR}^+) & 0 & \hat{k}_{NTR}^+ \\
0 & 0 & 0 & 0 & 0 & 0 & \hat{k}_{TR}^- & 0 & 1-\hat{k}_{TR}^- & 0 \\
0 & 0 & 0 & 0 & 0 & 0 & 0 & \hat{k}_{NTR}^- & 0 & 1-\hat{k}_{NTR}^-
\end{bmatrix} \tag{3.26}$$

Table 3.5: Association/dissociation rates: the association and dissociation rates of the signalling and nonsignalling complexes of the receptor antagonist, where SR is the signalling binary and NSR the nonsignalling binary.

Agent	Binds	Assoc. $(M^{-1}s^{-1})$	Dissoc. (s^{-1})
IL-1RI[1]	IL-1Ra	4.3×10^6	1.25×10^{-4}
SR [1]	IL-1RAcP	4.3×10^6	1.25×10^{-4}
IL-1RII [2]	IL-1Ra	2.0×10^6	5.44×10^{-4}
NSR [2]	IL-1RAcP	1.73×10^6	5.41×10^{-4}

[1] Source: (37), (4), (24)   [2] Source: (95), (4), (24)

Table 3.6: Probabilities $\mathbb{P}(X)$ such that $\hat{k}_u^{\pm} \in [0, 1]$ derived from association and dissociation rates $k_u^{\pm}$ given in table 3.5, after applying the conversion factor given by equation (3.24).

Antagonist association probabilities		
Complex	Symbol	$\mathbb{P}(X)$
Signalling binary	$\hat{k}_{SR}^+$	2.54×10^{-6}
Nonsignalling binary	$\hat{k}_{NSR}^+$	1.18×10^{-6}
Signalling ternary	$\hat{k}_{TR}^+$	2.54×10^{-6}
Nonsignalling ternary	$\hat{k}_{NTR}^+$	1.02×10^{-6}
Antagonist dissociation probabilities		
Complex	Symbol	$\mathbb{P}(X)$
Signalling binary	$\hat{k}_{SR}^-$	7.38×10^{-17}
Nonsignalling binary	$\hat{k}_{NSR}^-$	3.21×10^{-16}
Signalling ternary	$\hat{k}_{TR}^-$	7.38×10^{-17}
Nonsignalling ternary	$\hat{k}_{NTR}^-$	3.20×10^{-16}

3.2.2 Markov chain model

We can experiment again to investigate the behaviour of the system in the presence of IL-1Ra, as in Section (3.1.1). Notice that the number of states in the model has expanded: once again, for completeness, we have the subnetwork formed by IL-1β (L); S, signalling binary; NS, nonsignalling binary; T, signalling ternary; NT, nonsignalling ternary; and the subnetwork formed by the receptor antagonist (R), the binary complex formed by the type-I receptor and IL-1Ra (SR), the binary complex formed by the type-II receptor and IL-1Ra (NSR), the ternary complex formed by the complex SR and the receptor accessory (TR), and the ternary complex formed by the complex NSR and the receptor accessory (NTR).

We would like to know how the system evolves in the presence of the receptor antagonist. In particular, does the receptor antagonist slow the average time taken to form ternary complexes? To investigate this question, we could modify the experimental protocol used in Section (3.1.2), including the receptor antagonist.

The system will have two initial states, corresponding to IL-1β and IL-1Ra. One way of thinking about this is that the ligand is in a superposition that remains undetermined until an association event takes place.

The protocol for the experiment is as follows: we suppose that the system is currently in state i, and we wish to consider which state it goes to next. The probability distribution which determines this is

$$\mathbf{p}_i = \{\pi_{i1}, \pi_{i2}, \mathbf{K}, \pi_{im}\} \tag{3.27}$$

where m is the number of possible states and p_{ij} is the transition probability from state i to state j. Then $\sum_{j=1}^{m} p_{ij} = 1$ for each i. State changes occur using the criteria given in section (3.2.3).

The termination criteria of the trial are as follows: if a signalling ternary complex is formed, the experimental trial will terminate, reporting the number of timesteps taken to reach this state; if the receptor antagonist forms a binary or ternary complex, then the trial will continue until either a dissociation event occurs, or the maximum number of timesteps is reached. The experiment will describe the length of the mean sample path in the presence of the receptor antagonist.

The experiment can best be described in the following way. Imagine that there is a state called U for unbound ligand, which is the *superposition* of L and R, with transition probabilities $1 - q : U \to L$ and $q : U \to R$, where q is the proportion of IL-1Ra units, and $1 - q$ is the proportion of IL-1β units in the extracellular concentration of ligand. The state transition diagram is given in figure 3.4, although ternary complex transitions are omitted.

When a ligand dissociates, it returns to the extracellular pool, which contains both IL-1β and IL-1Ra. At the next association event, a ligand is chosen from this at random, so that it is of type L with probability $1 - q$ and of type R with probability q. Therefore there is in effect only one unbound ligand state, U, with four possible association event transitions
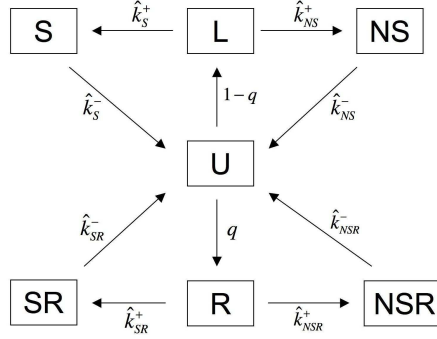
Figure 3.4: State transition diagram for IL-1β network including the receptor antagonist, where U is the unbound ligand state, L is IL-1β, R is IL-1Ra, S is the signalling binary complex, SR is the complex formed by IL-1Ra and the type-I receptor, NS is the nonsignalling binary complex, NSR the binary complex formed by IL-1Ra and the type-II receptor. Transitions to and from ternary complexes are not shown.

$$U \xrightarrow{(1-q)\,\hat{k}_S^+} S \tag{3.28}$$

$$U \xrightarrow{(1-q)\,\hat{k}_{NS}^+} NS \tag{3.29}$$

$$U \xrightarrow{q\hat{k}_{SR}^+} SR \tag{3.30}$$

$$U \xrightarrow{q\hat{k}_{NSR}^+} NSR \tag{3.31}$$

The probability that there is no transition out of state U is therefore

$$\bar{k}_U = 1 - \left((1-q)\left(\hat{k}_S^+ + \hat{k}_{NS}^+\right) + q\left(\hat{k}_{SR}^+ + \hat{k}_{NSR}^+\right) \right) \tag{3.32}$$

We can also add nonsignalling binary and ternary complex formation in a second experiment, so that we can find the effect of two inhibitors on the length of the average sample path. The system will consist of two initial states, as described above, consisting of IL-1β and IL-1Ra. Two association events are available to each ligand to form a binary complex, and there are two further ternary complex association events. The experimental trial will terminate if the system reaches the signalling ternary state; otherwise, the system will continue until it reaches the maximum number of iterations, to provide for dissociation of the complex.

The results from the experiments are given in Table (3.7). The first entry gives us the results for the average sample path taken to form a signalling ternary complex, where the system consists of IL-1β, the signalling binary, and the signalling ternary. The second shows the longer average sample path where the nonsignalling binary and ternary states are introduced into the system. The third shows the effect of the receptor antagonist, without the type-II receptor, and the fourth shows the effect of both antagonist and type-II receptor on

Table 3.7: Mean sample path length from experiments: effect of the type-II receptor and receptor antagonist. The first experiment shows the average sample path without the type-II receptor or receptor antagonist, the second with the type-II receptor present, the third with the receptor antagonist present and the type-II receptor absent, the fourth with both the antagonist and the type-II receptor present. The average sample path clearly increases.

Type-II	IL-1Ra	Mean
N	N	363.96
Y	N	3713.96
N	Y	6455.14
Y	Y	7811.12

the system. From these experiments, it seems reasonable to conclude that the receptor antagonist increases the average sample path taken to form signalling ternary complexes. IL-1Ra can be said to perform a similar role to the type-II receptor in the IL-1β network. Furthermore, both the antagonist and the type-II receptor appear to have a synergistic effect on the network, acting in concert to slow the formation of signalling ternaries and thus signalling transduction.

3.2.3   Long term behaviour of the system

We can find the stationary distribution by solving the equation $\pi\mathbf{P} = \pi$ for the stochastic matrix $\mathbf{P}$ such that $\pi_{\mathbf{j}} > 0$. We can solve the equation $\pi\mathbf{P} = \pi$ algebraically. The solutions are given in equations (3.33)-(3.42). Solving numerically, we find once again that the signalling ternary complex formed by IL-1β is approximately equal to one. In the presence of the receptor antagonist, we have a robust solution $\pi_4 \approx 1$, which corresponds to the signalling ternary complex; the next largest, π_8, corresponds to the antagonist ternary complex. We can conclude from this that the stationary distribution of the stochastic matrix $\mathbf{P}$ is the signalling ternary complex.

To simplify, let: $\psi = \dfrac{\hat{k}^+_{SR}\hat{k}^+_{TR}\hat{k}^-_{NSR}\hat{k}^-_{NTR}}{\hat{k}^+_{SR}\hat{k}^+_{NTR}\hat{k}^-_{SR}\hat{k}^-_{TR}+\hat{k}^+_{SR}\hat{k}^+_{TR}\hat{k}^-_{NSR}\hat{k}^-_{NTR}+\hat{k}^+_{NSR}\hat{k}^-_{SR}\hat{k}^-_{TR}\hat{k}^-_{NTR}+\hat{k}^+_{SR}\hat{k}^-_{NSR}\hat{k}^-_{TR}\hat{k}^-_{NTR}+\hat{k}^-_{SR}\hat{k}^-_{NSR}\hat{k}^-_{TR}\hat{k}^-_{NTR}}$

Then:

$$\pi_1 = \frac{(\hat{k}^-_S\hat{k}^-_{NS}\hat{k}^-_T\hat{k}^-_{NT}(-\hat{k}^-_{NSR}(\hat{k}^-_{SR}\hat{k}^-_{TR}+\hat{k}^+_{SR}(\hat{k}^+_{TR}+\hat{k}^-_{TR}))\hat{k}^-_{NTR}\psi+\hat{k}^+_{NSR}\hat{k}^-_{SR}\hat{k}^-_{TR}(\hat{k}^-_{NTR}-(\hat{k}^+_{NTR}+\hat{k}^-_{NTR})\psi)))}{((\hat{k}^-_{NS}(\hat{k}^-_S\hat{k}^-_T+\hat{k}^+_S(\hat{k}^+_T+\hat{k}^-_T))\hat{k}^-_{NT}+b\hat{k}^-_S\hat{k}^-_T(\hat{k}^+_{NT}+\hat{k}^-_{NT}))\hat{k}^+_{NSR}\hat{k}^-_{SR}\hat{k}^-_{TR}\hat{k}^-_{NTR})} \tag{3.33}$$

$$\pi_2 = \frac{(\hat{k}^+_S\hat{k}^-_{NS}\hat{k}^-_T\hat{k}^-_{NT}(-\hat{k}^-_{NSR}(\hat{k}^-_{SR}\hat{k}^-_{TR}+\hat{k}^+_{SR}(\hat{k}^+_{TR}+\hat{k}^-_{TR}))\hat{k}^-_{NTR}\psi+\hat{k}^+_{NSR}\hat{k}^-_{SR}\hat{k}^-_{TR}(\hat{k}^-_{NTR}-(\hat{k}^+_{NTR}+\hat{k}^-_{NTR})\psi)))}{((\hat{k}^-_{NS}(\hat{k}^-_S\hat{k}^-_T+\hat{k}^+_S(\hat{k}^+_T+\hat{k}^-_T))\hat{k}^-_{NT}+\hat{k}^+_{NS}\hat{k}^-_S\hat{k}^-_T(\hat{k}^+_{NT}+\hat{k}^-_{NT}))\hat{k}^+_{NSR}\hat{k}^-_{SR}\hat{k}^-_{TR}\hat{k}^-_{NTR})} \tag{3.34}$$

$$\pi_3 = \frac{(\hat{k}^+_{NS}\hat{k}^-_S\hat{k}^-_T\hat{k}^-_{NT}(-\hat{k}^-_{NSR}(\hat{k}^-_{SR}\hat{k}^-_{TR}+\hat{k}^+_{SR}(\hat{k}^+_{TR}+\hat{k}^-_{TR}))\hat{k}^-_{NTR}\psi+\hat{k}^+_{NSR}\hat{k}^-_{SR}\hat{k}^-_{TR}(\hat{k}^-_{NTR}-(\hat{k}^+_{NTR}+\hat{k}^-_{NTR})\psi)))}{((\hat{k}^-_{NS}(\hat{k}^-_S\hat{k}^-_T+\hat{k}^+_S(\hat{k}^+_T+\hat{k}^-_T))\hat{k}^-_{NT}+\hat{k}^+_{NS}\hat{k}^-_S\hat{k}^-_T(\hat{k}^+_{NT}+\hat{k}^-_{NT}))\hat{k}^+_{NSR}\hat{k}^-_{SR}\hat{k}^-_{TR}\hat{k}^-_{NTR})} \tag{3.35}$$

$$\pi_4 = \frac{(\hat{k}^+_S\hat{k}^+_T\hat{k}^-_{NS}\hat{k}^-_{NT}(-\hat{k}^-_{NSR}(\hat{k}^-_{SR}\hat{k}^-_{TR}+\hat{k}^+_{SR}(\hat{k}^+_{TR}+\hat{k}^-_{TR}))\hat{k}^-_{NTR}\psi+\hat{k}^+_{NSR}\hat{k}^-_{SR}\hat{k}^-_{TR}(\hat{k}^-_{NTR}-(\hat{k}^+_{NTR}+\hat{k}^-_{NTR})\psi)))}{((\hat{k}^-_{NS}(\hat{k}^-_S\hat{k}^-_T+\hat{k}^+_S(\hat{k}^+_T+\hat{k}^-_T))\hat{k}^-_{NT}+\hat{k}^+_{NS}\hat{k}^-_S\hat{k}^-_T(\hat{k}^+_{NT}+\hat{k}^-_{NT}))\hat{k}^+_{NSR}\hat{k}^-_{SR}\hat{k}^-_{TR}\hat{k}^-_{NTR})} \tag{3.36}$$

$$\pi_5 = \frac{(\hat{k}^+_{NS}\hat{k}^+_{NT}\hat{k}^-_S\hat{k}^-_T(-\hat{k}^-_{NSR}(\hat{k}^-_{SR}\hat{k}^-_{TR}+\hat{k}^+_{SR}(\hat{k}^+_{TR}+\hat{k}^-_{TR}))\hat{k}^-_{NTR}\psi+\hat{k}^+_{NSR}\hat{k}^-_{SR}\hat{k}^-_{TR}(\hat{k}^-_{NTR}-(\hat{k}^+_{NTR}+\hat{k}^-_{NTR})\psi)))}{((\hat{k}^-_{NS}(\hat{k}^-_S\hat{k}^-_T+\hat{k}^+_S(\hat{k}^+_T+\hat{k}^-_T))\hat{k}^-_{NT}+\hat{k}^+_{NS}\hat{k}^-_S\hat{k}^-_T(\hat{k}^+_{NT}+\hat{k}^-_{NT}))\hat{k}^+_{NSR}\hat{k}^-_{SR}\hat{k}^-_{TR}\hat{k}^-_{NTR})} \tag{3.37}$$

$$\pi_6 = \frac{(\hat{k}^-_{NSR}\psi)}{\hat{k}^+_{NSR}} \tag{3.38}$$

$$\pi_7 = \frac{(\hat{k}^+_{SR}\hat{k}^-_{NSR}\psi)}{(\hat{k}^+_{NSR}\hat{k}^-_{SR})} \tag{3.39}$$

$$\pi_8 = \psi \tag{3.40}$$

$$\pi_9 = \frac{(\hat{k}^+_{SR}\hat{k}^+_{TR}\hat{k}^-_{NSR}\psi)}{(\hat{k}^+_{NSR}\hat{k}^-_{SR}\hat{k}^-_{TR})} \tag{3.41}$$

$$\pi_{10} = \frac{(\hat{k}^+_{NTR}\psi)}{\hat{k}^-_{NTR}} \tag{3.42}$$

The system described in the previous section was investigated for values of $U \in [100, 500, 1000]$; we vary q between zero and one. The number of iterations is set to 5×10^8; this a large and computationally expensive number of iterations, intended to show the long term behaviour of the system, and is not intended to be biologically realistic. For each value of U, we have 100 experimental trials. The association and dissociation probabilities given in table (3.6) are used, and the states are as given in figure (3.4).

At each iteration i, the simulation generates a random number and compares it with the probabilities given in equations (3.28) - (3.32), determining if a state change will occur. The state of the unbound ligand, whether it is IL-1β or IL-1Ra, is chosen at this point by comparing a second random number to q. A third random number is generated to determine which state change the ligand will undergo, using the criteria given in section (3.2.3).

The state change then occurs, if it is possible - for instance, a signalling ternary state change can only occur if a signalling binary is present in the system.

3.3   Varying q

The value of q will clearly have a major effect on the dynamics of the system. An experiment was designed to investigate these dynamics. The system starts with a single ligand in the superposition state, as described previously. The system has a single parameter, the value of q, such that $0.01 \le q \le 0.99$, and the increment $\delta = 0.01$ is applied to q after $N = 1000$ trials. Each trial was given a large number of iterations $n = 5 \times 10^5$ before termination. Notice that this is not necessarily a biologically feasible number if thought of in terms of time steps, for example if each iteration represents a second; however, this is not the intention of the experiment, since it is of more interest to give the system as many opportunities to change state with the low probabilities which certain values of q may engender. It is worth noting that the simulation took far fewer iterations to reach a ternary state, and that none of the ligand remained unbound for n iterations.

The system determines the state of the ligand in the following way: it generates a random number d and compares it to the q parameter. If $d > q$, the ligand is assigned to be a protein of IL-1β, and if not, a receptor antagonist. The system then goes through each iteration, generating a random number, and comparing this to the probabilities of each state change, as given in section (3.2.3). The probabilities, as noted, change with the value of q. The system generally terminates long before the maximum number of iterations n has been reached, as would be expected from the mean Markov chain length of the simulations in section (3.2).

After the ligand changes from its superposition to a defined state, only appropriate state changes are available to it. If a change in state occurs, the simulation immediately prints out this information. The final state of the system is printed just before the simulation terminates, which allows us to capture those trials where the ligand remains unbound.

Figure 3.5: Ternary formation for IL-1β and IL-1Ra: mean sample path length. Only the Type-I receptor is available for binding. The signalling ternary complexes, T, are given in red, and the antagonist-bound ternaries, TR, are given in orange.
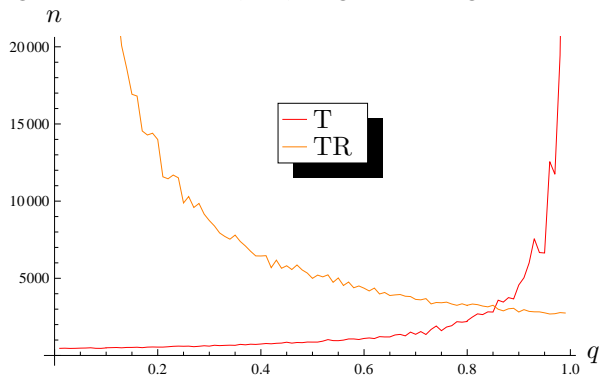
3.3.1 Varying q: results

The simulations initially excised the Type-II receptor from the system, so that the effects of the receptor antagonist on IL-1β binding to Type-I can be seen without the additional effects of the nonsignalling receptor. The effect of q on the mean sample path length and the standard deviation can be seen in Table (3.8) for both ligands. The simulation starts with $q = 0.01$ and ends with $q = 0.99$; both start points and end points are given in the table, however, for reasons of brevity, some of the data is elided from the table.

The table shows that for increasing q, the mean Markov chain length increases for IL-1β-bound ternary complexes, and decreases for IL-1Ra-bound ternary complexes. The effect of IL-1Ra can be seen in the increased mean sample path, which is to be expected from the results given in section (3.2.2), Table (3.7). Increasing q decreases the number of iterations taken to form an IL-1Ra-bound ternary complex. Standard deviations σ for both type of complexes are relatively large, which again accords with the results given in section (3.2.2).

To summarise, as the probability of the determination of the ligand superposition U becoming IL-1β becomes less, the mean path length to signalling ternary complex formation becomes much greater, and IL-1Ra-bound ternary complex formation takes on average much fewer iterations.

Figure (3.5) shows the mean sample paths of the IL-1β- and antagonist-bound ternary complexes, showing the inhibitory effect of q on signalling complex formation. Figure (3.6) gives the results of ternary formation, for varying q, including the Type-II nonsignalling receptor.

The mean Markov chain length for IL-1β-bound ternary complexes is given in figure (3.6(a)). Recall that the simulation will terminate when it reaches a *ternary* complex, either signalling or antagonistic. Dividing by the number of trials N gives the mean number of iterations, or the mean Markov chain length, for the value of n for each value of q. The signalling ternary T, given in red, has an initially short Markov chain length, as does the nonsignalling ternary NT; however, the nonsignalling ternary has a longer Markov chain length than the signalling ternary, since it has a lower probability of association.

Table 3.8: The mean sample path length and standard deviation taken to form a ternary complex for increasing q. Only the Type-I receptor is available to the ligand. The results are given for $0.01 \leq q \leq 0.99$, however some data has been elided for brevity. Both the mean Markov chain length and the standard deviation increase on increasing q; notice the large standard deviation σ, which is similar to the results given in Table (3.7) in Section (3.2.2). Each experiment ran for $N = 1000$ trials.

IL-1β ternaries		
q	Mean	σ
0.01	460.54	327.91
0.10	489.00	497.83
0.20	542.13	382.52
0.30	603.79	432.09
0.40	741.54	520.33
0.50	866.14	603.93
0.60	1102.33	820.76
0.70	1369.71	1026.42
0.80	2199.96	2250.12
0.90	4567.42	3044.91
0.99	40216.55	25890.93
IL-1Ra ternaries		
q	Mean	σ
0.01	217033.83	116674.52
0.10	25245.14	25553.04
0.20	13992.41	10923.43
0.30	8741.16	6378.66
0.40	6445.02	5020.79
0.50	4995.19	4161.98
0.60	4359.01	3379.97
0.70	3631.61	2984.28
0.80	3240.03	3252.19
0.90	2814.62	2312.00
0.99	2749.94	2044.33

Table 3.9: The mean sample path length and standard deviation taken to form a ternary complex for increasing q. Both receptor types are available to the ligand. The results are given for $0.01 \leq q \leq 0.99$. Each experiment ran for $N = 1000$ trials.

	IL-1β-Type-I ternaries		IL-1β-Type-II ternaries		
q	Mean	σ	q	Mean	σ
0.01	648.27	890.10	0.01	2885.68	3207.06
0.1	716.29	676.15	0.1	2988.17	3630.40
0.2	754.51	1070.19	0.2	3475.86	3649.50
0.3	904.94	1222.99	0.3	4014.20	4430.14
0.4	1258.55	1590.91	0.4	4416.97	5265.09
0.5	1331.34	1907.90	0.5	4979.98	6606.21
0.6	1574.13	2135.48	0.6	7671.85	8235.41
0.7	2239.37	2908.04	0.7	6927.02	10032.39
0.8	3458.06	3137.40	0.8	16899.12	14667.24
0.9	4633.86	8564.09	0.9	23025.96	32150.83
0.99	74907.14	103813.92	N/A	N/A	N/A
	IL-1Ra-Type-I ternaries		IL-1Ra-Type-II ternaries		
q	Mean	σ	q	Mean	σ
0.01	72118.94	119477.71	0.01	121111.00	160494.00
0.1	16749.50	13784.86	0.1	81394.92	65059.96
0.2	9506.58	11162.66	0.2	27017.45	33680.04
0.3	7625.03	8636.01	0.3	18940.65	20536.23
0.4	5558.49	6301.98	0.4	17206.61	15669.32
0.5	4292.39	4987.36	0.5	12771.29	13322.85
0.6	3611.62	4032.81	0.6	10920.79	11525.91
0.7	2818.33	3332.33	0.7	9528.51	9405.60
0.8	2579.12	2464.02	0.8	7104.74	7780.27
0.9	2051.89	2589.29	0.9	6123.82	6932.59
0.99	2088.73	2623.58	0.99	5741.87	6853.09
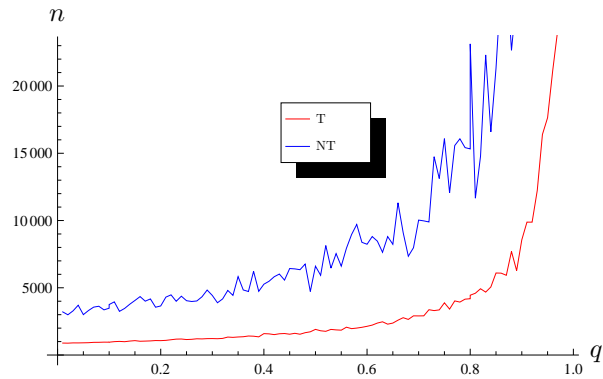
(a) IL-1β signalling/nonsignalling ternary
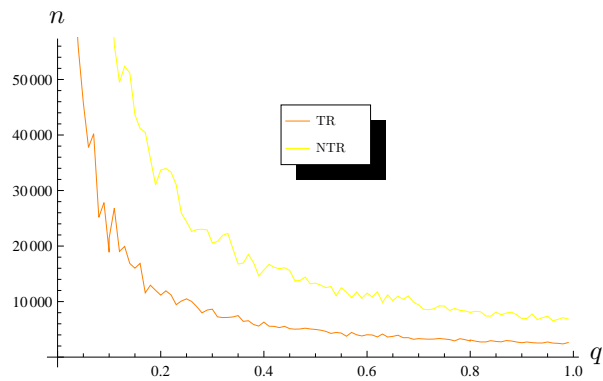
(b) IL-1Ra signalling/nonsignalling ternary
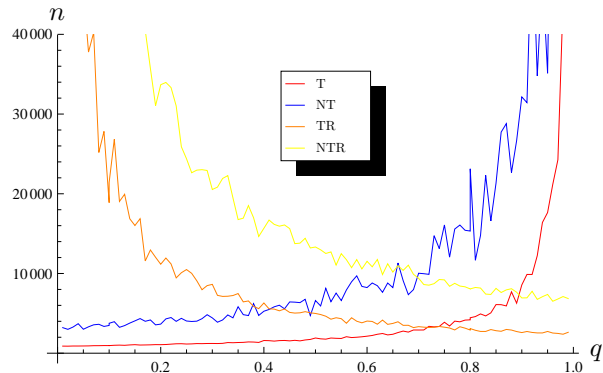
(c) Comparison of all complexes

Figure 3.6: Ternary complex formation with two ligands: IL-1β and IL-1Ra. Figure 3.6(a) shows ternary complexes T bound to IL-1β, where the signalling ternary complex is given in red, and the nonsignalling ternary complex NT is given in blue. Initially, the Markov chain length has a low mean number of iterations. The chain length for both ternary complexes increases on increasing values of q. Figure 3.6(b) shows ternary formation for IL-1Ra, where the Type-I bound complex TR is given in orange, and the Type-II bound complex is given in yellow. The Markov chain length is initially high and decreases on increasing n. Figure 3.6(c) shows all the complexes for comparison purposes.

The mean number of iterations n taken to form either complex again increases with increasing q. Despite the figure showing mean Markov chain lengths, the plot tends to fluctuate, particularly the nonsignalling ternary; the formation of nonsignalling ternaries is a less frequent event, due to its lower probability, and the simulation prints out any change of state as soon as it happens to the system, which will occur at an unpredictable number of timesteps, accounting for the stochastic appearance of the plot.

Figure (3.6(b)) gives the antagonist-bound ternary complexes, those bound to both Type-I and Type-II receptors and the receptor accessory protein. The IL-1Ra-Type-I-IL-1RAcP ternary TR is given in the figure in orange, and the Type-II-based ternary NTR is given in yellow. The formation of NTR takes a higher number of iterations than formation of TR, as with the signalling and nonsignalling ternaries T and NT. Similarly, formation of antagonist-bound complexes take longer than IL-1β-bound complexes.

Comparing Table (3.8) and Table (3.9), we can confirm that, as found previously in Section (3.2.2), the receptor antagonist and the Type-II receptor act to slow formation of signalling ternaries. There is therefore a synergy between the Type-II receptor and the receptor antagonist, enhancing the inhibition of IL-1β.

Figure (3.6) shows that there are two effects on binary and ternary complex formation. The first is to slow the formation of signalling complexes; the second is to block the formation of signalling complexes. If a Type-I receptor is consumed by its formation with a receptor antagonist, it is not available for binding IL-1β. Similarly, an antagonist ternary complex will make a Type-I receptor and a receptor accessory protein unavailable for binding. This means that the interaction between the Type-II receptor and the antagonist significantly decrease the mean number of iterations taken to form a signalling ternary complex, and therefore the interaction between the Type-II receptor and the antagonist are not noticeably mutually inhibitory.

The antagonist can go on to form antagonist ternary complexes, where it has consumed a receptor accessory protein. Each receptor accessory consumed is one that is not available for the formation of a signalling ternary complex, and therefore impedes a possible signal transduction event.

To summarise, the following effects have been found:

- IL-1Ra without Type-II:

    - slows signalling complex formation: the formation of signalling complexes is noticeably slower for higher values of q

    - sequesters Type-I receptors: prevents formation of signalling by consuming Type-I receptors, making them unavailable for signalling complex formation

    - sequesters receptor accessory protein: prevents formation of signalling by consuming receptor accessory proteins, making them unavailable for signalling complex formation

- IL-1Ra with Type-II:

    - further slows signalling complex formation: a synergistic interaction between the antagonist and the nonsignalling receptor slows sig-

   nalling complex formation, confirming what was shown in section (3.2), with increasing q

   – sequesters both Type-I receptor and receptor accessory protein: antagonistic ternaries consume the receptor accessory protein, therefore impeding formation of signalling ternary complexes.

3.4   Discussion

Two stochastic models of the IL-1β network have been presented, investigating the respective roles of the type-II receptor and the receptor antagonist. The behaviour of the Markov processes have been described both computationally and analytically. IL-1β is a very active cytokine, requiring only tens of receptors to invoke a cellular response. Many inhibitory control mechanisms have evolved alongside the IL-1β network, possibly due to its potency (29). Two inhibitory control mechanisms, the type-II nonsignalling receptor and the receptor antagonist, have been modelled in the stochastic models analysed above.

   It was found that the model including type-II receptor has a unique stationary distribution in which the system occupies the ternary signalling complex with probability close to one. Given the relative size of the association and dissociation rates of the type-I and type-II receptors, this is perhaps unsurprising, since IL-1β is a fundamentally important cytokine. This has implications for the biology of the network. The potency of IL-1β is such that, without some form of inhibition, it could potentially cause considerable damage.

   It has been argued that the type-II receptor acts as a decoy, or *sink*, for IL-1β (15), by absorbing any of it that has not yet bound to type-I receptors. However, the Markov chain model, as described in Section (3.1.2), has shown that the type-II receptor is not an effective competitor for IL-1β, or for receptor accessory protein. Rather, its presence acts more to *delay* the network going to the signalling ternary complex state, if the experimental protocol allows the possibility of dissociation.

   The *modelled* network exhibited a stationary distribution, but could a *biological* system be said to have an equilibrium? This is a difficult question, and not one that could easily be addressed here, but certainly a chronic inflammatory disease such as rheumatoid arthritis appears to have an equilibrium, sustained by a low, but persistent, level of stimulus. If the extracellular IL-1β stimulus is sustained at a constant level, then the system will have time to reach equilibrium. However, if the stimulus is transient, it may not. Since the type-II receptor acts to delay passage to the signalling state, its function could be to protect the cell from activation by transient IL-1 stimulation.

   The dissociation rates of the system are extremely small, relative to the association rates. When the dissociation rates were set to zero, an exploration of the Markov chain behaviour revealed that, without the possibility of dissociation, the system no longer has a unique stationary distribution. It appears that the dissociation rates, despite their apparent numerical insignificance, have a significant role to play in the dynamics of the IL-1β network.

   The receptor antagonist model, as described in Section (3.2.1) and modelled in Section (3.2.2), introduced a second ligand into the IL-1β network. The antagonist IL-1Ra binds to both type-I and type-II receptors, and also sequesters the receptor accessory protein. It could therefore be considered a competitor for

IL-1β, and an inhibitory influence on the network. Analysis of the stochastic matrix showed that the signalling ternary complex was, once again, the state with the highest probability distribution, although the signalling ternary complex formed by the receptor antagonist was the second highest.

In section (3.3.1) we introduced a parameter q, the purpose of which was to affect the probability of the ligand U being determined randomly as either IL-1β or IL-1Ra. q varied such that $0.01 \leq q \leq 0.99$. As q increased, the mean Markov chain length for the formation of ternary signalling complexes was found to increase, and antagonist ternary complex mean path length was found to decrease. From this, and the results in section (3.2.2), it was found that the presence of the receptor antagonist slows the formation of signalling complexes, and by sequestering the Type-I receptor and the receptor accessory, impedes formation of signalling complexes.

Adding the Type-II receptor to the simulation was found to further slow formation of signalling complexes on increasing q, confirming results in section (3.2.2). The antagonist and Type-II receptor were found not to be significantly mutually inhibitory, although some antagonist-Type-II ternary complexes were formed. Furthermore, antagonist complexes could consume both Type-I receptors and receptor accessory protein, obstructing ongoing signal complex formation.

The ongoing consumption of receptors and accessories, inhibiting further signalling ternary complex formation, suggests a further control mechanism. Imagine a cell that has been subjected to an IL-1β stimulus in the presence of some injury or infection. It is highly likely that immune system cells or other inured cells in the immediate neighbourhood would be emitting cytokines, including IL-1, at random intervals. Sequestration of receptors and accessories by elements of the network, which do not contribute to signal transduction, could prevent the cell from being able to respond to further IL-1β. IL-1β is a very potent chemical, and the consumption of limited resources could have evolved as a means to limit the physiological response of cells.

Chapter 4

Constrained resources model

In the previous chapter, we considered a model of the IL-1β network where the receptors and accessory proteins were not constrained. This chapter considers the effect of constraining receptors and accessories on system dynamics.

The first Markov chain model consists of IL-1β, Type-I and Type-II receptors, and the receptor accessory, along with subsequent protein products. We decompose the network into a set of elementary events, and explore the transition between the various states. This model builds on the work in the previous chapter, analysing the effect of the Type-II receptor on signal transduction.

The second Markov chain model examines the effect on the formation of signalling ternary complexes in the presence of the receptor antagonist protein, IL-1Ra. This entails further event decomposition, since the system has a number of extra states available to it. Experiments take place both with and without the Type-II receptor. A further experiment, based on an estimation of the likely range of receptor and accessory populations on a human cell membrane, indicates the likely behaviour of the system in the vicinity of a single human cell.

4.1 IL-1β Markov process: finite receptors and accessories

The model takes into account the central event of the IL-1β network, binding of the ligand to the Type-I receptor. The components modelled are: IL-1β, IL-1RI, IL-1RII, IL-1RAcP, signalling and nonsignalling binary complexes, and signalling and nonsignalling ternary complexes.

Consider a population consisting of a number N of units, each of which can be in one of $S+1$ possible states, indexed by $u = 0, 1, \ldots, S$. If N_u is the number of units in state u, then $\mathbf{N} = (N_0, \ldots, N_S)$ is the population state vector. The simplex over the set of states S can be given by:

$$\Delta[S] = \left\{ \mathbf{s} \in (s_0, \ldots, s_S) \in \mathbb{R}^{S+1} : 0 \le s_u \le 1, \text{ and} \sum_{u=0}^{S} s_u = 1 \right\} \qquad (4.1)$$

Inside this S-dimensional simplex is the rational lattice:

$$\Omega_N = \{\mathbf{s} \in \Delta[S] : Ns_u = N_u \quad \text{is an integer} \quad \forall\, u \in S\} \tag{4.2}$$

Elements of this set specify the state of the system (at any given time). We assume that elementary events change the population state, and that each elementary event can take place in an elementary time step. At most, one elementary event can occur to each population unit in an elementary time step. If a particular population unit is in some state u, and an elementary event occurs, the state of the unit may change, and therefore the population state will change: $\mathbf{N} \to \mathbf{N} + \varepsilon$, where the vector representing the change-of-state is given by $\varepsilon = (\varepsilon_0, \ldots, \varepsilon_S)$ and satisfies $\varepsilon \in \{0, \pm 1\}$ with $\sum_w \varepsilon_w = 0$. This ensures that N, the total number of units in the population, is conserved.

We denote all the possible population state change vectors by the set:

$$\epsilon = \left\{ \varepsilon = (\varepsilon_0, \varepsilon_1, \ldots, \varepsilon_s) : \varepsilon_u \in \{0, \pm 1\} \text{ and } \sum_w \varepsilon_w = 0 \right\} \tag{4.3}$$

We will restrict the state changes of the system to *allowable* elementary events. It is allowable, for example, for a binary signalling complex to change state to a ternary signalling complex, but not allowable for a ligand to change state to a ternary signalling complex. Let $\mathcal{E}$ be the set of allowable elementary events and let it be partitioned in the form:

$$\mathcal{E} = \bigcup_{u=0}^{S} \mathcal{E}_u \tag{4.4}$$

which is the disjoint union of events (since the elementary events are mutually exclusive), so that each elementary event is associated with a particular population unit state u. A population unit that is currently in state u can only be affected by an elementary event in $\mathcal{E}_u$. Also, each set $\mathcal{E}_u$ contains an element signifying a nonevent, $\emptyset_u$, indicating that nothing happens.

For each elementary event $e \in \mathcal{E}_u$, we have:

$$\sum_{e \in \mathcal{E}_u} p(e|\mathbf{s}) = 1 \tag{4.5}$$

where $p(e|\mathbf{s})$ is the conditional probability that the elementary event e occurs, conditional on the state of the system being $\mathbf{s}$; the elementary events in $\mathcal{E}_u$ exhaust all the possible single-step changes of state that can occur to a population unit in a state u.

We wish to model the major components in membrane-bound binding events in the IL-1β network, and so need state variables which correspond to these components. To simplify, we can use some of the conservation relations introduced in the differential equations model (see 2.1); these conserved quantities are:

$$\begin{aligned}
\text{Total number of ligand molecules} &= L_T & (4.6)\\
\text{Total number of Type-I receptors} &= N_{R1} & (4.7)\\
\text{Total number of Type-II receptors} &= N_{R2} & (4.8)\\
\text{Total number of accessory proteins} &= N_{CP} & (4.9)
\end{aligned}$$

We introduce the state variables:

$$\begin{aligned}
\text{Number of free ligand molecules} &= L && (4.10) \\
\text{Number of binary Type-I complexes} &= C_1 && (4.11) \\
\text{Number of binary Type-II complexes} &= C_2 && (4.12) \\
\text{Number of ternary Type-I complexes} &= T_1 && (4.13) \\
\text{Number of ternary Type-II complexes} &= T_2 && (4.14)
\end{aligned}$$

A further conservation relation for the total number of the various protein species, or units, in the system L_T is given by:

$$L_T = L + C_1 + C_2 + T_1 + T_2 \qquad (4.15)$$

The total number of units in the system $\mathbf{N} = (L, C_1, C_2, T_1, T_2)$, and the corresponding state probability distribution $\mathbf{s} = \frac{\mathbf{N}}{L_T} = (s_0, s_1, s_2, s_3, s_4)$. Note that, as required of a probability distribution, $s_0 + s_1 + s_2 + s_3 + s_4 = 1$. We should also note that:

$$\begin{aligned}
\text{Free ligand molecules} &= L && (4.16) \\
&= L_T - (C_1 + C_2 + T_1 + T_2) \\
\text{Unbound Type-I receptors} &= N_{R1} - C_1 - T_1 && (4.17) \\
\text{Unbound Type-II receptors} &= N_{R2} - C_2 - T_2 && (4.18) \\
\text{Unbound IL-1RAcP} &= N_{CP} - T_1 - T_2 && (4.19)
\end{aligned}$$

The states we shall consider are as follows:

- $S0$: ligand

- $S1$: binary signalling complex

- $S2$: binary nonsignalling complex

- $S3$: ternary signalling complex

- $S4$: ternary nonsignalling complex

From this, we have $S = 5$. A state transition diagram is given in Figure (4.1), which shows the components we are simulating in the experiments and their relationship to each other.

4.2 Elementary events

This section details the elementary events which take the system from one state to the next. Notice that the probabilities utilise the association and dissociation rates $k_u^\pm$; however, in this context rate means probability per unit time, and so need to be scaled to convert them into probabilities. We choose the scaling so that they satisfy $\kappa k_u^\pm = \hat{k}_u^\pm \in [0, 1]$, which will be described later.
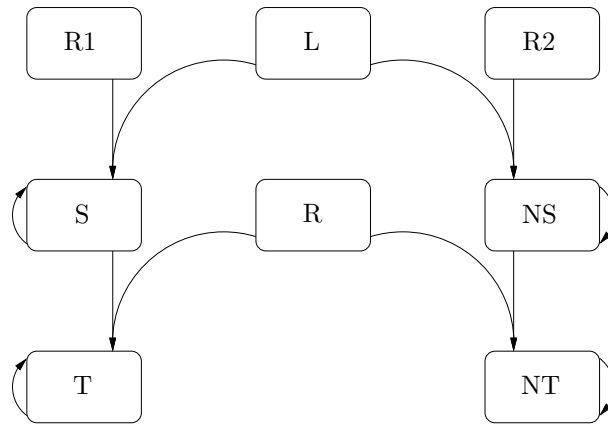
Figure 4.1: State transition diagram for the IL-1β network, where L is IL-1β, R1 is the Type-I receptor, R2 is the Type-II receptor, R is the receptor accessory, S is the signalling binary complex, NS is the nonsignalling binary complex, T is the signalling ternary complex, and NT the nonsignalling ternary complex.

4.2.1 $E1$: **Ligand binds to Type-I receptor**

Ligand encounters and binds IL-1RI, creating a signalling binary complex. If the amount of free ligand $L = 0$, state change cannot occur; neither can it occur if no free signalling receptor is available.

$$
\begin{aligned}
\text{State transition} \quad &: \quad (L, C_1) \rightarrow (L - 1, C_1 + 1) \\
\text{Probability} \quad &: \quad p(E_1|\mathbf{s}) = \hat{k}_w^+(n_{R1} - s_1 - s_3) \quad \text{per unit of free ligand} \\
\text{Change vector} \quad &: \quad \varepsilon_\mathbf{1} = (-1, 1, 0, 0, 0)
\end{aligned}
$$

where $n_{R1} = \frac{N_{R1}}{L_T}$, and $\hat{k}_w^+$ is the association rate expressed as a probability per unit time.

4.2.2 $E2$: **Ligand binds to Type-II receptor**

Ligand encounters and binds IL-1RII, creating a nonsignalling binary complex. If the amount of free ligand $L = 0$, or $C_2 = 0$, state change cannot occur.

$$
\begin{aligned}
\text{State transition} \quad &: \quad (L, C_2) \rightarrow (L - 1, C_2 + 1) \\
\text{Probability} \quad &: \quad p(E_2|\mathbf{s}) = \hat{k}_x^+(n_{R2} - s_2 - s_4) \quad \text{per unit of free ligand} \\
\text{Change vector} \quad &: \quad \varepsilon_\mathbf{2} = (-1, 0, 1, 0, 0)
\end{aligned}
$$

where $n_{R2} = \frac{N_{R2}}{L_T}$, and $\hat{k}_x^+$ is the association rate expressed as a probability per unit time.

4.2.3 $E3$: **Signalling binary binds to IL-1RAcP**

The signalling binary binds to the receptor accessory protein, creating a signalling ternary complex. If the amount of signalling binaries $C_1 = 0$, the state change cannot occur.

$$
\begin{aligned}
\text{State transition} \quad &: \quad (C_1, T_1) \rightarrow (C_1 - 1, T_1 + 1) \\
\text{Probability} \quad &: \quad p(E_3|\mathbf{s}) = \hat{k}_y^+(n_{CP} - s_3 - s_4) \\
&\qquad\qquad \text{per unit of Type-I binary complexes} \\
\text{Change vector} \quad &: \quad \varepsilon_\mathbf{3} = (0, -1, 0, 1, 0)
\end{aligned}
$$

where $n_{CP} = \frac{N_{CP}}{L_T}$, and $\hat{k}_y^+$ is the association rate between the binary Type-I complex and the accessory protein expressed as a probability per unit time.

4.2.4 $E4$: **Nonsignalling binary binds to IL-1RAcP**

The nonsignalling binary binds to the receptor accessory protein, creating a nonsignalling ternary complex. If the amount of nonsignalling binaries $C_2 = 0$, the state change cannot occur.

$$\begin{aligned}
\text{State transition} \quad &: \quad (C_2, T_2) \rightarrow (C_2 - 1, T_2 + 1) \\
\text{Probability} \quad &: \quad p(E_4|\mathbf{s}) = \hat{k}_z^+(n_{CP} - s_3 - s_4) \\
&\qquad \text{per unit of Type-II binary complexes} \\
\text{Change vector} \quad &: \quad \varepsilon_4 = (0, 0, -1, 0, 1)
\end{aligned}$$

where n_{CP} is as above, and $\hat{k}_z^+$ is the association rate between the binary Type-II complex and the accessory protein expressed as a probability per unit time.

4.2.5 $E5$: Signalling binary complex dissociates

The signalling binary complex dissociates, yielding an unbound ligand and an unbound Type-I receptor.

$$\begin{aligned}
\text{State transition} \quad &: \quad (L, C_1) \rightarrow (L + 1, C_1 - 1) \\
\text{Probability} \quad &: \quad p(E_5|\mathbf{s}) = \hat{k}_w^- \quad \text{per unit of Type-I binary complexes} \\
\text{Change vector} \quad &: \quad \varepsilon_5 = (1, -1, 0, 0, 0)
\end{aligned}$$

4.2.6 $E6$: Nonsignalling binary complex dissociates

The nonsignalling binary complex dissociates, yielding an unbound ligand and an unbound Type-II receptor.

$$\begin{aligned}
\text{State transition} \quad &: \quad (L, C_2) \rightarrow (L + 1, C_2 - 1) \\
\text{Probability} \quad &: \quad p(E_6|\mathbf{s}) = \hat{k}_x^- \quad \text{per unit of Type-II binary complexes} \\
\text{Change vector} \quad &: \quad \varepsilon_6 = (1, 0, -1, 0, 0)
\end{aligned}$$

4.2.7 $E7$: Signalling ternary complex dissociates

The signalling ternary complex dissociates, creating a signalling binary complex and a receptor accessory protein.

$$\begin{aligned}
\text{State transition} \quad &: \quad (C_1, T_1) \rightarrow (C_1 + 1, T_1 - 1) \\
\text{Probability} \quad &: \quad p(E_7|\mathbf{s}) = \hat{k}_y^- \quad \text{per unit of Type-I ternary complexes} \\
\text{Change vector} \quad &: \quad \varepsilon_7 = (0, 1, 0, -1, 0)
\end{aligned}$$

4.2.8 $E8$: Nonsignalling ternary complex dissociates

The nonsignalling ternary complex dissociates, creating a nonsignalling binary complex and a receptor accessory protein.

$$\begin{aligned}
\text{State transition} \quad &: \quad (C_2, T_2) \rightarrow (C_2 + 1, T_2 - 1) \\
\text{Probability} \quad &: \quad p(E_8|\mathbf{s}) = \hat{k}_z^- \quad \text{per unit of Type-II ternary complexes} \\
\text{Change vector} \quad &: \quad \varepsilon_8 = (0, 0, 1, 0, -1)
\end{aligned}$$

4.2.9 Event decomposition

The change-of-state vectors, along with their associated events, are:

$$E1 \quad : \quad (-1, 1, 0, 0, 0) \tag{4.20}$$
$$E2 \quad : \quad (-1, 0, 1, 0, 0) \tag{4.21}$$
$$E3 \quad : \quad (0, -1, 0, 1, 0) \tag{4.22}$$
$$E4 \quad : \quad (0, 0, -1, 0, 1) \tag{4.23}$$
$$E5 \quad : \quad (1, -1, 0, 0, 0) \tag{4.24}$$
$$E6 \quad : \quad (1, 0, -1, 0, 0) \tag{4.25}$$
$$E7 \quad : \quad (0, 1, 0, -1, 0) \tag{4.26}$$
$$E8 \quad : \quad (0, 0, 1, 0, -1) \tag{4.27}$$

where the vectors are applied to the total number of units in the system $\mathbf{N} = (L, C_1, C_2, T_1, T_2)$ such that, for example, the change-of-state vector $(-1, 1, 0, 0, 0)$ would leave the system with one less ligand and one more signalling binary.

Grouping by the units of the modified quantity:

$$\mathcal{E}_0 \quad = \quad \{\emptyset_0, E1, E2\} \quad \text{per unit of free ligand} \tag{4.28}$$
$$\mathcal{E}_1 \quad = \quad \{\emptyset_1, E3, E5\} \quad \text{per unit of Type-I binary complexes} \tag{4.29}$$
$$\mathcal{E}_2 \quad = \quad \{\emptyset_2, E4, E6\} \quad \text{per unit of Type-II binary complexes} \tag{4.30}$$
$$\mathcal{E}_3 \quad = \quad \{\emptyset_3, E7\} \quad \text{per unit of Type-I ternary complexes} \tag{4.31}$$
$$\mathcal{E}_4 \quad = \quad \{\emptyset_4, E8\} \quad \text{per unit of Type-II ternary complexes} \tag{4.32}$$

Also:

$$\mathcal{E}_0(0, 0, 0, 0, 0) \quad = \quad \{\emptyset_0\}$$
$$\mathcal{E}_0(-1, 1, 0, 0, 0) \quad = \quad \{E1\} \quad \text{per unit of free ligand}$$
$$\mathcal{E}_0(-1, 0, 1, 0, 0) \quad = \quad \{E2\} \quad \text{per unit of free ligand}$$
$$\mathcal{E}_1(0, 0, 0, 0, 0) \quad = \quad \{\emptyset_1\}$$
$$\mathcal{E}_1(0, -1, 0, 1, 0) \quad = \quad \{E3\} \quad \text{per unit of Type-I binary complexes}$$
$$\mathcal{E}_1(1, -1, 0, 0, 0) \quad = \quad \{E5\} \quad \text{per unit of Type-I binary complexes}$$
$$\mathcal{E}_2(0, 0, 0, 0, 0) \quad = \quad \{\emptyset_2\}$$
$$\mathcal{E}_2(0, 0, -1, 0, 1) \quad = \quad \{E4\} \quad \text{per unit of Type-II binary complexes}$$
$$\mathcal{E}_2(1, 0, -1, 0, 0) \quad = \quad \{E6\} \quad \text{per unit of Type-II binary complexes}$$
$$\mathcal{E}_3(0, 0, 0, 0, 0) \quad = \quad \{\emptyset_3\}$$
$$\mathcal{E}_3(0, 1, 0, -1, 0) \quad = \quad \{E7\} \quad \text{per unit of Type-I ternary complexes}$$
$$\mathcal{E}_4(0, 0, 0, 0, 0) \quad = \quad \{\emptyset_4\}$$
$$\mathcal{E}_4(0, 0, 1, 0, -1) \quad = \quad \{E8\} \quad \text{per unit of Type-II ternary complexes}$$

4.2.10 Updating the system

In this section we will look at algorithms for updating the system. Note that only certain operations can be applied to the population units when they are

in a certain state. In general, a binary or ternary complex may associate or dissociate, and a receptor may bind, but some operations are forbidden. For example, it is obviously impossible for a nonsignalling binary to become a signalling ternary.

At a systemic level, we have two options for updating the system. One of these would be sequential updating, whereby the change to a population unit would be reflected immediately in the state of the rest of the system. The other, simultaneous updating, would mean that the system state remains the same until updates have occurred to all the population units, and then applied as a whole to the rest of the system. The simultaneous update algorithm is given in algorithm (1); notice that, for brevity, only the association events are shown in the algorithm. The notation is due to the pseudocode convention of the widely used `algorithmic` package available with the text processing system LaTeX.

The simultaneous algorithm begins by making a copy of the current system state, where the state vector after updating is $\tilde{\mathbf{N}}$. The algorithm loops over the population units in the order of the units to which state changes are applicable, so that association of signalling and nonsignalling binary complexes takes place on the units of free ligand. A randomly-generated number in the range $x \in [0, 1]$ is compared to the various state change probabilities by the appropriate function invocation, for example `probabilitySignallingBinaryAssociation()`. If the random variable x is less than the probability p, a change is made, such as the formation of a signalling binary complex; if not, the algorithm goes on to the next state change for this unit.

If the state change is applicable to the currently-selected population unit, then the population unit is updated with the state change; this prevents illegal operations, for example, a binary signalling complex from binding another ligand, or becoming a ternary nonsignalling complex. Finally, once the population units have been iterated over, the modified system is copied en masse to the population unit vector ($\tilde{\mathbf{N}} \Leftarrow \mathbf{N}$).

We can now perform an experiment which looks at the role of the Type-II receptor in a Markov chain model where the resources, of receptors and receptor accessories, are constrained. Previous experiments suggest that rather a large number of Type-II receptors would be needed to form nonsignalling ternary complexes. Subsequently, we introduce a parameter q which will be used to multiply the size of the population of Type-II receptors in the system. q will be in the range $0 \le q \le 20$. The number of Type-II receptors will initially be equal to Type-I, but for $q = 0$ the receptors in the system will consist of only signalling receptors. The number of Type-II receptors will gradually increase until they are more than an order of magnitude greater in number than Type-I receptors.

Figure (4.2) shows the behaviour of the IL-1β network with constrained receptors and accessories. For low values of q, where there are very few Type-II receptors in the system, signalling ternaries form without constraint. As q, and the size of the Type-II population, increase, nonsignalling ternaries begin to increase until they reach parity with signalling ternaries.

After this point, nonsignalling ternaries form more frequently than their signalling counterparts, and the Type-II receptor would have a significant inhibitory effect on signal transduction. Also, at this point, the constrained supply of receptor accessory would have been consumed mainly by nonsignalling binary

$\tilde{\mathbf{N}} \Leftarrow \text{copySystemState}(\mathbf{N})$
$\mathbf{L} \Leftarrow \text{getLigand}(\tilde{\mathbf{N}})$ { get the free ligand state variable}
$\mathbf{R1} \Leftarrow \text{getSignallingReceptors}(\tilde{\mathbf{N}})$ { get the free ligand Type-I receptor state variable}
$\mathbf{R2} \Leftarrow \text{getNonsignallingReceptors}(\tilde{\mathbf{N}})$ { ... Type-II receptors }
$\mathbf{C1} \Leftarrow \text{getSignallingComplexes}(\tilde{\mathbf{N}})$ { ... signalling binaries }
$\mathbf{C2} \Leftarrow \text{getNonsignallingComplexes}(\tilde{\mathbf{N}})$ { ... nonsignalling binaries }
$\mathbf{RAcP} \Leftarrow \text{getReceptorAccessory}(\tilde{\mathbf{N}})$ {free receptor accessory state variable}
$\mathbf{T1} \Leftarrow \text{getSignallingTernaries}(\tilde{\mathbf{N}})$ {signalling ternaries (for possible dissociation event)}
$\mathbf{T2} \Leftarrow \text{getNonsignallingTernaries}(\tilde{\mathbf{N}})$ {nonsignalling ternaries (for possible dissociation event)}
for all i such that $0 \leq i \leq \mathbf{L}$ **do**
  $x \Leftarrow x \in [0, 1]$ {generate a random number}
  $p = \text{probabilitySignallingBinaryAssociation}()$
  if $x < p$ **then**
    $\mathbf{L} \Leftarrow \mathbf{L} - 1$ {decrement ligand state variable}
    $\mathbf{R1} \Leftarrow \mathbf{R1} - 1$ {decrement Type-I receptors}
    $\mathbf{C1} \Leftarrow \mathbf{C1} + 1$ {increment signalling binary complexes}
  end if
  $x \Leftarrow x \in [0, 1]$ {get a fresh random number}
  $p = \text{probabilityNonsignallingBinaryAssociation}()$
  if $x < p$ **then**
    $\mathbf{L} \Leftarrow \mathbf{L} - 1$ {decrement ligand state variable}
    $\mathbf{R2} \Leftarrow \mathbf{R2} - 1$ {decrement Type-II receptors}
    $\mathbf{C2} \Leftarrow \mathbf{C2} + 1$ {increment nonsignalling binary complexes}
  end if
  $x \Leftarrow x \in [0, 1]$ {this class of events works on units of Type-I binaries}
  $p = \text{probabilitySignallingTernaryAssociation}()$
  if $x < p$ **then**
    $\mathbf{C1} \Leftarrow \mathbf{C1} - 1$ {decrement signalling binary}
    $\mathbf{RAcP} \Leftarrow \mathbf{RAcP} - 1$ {decrement free receptor accessory}
    $\mathbf{T1} \Leftarrow \mathbf{T1} + 1$ {increment signalling ternaries}
  end if
  $x \Leftarrow x \in [0, 1]$ {this class of events works on units of Type-II binaries}
  $p = \text{probabilityNonsignallingTernaryAssociation}()$
  if $x < p$ **then**
    $\mathbf{C2} \Leftarrow \mathbf{C2} - 1$ {decrement nonsignalling binary}
    $\mathbf{RAcP} \Leftarrow \mathbf{RAcP} - 1$ {decrement receptor accessory}
    $\mathbf{T2} \Leftarrow \mathbf{T2} + 1$ {increment nonsignalling ternaries}
  end if
end for
$\mathbf{N} \Leftarrow \text{copySystemState}(\tilde{\mathbf{N}})$ {copy the changed units back}

Algorithm 1: `Simultaneous update` method
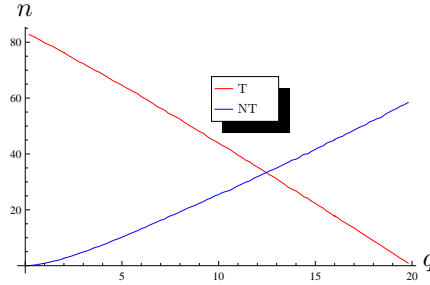
Figure 4.2: Ternary complex formation, both signalling and nonsignalling. The Type-I receptor and receptor accessory are held constant at 100. Signalling complexes T formed from IL-1β are given in red, and nonsignalling ternaries NT in blue. The number of ternaries formed is given by n. The parameter q acts as a multiplier of the Type-II receptor population. Signalling ternaries initially form rapidly, but as q increases, nonsignalling ternaries begin to dominate; at larger values of q, nonsignalling ternary formation becomes more frequent than signalling ternary.

and ternary complexes. If we accept some tens of signalling ternaries as sufficient for inducing a physiological response from a cell, a value of $q \approx 10$ would have a substantial inhibitory effect.

4.3 Stochastic model of IL-1β: receptor antagonist

In this section, we examine the effects of the interleukin-1 receptor antagonist on the dynamics of the IL-1β network, by expanding the stochastic system presented in the previous section.

We can proceed to empirically investigate the behaviour of the system, once again using stochastic simulation techniques. We develop the stochastic model by continuing the process given in Section (4.1), considering the additional elements demanded by the inclusion of the receptor antagonist. In the previous section, we assumed that there were always sufficient pools of receptors and accessory proteins to form a complex. In this section, we shall limit the number of receptors and accessory proteins and observe the effect on ternary complex formation.

Recall that $\mathcal{E}$ is the set of allowable elementary events, and let it be partitioned in the form:

$$\mathcal{E} = \bigcup_{u=0}^{S} \mathcal{E}_u \qquad (4.33)$$

which is the disjoint union of the set of events (since the elementary events are mutually exclusive), so that each event is associated with a particular population unit state u. Also, each set $\mathcal{E}_u$ contains an element signifying a nonevent, $\emptyset_u$. A population unit that is currently in state u can only be affected by those elementary events in $\mathcal{E}_u$.

Once again, we consider a large population consisting of a large number N of units, each of which can be in one of $S + 1$ possible states, indexed by

$S = 0, 1, \ldots, S$. If N_u is the number of units in a state u, then $\mathbf{N} = (N_0, \ldots, N_s)$ is the population state vector. The states we shall consider are as follows:

- $S0$: ligand

- $S1$: receptor antagonist

- $S2$: binary signalling complex

- $S3$: binary nonsignalling complex

- $S4$: ternary signalling complex

- $S5$: ternary nonsignalling complex

- $S6$: IL-1Ra/Type-I binary complex

- $S7$: IL-1RA/Type-II binary complex

- $S8$: IL-1Ra/Type-I/RAcP ternary complex

- $S9$: IL-1Ra/Type-II/RAcP ternary complex

From this, we have $S = 10$.

Before introducing state variables we make use of some conservation relations; these conserved quantities are:

$$
\begin{array}{rcll}
\text{Total number of ligand molecules} & = & L_T & (4.34) \\
\text{Total number of IL-1}\beta\text{ molecules} & = & L_\beta & (4.35) \\
\text{Total number of IL-1Ra molecules} & = & L_R & (4.36) \\
\text{Total number of Type-I receptors} & = & N_{R1} & (4.37) \\
\text{Total number of Type-II receptors} & = & N_{R2} & (4.38) \\
\text{Total number of accessory proteins} & = & N_{CP} & (4.39)
\end{array}
$$

We introduce the state variables:

$$
\begin{array}{rcll}
\text{Number of free IL-1}\beta\text{ molecules} & = & L & (4.40) \\
\text{Number of free IL-1Ra molecules} & = & R & (4.41) \\
\text{Number of binary Type-I complexes} & = & C_1 & (4.42) \\
\text{Number of binary Type-II complexes} & = & C_2 & (4.43) \\
\text{Number of ternary Type-I complexes} & = & T_1 & (4.44) \\
\text{Number of ternary Type-II complexes} & = & T_2 & (4.45) \\
\text{Number of antagonist binary Type-I complexes} & = & C_{1R} & (4.46) \\
\text{Number of antagonist binary Type-II complexes} & = & C_{2R} & (4.47) \\
\text{Number of antagonist ternary Type-I complexes} & = & T_{1R} & (4.48) \\
\text{Number of antagonist ternary Type-II complexes} & = & T_{2R} & (4.49)
\end{array}
$$

Further conservation relations for the total ligand in the system L_T can be derived from this:

$$
\begin{aligned}
L_T &= L + R + C_1 + C_2 + T_1 + T_2 + C_{1R} + C_{2R} + T_{1R} + T_{2R} \quad (4.50)\\
L_\beta &= L + C_1 + C_2 + T_1 + T_2 \quad (4.51)\\
L_R &= R + C_{1R} + C_{2R} + T_{1R} + T_{2R} = L_T - L_\beta \quad (4.52)
\end{aligned}
$$

The independent variables can be taken as $\mathbf{N} = (L, R, C_1, C_2, \cdots, T_{2R})$, and the corresponding state probability distribution as $\mathbf{s} = \frac{\mathbf{N}}{L_T} = (s_0, s_1, \cdots, s_9)$. Note that, as required of a probability distribution, $s_0 + s_1 + s_2 + s_3 + s_4 + s_5 + s_6 + s_7 + s_8 + s_9 = 1$. We should also note that:

$$
\begin{aligned}
\text{Free ligand molecules} &= L_T - (C_1 + C_2 + T_1 + T_2 \quad (4.53)\\
&\quad + C_{1R} + C_{2R} + T_{1R} + T_{2R})\\
\text{Free IL-1}\beta\text{ molecules} &= L \quad (4.54)\\
&= L_\beta - (C_1 + C_2 + T_1 + T_2)\\
\text{Free IL-1Ra molecules} &= R \quad (4.55)\\
&= L_R - (C_{1R} + C_{2R} + T_{1R} + T_{2R})\\
\text{Unbound Type-I receptors} &= N_{R1} - (C_1 + T_1 + C_{1R} + T_{1R}) \quad (4.56)\\
\text{Unbound Type-II receptors} &= N_{R2} - (C_2 + T_2 + C_{2R} + T_{2R}) \quad (4.57)\\
\text{Unbound IL-1RAcP} &= N_{CP} - (T_1 + T_2 + T_{1R} + T_{2R}) \quad (4.58)
\end{aligned}
$$

The state transition diagram given in Figure (4.3) shows the relationships between the various components being modelled. Notice the centrality of both receptors, and the receptor accessory protein, to the IL-1β network.

4.4   Elementary events

This section details the elementary events which takes the enhanced IL-1Ra system from one state to the next. Notice that the probabilities utilise the association and dissociation rates $k_u^{\pm}$; however, these rates must be scaled so that they satisfy $\kappa k_u^{\pm} = \hat{k}_u^{\pm} \in [0, 1]$, which will be described later. The previous set of elementary events, which also apply to this model, are given in Section (4.2), and so will not be given here.

4.4.1 $E9$: IL-1Ra binds to Type-I receptor

A particle of IL-1Ra encounters and binds to IL-1RI, creating a binary complex. If the amount of free receptor antagonist $R = 0$, the state change cannot occur.

$$
\begin{aligned}
\text{State transition} \quad &: \quad (R, C_{1R}) \to (R - 1, C_{1R} + 1)\\
\text{Probability} \quad &: \quad p(E_9|\mathbf{s}) = \hat{k}_{raw}^{+}(n_{R1} - s_2 - s_4 - s_6 - s_8) \quad \text{per unit of free IL-1Ra}\\
\text{Change vector} \quad &: \quad \varepsilon_{\mathbf{9}} = (0, -1, 0, 0, 0, 0, 1, 0, 0, 0)
\end{aligned}
$$

where $n_{R1} = \frac{N_{R1}}{L_T}$, and $\hat{k}_{raw}^{+}$ is the association rate expressed as a probability per unit time.
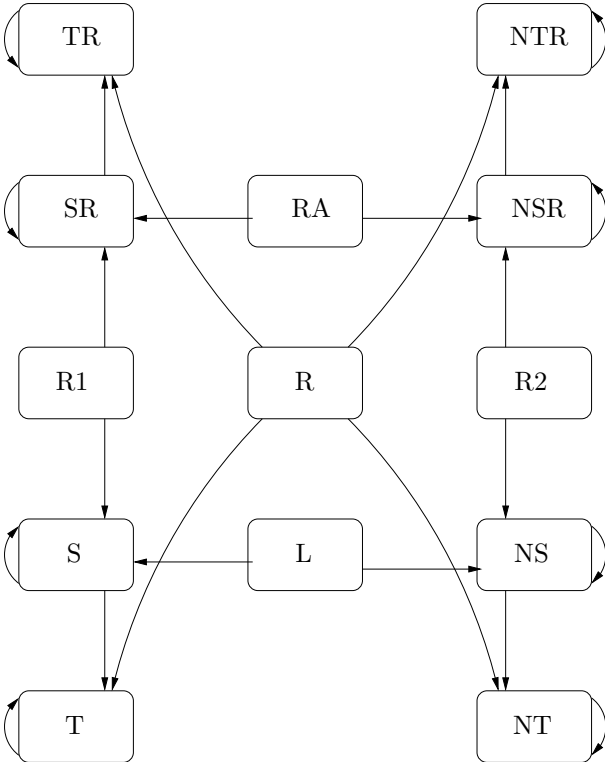
Figure 4.3: State transition diagram for IL-1β network, where L is IL-1β, R1 is the Type-I receptor, R2 is the Type-II receptor, R is the receptor accessory, S is the signalling binary complex, NS is the nonsignalling binary complex, T is the signalling ternary complex, NT the nonsignalling ternary complex, RA is the receptor antagonist, SR is the signalling binary (antagonist) complex, NSR is the nonsignalling binary (antagonist) complex, TR is the signalling ternary (antagonist) complex, and NTR the nonsignalling ternary (antagonist) complex.

4.4.2 $E10$: **IL-1Ra binds to Type-II receptor**

The receptor antagonist ligand encounters and binds to IL-1RII, creating a binary complex. If the amount of free ligand $R = 0$, the state change cannot occur.

$$\text{State transition} \quad : \quad (R, C_{2R}) \to (R - 1, C_{2R} + 1)$$
$$\text{Probability} \quad : \quad p(E_{10}|\mathbf{s}) = \hat{k}_{rax}^{+}(n_{R2} - s_3 - s_5 - s_7 - s_9) \quad \text{per unit of free IL-1Ra}$$
$$\text{Change vector} \quad : \quad \varepsilon_{\mathbf{10}} = (0, -1, 0, 0, 0, 0, 0, 1, 0, 0)$$

where $n_{R2} = \frac{N_{R2}}{L_T}$, and $\hat{k}_{rax}^{+}$ is the association rate expressed as a probability per unit time.

4.4.3 $E11$: **IL-1Ra/Type-I binary binds to IL-1RAcP**

The IL-1Ra/Type-I binary binds to the receptor accessory protein, creating a IL-1Ra/Type-I/RAcP ternary complex. If the amount of IL-1Ra/Type-I binaries $C_{1R} = 0$, the state change cannot occur.

$$\text{State transition} \quad : \quad (C_{1R}, T_{1R}) \to (C_{1R} - 1, T_{1R} + 1)$$
$$\text{Probability} \quad : \quad p(E_{11}|\mathbf{s}) = \hat{k}_{ray}^{+}(n_{cp} - s_3 - s_4)$$
$$\text{per unit of IL-1Ra/Type-I binary complexes}$$
$$\text{Change vector} \quad : \quad \varepsilon_{\mathbf{11}} = (0, 0, 0, 0, 0, 0, -1, 0, 1, 0)$$

where $n_{CP} = \frac{N_{CP}}{L_T}$, and $\hat{k}_{ray}^{+}$ is the association rate between the antagonist/Type-I complex and the accessory protein expressed as a probability per unit time.

4.4.4 $E12$: **IL-1Ra/Type-II binary binds to IL-1RAcP**

The IL-1Ra/Type-II binary binds to the receptor accessory protein, creating a IL-1Ra/Type-II/RAcP ternary complex. If the amount of IL-1Ra/Type-II binaries $C_{2R} = 0$, the state change cannot occur.

$$\text{State transition} \quad : \quad (C_{2R}, T_{2R}) \to (C_{2R} - 1, T_{2R} + 1)$$
$$\text{Probability} \quad : \quad p(E_{12}|\mathbf{s}) = \hat{k}_{raz}^{+}(n_{cp} - s_3 - s_5 - s_8 - s_9)$$
$$\text{per unit of IL-1Ra/Type-II binary complexes}$$
$$\text{Change vector} \quad : \quad \varepsilon_{\mathbf{12}} = (0, 0, 0, 0, 0, 0, 0, -1, 0, 1)$$

where n_{CP} is as above, and $\hat{k}_{raz}^{+}$ is the association rate between the IL-1Ra/Type-II complex and the accessory protein expressed as a probability per unit time.

4.4.5 $E13$: **IL-1Ra/Type-I binary complex dissociates**

The IL-1Ra/Type-I binary complex dissociates, yielding an unbound receptor antagonist and an unbound Type-I receptor.

State transition   : $(R, C_{1R}) \rightarrow (R+1, C_{1R}-1)$

Probability   : $p(E_{13}|\mathbf{s}) = \hat{k}_{raw}^{-}$ per unit of IL-1Ra/Type-I binary complexes

Change vector   : $\varepsilon_{\mathbf{13}} = (0, 1, 0, 0, 0, 0, -1, 0, 0, 0)$

4.4.6 $E14$: IL-1Ra/Type-II binary complex dissociates

The IL-1Ra/Type-II binary complex dissociates, yielding an unbound receptor antagonist and an unbound Type-II receptor.

State transition   : $(R, C_{2R}) \rightarrow (R+1, C_{2R}-1)$

Probability   : $p(E_{14}|\mathbf{s}) = \hat{k}_{rax}^{-}$ per unit of IL-1Ra/Type-II binary complexes

Change vector   : $\varepsilon_{\mathbf{14}} = (0, 1, 0, 0, 0, 0, 0, -1, 0, 0)$

4.4.7 $E15$: IL-1Ra/Type-I/RAcP ternary complex dissociates

The IL-1Ra/Type-I/RAcP ternary complex dissociates, creating a IL-1Ra/Type-I binary complex and a receptor accessory protein.

State transition   : $(C_{1R}, T_{1R}) \rightarrow (C_{1R}+1, T_{1R}-1)$

Probability   : $p(E_{15}|\mathbf{s}) = \hat{k}_{ray}^{-}$ per unit of IL-1Ra/Type-I/RAcP ternary complexes

Change vector   : $\varepsilon_{\mathbf{15}} = (0, 0, 0, 0, 0, 0, 1, 0, -1, 0)$

4.4.8 $E16$: IL-1Ra/Type-II/RAcP ternary complex dissociates

The IL-1Ra/Type-II/RAcP ternary complex dissociates, creating a IL-1Ra/Type-II binary complex and a receptor accessory protein.

State transition   : $(C_{2R}, T_{2R}) \rightarrow (C_{2R}+1, T_{2R}-1)$

Probability   : $p(E_{16}|\mathbf{s}) = \hat{k}_{ray}^{-}$ per unit of IL-1Ra/Type-II/RAcP ternary complexes

Change vector   : $\varepsilon_{\mathbf{16}} = (0, 0, 0, 0, 0, 0, 0, 1, 0, -1)$

4.4.9   Event decomposition

The change-of-state vectors, including those adapted from the stochastic model without the receptor antagonist (see ...),along with their associated events, are:

$$
\begin{array}{rll}
E1 & : & (-1,0,1,0,0,0,0,0,0,0) & (4.59) \\
E2 & : & (-1,0,0,1,0,0,0,0,0,0) & (4.60) \\
E3 & : & (0,0,-1,0,1,0,0,0,0,0) & (4.61) \\
E4 & : & (0,0,0,-1,0,1,0,0,0,0) & (4.62) \\
E5 & : & (1,0,-1,0,0,0,0,0,0,0) & (4.63) \\
E6 & : & (1,0,0,-1,0,0,0,0,0,0) & (4.64) \\
E7 & : & (0,0,1,0,-1,0,0,0,0,0) & (4.65) \\
E8 & : & (0,0,0,1,0,-1,0,0,0,0) & (4.66) \\
E9 & : & (0,-1,0,0,0,0,1,0,0,0) & (4.67) \\
E10 & : & (0,-1,0,0,0,0,0,1,0,0) & (4.68) \\
E11 & : & (0,0,0,0,0,0,-1,0,1,0) & (4.69) \\
E12 & : & (0,0,0,0,0,0,0,-1,0,1) & (4.70) \\
E13 & : & (0,1,0,0,0,0,-1,0,0,0) & (4.71) \\
E14 & : & (0,1,0,0,0,0,0,-1,0,0) & (4.72) \\
E15 & : & (0,0,0,0,0,0,0,1,0,-1,0) & (4.73) \\
E16 & : & (0,0,0,0,0,0,0,0,1,0,-1) & (4.74)
\end{array}
$$

and so, grouping by the units of the modified quantity:

$$
\begin{array}{rll}
\mathcal{E}_0 & = & \{\emptyset_0, E1, E2\} \quad \text{per unit of free ligand} & (4.75) \\
\mathcal{E}_1 & = & \{\emptyset_1, E3, E5\} \quad \text{per unit of Type-I binary complexes} & (4.76) \\
\mathcal{E}_2 & = & \{\emptyset_2, E4, E6\} \quad \text{per unit of Type-II binary complexes} & (4.77) \\
\mathcal{E}_3 & = & \{\emptyset_3, E7\} \quad \text{per unit of Type-I ternary complexes} & (4.78) \\
\mathcal{E}_4 & = & \{\emptyset_4, E8\} \quad \text{per unit of Type-II ternary complexes} & (4.79) \\
\mathcal{E}_5 & = & \{\emptyset_5, E9, E10\} \quad \text{per unit of free receptor antagonist} & (4.80) \\
\mathcal{E}_6 & = & \{\emptyset_6, E11, E13\} \quad \text{per unit of free IL-1Ra/Type-I binary} & (4.81) \\
\mathcal{E}_7 & = & \{\emptyset_7, E12, E14\} \quad \text{per unit of free IL-1Ra/Type-II binary} & (4.82) \\
\mathcal{E}_8 & = & \{\emptyset_8, E15\} \quad \text{per unit of IL-1Ra/Type-I/RAcP ternary} & (4.83) \\
\mathcal{E}_9 & = & \{\emptyset_9, E16\} \quad \text{per unit of IL-1Ra/Type-II/RAcP ternary} & (4.84)
\end{array}
$$

4.5   Ternary complex formation in presence of IL-1Ra

Using the constrained resources model, where receptors and accessory proteins have a limited supply, we can experiment to observe the effect of the presence of the receptor antagonist on the formation of signalling ternary. The experiment considers competition for the Type-I receptor between IL-1β and IL-1Ra, and further competition between both types of binary complexes (signalling and antagonist signalling) for the receptor accessory.

We will begin by looking at the effect on IL-1β ternary signalling complex formation in the presence of the receptor antagonist, gradually increasing the
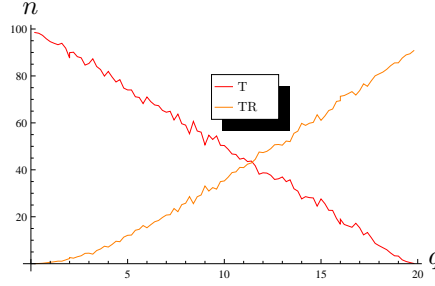
Figure 4.4: Ternary complex formation, both signalling and antagonist. The Type-I receptor and receptor accessory are held constant at 100. Signalling complexes formed from IL-1β are given in red, and antagonist ternaries in orange. The number of ternaries formed is given by n. The parameter q acts as a multiplier of the antagonist population, while the amount of IL-1β is held constant. Signalling ternaries initially form rapidly, but as q increases, antagonist ternaries begin to dominate; at larger values of q, antagonist ternary formation becomes more frequent than signalling ternary.

amount of IL-1Ra in the system. The simulation will initially have the same amount of IL-1β and receptor antagonist; however, we once again make use of a parameter q, where $0 \leq q \leq 20$, which is used as a multiplier of the antagonist population. The number of Type-I receptors and accessory proteins are kept constant throughout. We will ignore the Type-II receptor for the moment, choosing to include it in a later experiment.

$$
\begin{aligned}
\text{Total number of IL-1}\beta \text{ molecules} \quad &= \quad L_\beta & (4.85)\\
\text{Total number of IL-1Ra molecules} \quad &= \quad L_R & (4.86)\\
\text{Total number of ligand molecules} \quad &= \quad L_T = L_\beta + L_R & (4.87)\\
\text{Total number of Type-I receptors} \quad &= \quad N_{R1} = L_\beta + L_R & (4.88)\\
\text{Total number of accessory proteins} \quad &= \quad N_{CP} = L_\beta + L_R & (4.89)
\end{aligned}
$$

The experiment was repeated for $N = 1000$ trials for each value of the parameter q. The maximum number of iterations available to each simulation is $n = 5.0 \times 10^5$.

The effect on signalling ternary formation is shown in Figure (4.4). The signalling ternaries are given in red, and the antagonist ternaries in orange. It can be seen that the effect of increasing the amount of antagonist in the system via increasing q has a significant effect on ternary formation.

The experiment allows us to observe that, for low values of q, IL-1β remains capable of forming a sufficient number of signalling complexes to initiate signal transduction. However, increasing values of q yields an increasingly large population of receptor antagonist, and a decreasing number of signalling ternary formation. This is to be expected from the relative size of the association probabilities.

As the receptor antagonist population reaches approximately ten times the size of the IL-1β population, it forms approximately the same amount of ternaries. For higher values of q, formation of antagonist ternaries outnumbers signalling ternaries. Recall that some tens of signalling ternary formation events are required for signalling transduction to evoke a significant physiological re-

sponse from the cell. The antagonist is competing with IL-1β for Type-I receptors and receptor accessory, and a significant value of q would be above ten, where we have approximately a ten-to-one ratio between IL-1Ra and IL-1β and a roughly equal formation of both types of ternaries.

Since the availability of Type-I receptors and receptor accessory are constrained, the experiment shows that a sufficiently large number of receptor antagonists are likely to inhibit signal transduction. A ratio of ten-to-one in favour of the receptor antagonist is likely to impede formation of sufficient signalling ternaries for signal transduction.

4.6   Ternary complex formation in the presence of IL-1Ra and Type-II receptor

The addition of the IL-1 receptor antagonist to the type of stochastic model given in the last chapter implies an increase in complexity in the model's structure. The receptor antagonist is a ligand capable of binding to the Type-I and Type-II receptors, capable of forming both binary and ternary complexes. This effectively doubles the dimensions of the stochastic model.

From earlier sections (Section (4.3), (4.5)) , we know that both the Type-II receptor and the antagonist can have an inhibitory effect on signalling ternary formation. Varying the amount of receptor antagonist, while keeping other quantities fixed, would show the degree of synergy between the antagonist and both receptors, and determine the inhibitory effect of the antagonist.

The results of the simulations are shown in Figure (4.5). All four species of ternary are shown. Figure (4.5(a)) shows ternaries formed with IL-1β, Figure (4.5(b)) those formed with the antagonist, and Figure (4.5(c)) shows both together for ease of comparison. The formation of signalling binaries grows gradually less frequent as q increases, and signalling ternary formation is eventually almost completely inhibited.

The q parameter varies over $0 \leq q \leq 20$ and multiplies the antagonist population. As in Section (3.2.2), there is a synergistic effect between the antagonist and the Type-II receptor. Since there are more receptor antagonists the system can change state to, IL-1β ligand is given greater opportunity to form nonsignalling ternaries. This would confirm the observation in the earlier section, where a slowing effect on signalling ternary formation was found to occur, since nonsignalling ternary and antagonist ternary formation would add to the mean Markov chain length of all ternaries. Similarly, the probability of association of antagonist binaries and nonsignalling binaries are quite similar, making the probabilistic choice between the two states difficult to distinguish.

4.7   Human parameter experiments

In order to explore biologically relevant and realistic ranges of these parameters, we turn to the literature to ascertain the likely number of molecules on an average human cell membrane. We require the number of Type-I and Type-II receptors, and the number of receptor accessory proteins, likely to be expressed on the average human cell.
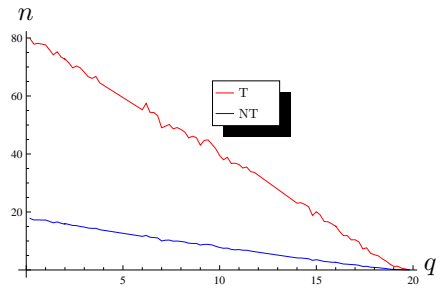
(a) IL-1β signalling/nonsignalling ternary
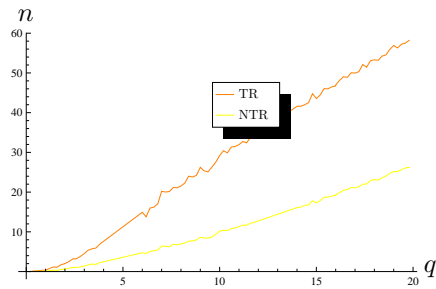
(b) IL-1Ra signalling/nonsignalling ternary
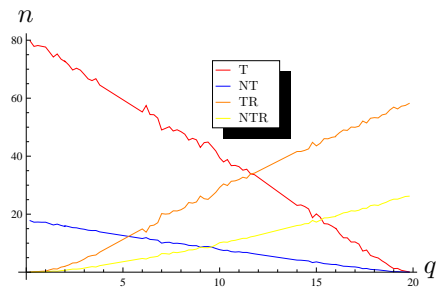
(c) Comparison of all complexes

Figure 4.5: Ternary complex formation: IL-1β, and the Type-I receptor and Type-II receptors are held constant at 100. In Figure (4.5(a)), signalling complexes T are given in red, and nonsignalling ternaries NT in blue. The number of ternaries formed is given by n. The parameter q acts as a multiplier of the antagonist population. The formation of signalling binaries grows gradually less frequent as q increases, and signalling ternary formation is eventually almost completely inhibited. Figure (4.5(b)) shows the formation of antagonist ternaries: the antagonist ternary formed with a Type-I receptor, TR, is given in orange, and the ternary formed with a Type-II receptor, NTR, is given in yellow. Both ternaries increase gradually on increasing q. Figure (4.5(c)) gives all the ternaries for ease of comparison.

Schotanus et al found a range of 900-1800 Type-I receptors expressed on the murine cell membrane on EL4 cells (85); Dubois et al found an average of 400 receptors were found to be expressed on both murine and human bone marrow cells (26); and an investigation of human synovial fibroblasts by Sadouk et al (79) found that they expressed an average of 1300 Type-I receptors on the cell membrane.

Given these observations, it seems that an estimated range for Type-I receptors R would be $200 \leq R \leq 2000$. Similar observations in both human and murine cells give a similar range for the Type-II receptor (61), (8), (9), (43), (14), and the receptor accessory protein (105),(58),(44), so that for a generalised parameter U, where U stands for any of the parameters in the system, we would have $200 \leq U \leq 2000$.

However, we are interested in the effect of constraints on ternary formation, particularly on signalling complexes, and so we shall restrict the experiment to the lower end of this range; in particular, we will investigate $50 \leq U \leq 500$. We assume that a significant cell response occurs at fifty signalling ternaries, and accordingly fix the amount of IL-1β available to the system to this amount; the other quantities will be allowed to vary.

An analysis of the parameters may reveal cases of redundancy, which will enable us to reduce the computational resources required by the experiment.

We can form the ratios

$$\alpha_1 = \frac{CRI}{CR} \quad = \quad \text{Type-I/complex formation proteins} \tag{4.90}$$

$$\alpha_2 = \frac{CRII}{CR} \quad = \quad \text{Type-II/complex formation proteins} \tag{4.91}$$

$$\beta = \frac{CAP}{CR} \quad = \quad \text{IL-1RAcP/complex formation proteins} \tag{4.92}$$

$$\frac{L}{CR} \quad = \quad \text{IL-1}\beta\text{/complex formation proteins} \tag{4.93}$$

$$\frac{Ra}{CR} \quad = \quad \text{IL-1Ra /complex formation proteins} \tag{4.94}$$

α_1 gives the ratio of the total number of signalling receptors to the total number of complex formation proteins; α_2 gives the ratio of the total number of nonsignalling receptors to the total number of complex formation proteins. β gives the total number of receptor accessory proteins to the complex formation proteins. $\frac{L}{CR}$ is ratio of the total IL-1β to the complex formation proteins, and $\frac{Ra}{CR}$ gives the total receptor antagonist to the complex formation proteins. Recall from the analysis in Chapter (2) that the ratios of the ligand and the receptor accessory protein to the total number of receptors are primary in determining the equilibrium of the system.

We wish to examine the effect of varying these parameters on system dynamics. For a general parameter U, we would vary the parameter such that, for example:

$$50 \leq U \leq 500, \{U : 100, 150, \cdots, 500\} \tag{4.95}$$

One advantage of considering the parameters as ratios is to identify equivalent sets of parameters; if the ratios are the same (after reduction to their simplest

Table 4.1: Parameter set: stochastic model of ternary complex formation in the presence of IL-1Ra and the Type-II receptor.

IL-1β	IL-1Ra	Type-I	Type-II	IL-1RAcP
50	50	100	100	200
50	100	150	150	300
50	150	200	200	400
50	200	250	250	500
50	250	300	300	600
50	300	350	350	700
50	350	400	400	800
50	400	450	450	900
50	450	500	500	1000

(a) 50 IL-1Ra, 100 R1, 100 R2, 200 RAcP   (b) 100 IL-1Ra, 150 R1, 150 R2, 300 RAcP

(c) 150 IL-1Ra, 200 R2, 200 R2, 200 RacP   (d) 200 IL-1Ra, 250 R1, 250 R2, 500 RAcP
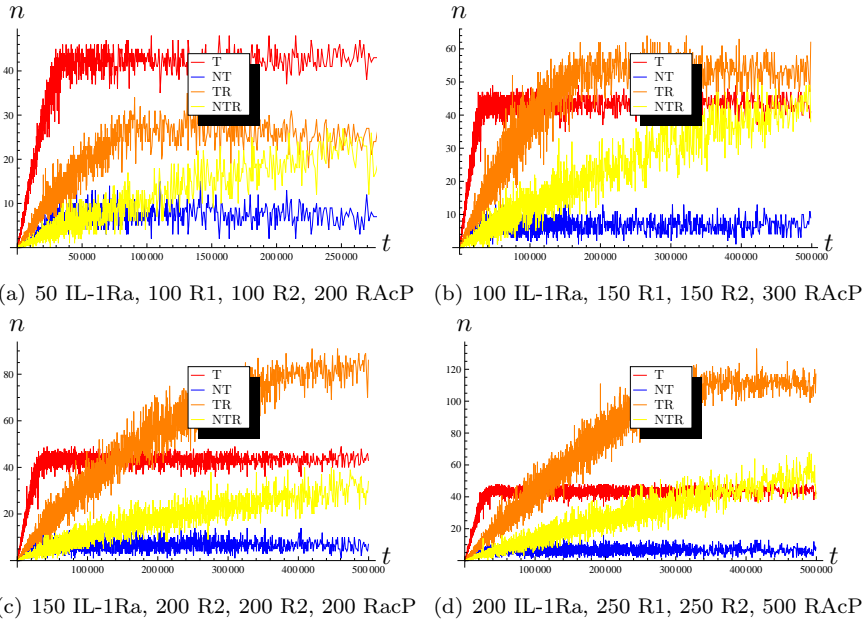
Figure 4.6: Ternary complex, all four species. Signalling complexes T are given in red, nonsignalling NT in blue; the antagonist ternary formed with a Type-I receptor, TR, is given in orange, and the ternary formed with a Type-II receptor, NTR, is given in yellow.

forms), we need consider only one of the identical sets of parameters, thereby eliminating redundancy and reducing the parameter space and the computational resources required.

We can set up an experiment to investigate what effect the introduction of ranges of parameters from the literature has on the system dynamics. The parameters used in the experiment are given in Table (4.1). Figure (4.6) shows the results of the experiment.

The data presented in the figure has been averaged, but the simulation can terminate whenever it has exhausted all the ligand. This leads to a stochastic or random appearance to the plots, since some simulations will terminate at a t which no other simulation terminates at, so that it is the only data point at

Table 4.2: Results of simulation: stochastic model of ternary complex formation in the presence of IL-1Ra and the Type-II receptor. IL-1β is held fixed at fifty. T gives the mean signalling ternaries, NT, the nonsignalling ternaries, TR the antagonist-Type-I ternaries, NTR the antagonist-Type-II ternaries.

IL-1Ra	Type-I	Type-II	IL-1RAcP	T	NT	TR	NTR
50	100	100	200	42.28	7.71	26.63	23.36
100	150	150	300	43.17	6.82	53.61	44.10
150	200	200	400	43.36	6.63	82.24	51.33
200	250	250	500	43.50	6.49	111.33	54.69
250	300	300	600	43.58	6.41	140.77	56.74
300	350	350	700	43.71	6.29	169.34	59.21
350	400	400	800	43.75	6.25	190.01	61.27
400	450	450	900	43.74	6.25	197.46	64.65
450	500	500	1000	43.81	6.18	202.67	62.81

this time t, and therefore cannot be averaged against other simulations. The simulations were repeated for $N = 1000$ trials. At no point in any of the trials did the required fifty signalling ternaries form, as can be seen from the figures and Table (4.2).

The figures show that the presence of Type-II receptors, where the numbers of Type-I and Type-II receptors are equal, seem to impede ternary complex formation sufficiently to prevent signal transduction, given the arbitrary (and conservative) requirement of fifty signalling ternaries. In the case of IL-1β, the complexes form rapidly, utilising many of the available Type-I receptors, whereas the receptor antagonist ligand forms ternary complexes at a slower rate. This is to be expected, given the respective association probabilities. Similarly, increasing amounts of receptor antagonist inhibits signalling ternary formation.

The effect of constraining the receptors and receptor accessories can be seen in the difference between, for example, the antagonist-IL-1β ternaries in Figure (4.6(a)) and Figure (4.6(b)). The parameters for the first figure are: IL-1$\beta = 50$, IL-1Ra = 50, Type-I = 100, Type-II = 100, IL-1RAcP = 200. In the second figure, we have the parameters: IL-1$\beta = 50$, IL-1Ra = 100, Type-I = 150, Type-II = 150, IL-1RAcP = 300.

In the first figure, the antagonist ternary complexes binding the Type-I receptor reach equilibrium at a level below that of the signalling ternary complexes. In the second figure, there are a greater number of both Type-I receptors and receptor accessories; the antagonist can continue to form ternary complexes and sequester resources that could be available to further IL-1β stimulus. The Type-II receptor and receptor antagonist can therefore both inhibit signal transduction, and consume resources which would be available to further interleukin stimulus.

Table (4.2) gives the mean number of ternaries formed for each set of parameters. This confirms that the mean number of signalling ternaries does not reach the arbitrary target of fifty. Relatively few nonsignalling ternaries, both IL-1β and antagonist-bound, are formed, but this is sufficient to prevent signalling transduction. As the number of available receptors and receptor accessories increases, the number of antagonist-bound ternaries increase. Some of these are bound to the Type-II receptor, but a greater number are bound to Type-I recep-

tors. Furthermore, nonsignalling complexes, both IL-1β- and antagonist-bound, continue to form after all possible signalling ternaries have been formed.

We have designed an experiment where the number of receptors and receptor accessories are constrained: it is not *assumed* that a protein will be available to form a binary complex, and an accessory protein to form a ternary complex; they must be assigned from a finite pool. Type-I receptors bound to the receptor antagonist, whether binary or ternary, make them unavailable to IL-1β. Similarly, ligand bound to the Type-II receptor may consume the accessory protein; insufficient available accessory protein will prevent signal transduction.

There are therefore two effects from the presence of the receptor antagonist on signalling transduction. Nonsignalling ternaries consume the receptor accessory, and Type-I-antagonist complexes consume the signalling receptor and the accessory protein, thereby making them unavailable for forming signalling ternary complexes. Antagonist ternaries also continue to form after IL-1β has been consumed, sequestering receptors and accessories and making them unavailable to further IL-1β stimulus.

Chapter 5

Lipid rafts and signalling

5.1 Introduction

In recent years the classical image of the plasma membrane lipid bilayer, a uniformly structured two-dimensional fluid acting as a medium for the diffusion of membrane proteins, has been modified substantially. It has been suggested that the plasma membrane is a more complex and compartmentalised structure than previously thought. This greater complexity is thought to be driven by a variety of lipid-lipid, lipid-protein and cytoskeletal interactions (2), (27), (57), (67). Separation of cholesterol enriched domains has been clearly demonstrated in both model and biological membranes, although the size and duration of lipid rafts is still to be determined (91).

Lipid rafts are areas of higher viscosity in comparison to the surrounding cell membrane, and this higher viscosity might capture membrane proteins as they move over the cell surface (66). It has been suggested that a major biological role which lipid rafts fulfil is to transport receptors and other related proteins around the cell membrane. If this is the case, they would play an important part in signal transduction (96), since they would intensify protein-protein interaction.

IL-1β is an essential part of the inflammatory process, triggering a rapid response to injury and/or infection, but has relatively few receptors expressed on the cell membrane. Since it plays such an integral part in mediating the host's defences, it is important that IL-1β signal transduction occurs rapidly. This work tests the hypothesis: do lipid rafts promote IL-1β signal transduction?

5.2 Lipid raft hypothesis

According to Cavalli (12), a lipid raft is a cholesterol-enriched microdomain in cell membranes. Lipids can broadly be defined as any hydrophobic naturally occurring molecule, and the term more specifically refers to fat-soluble acids such as cholesterol.

In 1972 the Singer-Nicolson fluid mosaic membrane model encapsulated the state-of-the-art theory on the organisation of membrane bound molecules in the plasma membrane of cells in general: a strong emphasis was placed on the dynamic behaviour of molecular elements in particular (94). The lipid microdomain concept, originally suggested more than two decades ago (52), was
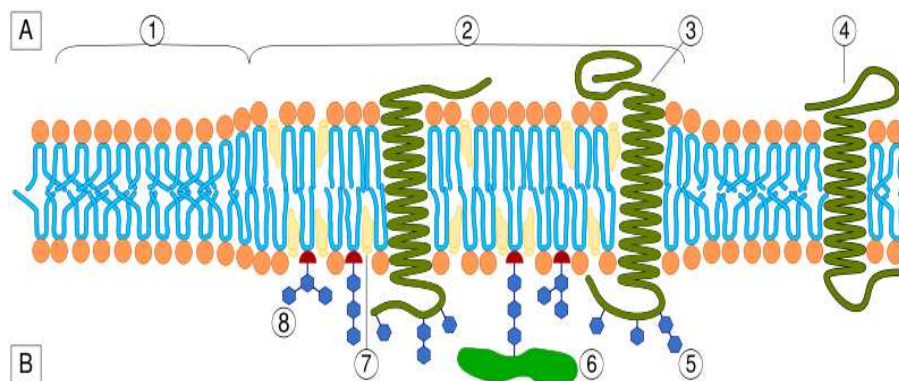
Figure 5.1: Schematic of lipid raft. ©Wikimedia Commons (freely licensed). The section labelled A represents intracellular, cytosolic space, and B, extracellular space. Furthermore, we have (1) Non-raft membrane, (2) Lipid raft, (3) Lipid raft associated transmembrane protein, (4) Non-raft membrane protein, (5) Glycosylation modifications (on glycoproteins and glycolipids), (6) GPI-anchored protein, (7) Cholesterol, (8) Glycolipid

based on lipid distribution heterogeneity analysis and structural perturbation assays in biomembranes. A number of observations reported on non-random and distinctive membrane associated patterns on the surface of live cells; many of these were made using fluorescence resonance energy transfer (FRET) techniques (100), (18). These observations raised questions about the widely-held fluid mosaic model of membranes.

Simons and Ikonen were the first to suggest the raft hypothesis (91). An overall view of the evidence and collected data indicate that glycosphigolipids (GSLs) form small, liquid ordered phase microdomains in phospholipid bilayers (107). These GSL microdomains are further stabilised with cholesterol, sometimes reinforced with cholesterol binding proteins such as caveolins. The microdomains may promote compartmentalisation of raft-associated proteins, such as receptors, and their spatial segregation from proteins excluded from rafts. These properties suggest that lipid rafts may be fundamental agents in the signal transduction process, through bringing together receptors with their signal transmitting, converting, and/or amplifying molecules while excluding other, for example inhibitory, proteins from these compartments. Figure (5.1) shows the structure of a lipid raft.

Novel single molecule techniques and FRET-based experiments showed that clusters of proteins consist of only a few proteins, and may only exist for a lifetime in the range of milliseconds (89). Rafts may facilitate distinct protein-protein interactions by increasing their local concentration and hence the probability for contact of signalling molecules. Moreover, results from single molecule tracking indicate that receptor ligation contributes to raft stabilisation, as shown for the receptor CD59 (57). A variety of other observational techniques have been applied to the problem of determining the size of lipid rafts. These have resulted in estimates converging on the region of five to fifty nm, with more recent estimates suggesting the lower end of this range (78), (77), (89).

Microdomains are larger than single membrane proteins, and so the rate of diffusion over the cell membrane of encapsulated proteins will be lower than that

of those anchored purely in the cell membrane itself (77). One way of approaching such questions would be to implement a stochastic, Monte Carlo model of the dynamics of protein interactions on a cell membrane, with signalling proteins encapsulated in microdomains of various sizes: such an approach has been tried in a recent paper (72). The paper allowed for a certain porousness of the microdomains, in that receptors and other associated proteins could enter and leave the raft; similarly, the work did not focus on the effect of the microdomains on the efficacy of signalling complex formation. The work was also quite generalised, since no specific types of receptor or ligand were modelled. We intend to apply a modelling technique to the IL-1β network derived from the approach by Nicolau et al, to attempt to determine a similar estimate of the size of the lipid rafts which are involved in supporting the formation of signalling and nonsignalling ternary complexes (72).

5.3   Simulation methods

The aim of the simulation is to see whether the presence of lipid rafts significantly enhances the formation of ternary complexes on the cell membrane. Cell membranes will be simulated both with and without lipid rafts, and the number of time steps taken to generate a fixed number of signalling complexes will be recorded.

It is appropriate at this point to consider the more general discussion surrounding lipid rafts. Despite many observation techniques and putative observations, the ontological status of lipid rafts is still mildly controversial. Given this, it may be better to suggest a more abstract entity, high viscosity regions (HVRs). This will enable us to investigate the effect which areas of higher viscosity have on the formation of signalling complexes, while remaining agnostic as to their cause.

The cell membrane is modelled as a two dimensional grid. A node, or grid point, is an element of the grid which can either be occupied or unoccupied by a protein at each time step. Only one protein may occupy a node at any one time, a principle known as volume exclusion. A protein may interact with another protein only if the two proteins are strictly contiguous, that is, they occupy neighbouring grid points. Each node is assumed to be 2 nm on each side, an estimate of the average size of a membrane (or microdomain) anchored protein (72). This gives a guide to the lower limit of the size of a HVR, and allows us to simply state the size of the cell membrane used in the simulation.

A HVR is modelled as a collection of nodes. A particularly simple representation would be to use a square: other models have used a disk in their simulation (72), although given the nature of the simulation (effectively a cellular automaton with Monte Carlo motivated probabilistic updating rules), it is arguable to what extent one representation is any more realistic than the other. It is likely that a microdomain is more amorphous, complex and ephemeral than either of these fixed shapes. The modelled HVRs will have different surface areas and densities on the simulated membrane, but these parameters will remain fixed for any particular execution of the simulation.

The simulation will initially randomly distribute a variety of different protein species among the HVRs; since we are investigating the IL-1β cytokine network, these species are IL-1RI and IL-1RAcP. The effect of extracellular inhibitory

proteins or receptors such as IL-1RII will not be included in this model, since we are interested in protein dynamics on the cell surface: for the purposes of the simulation, the total number of ternary complexes are more important than whether or not the complex initiates a signalling cascade.

The microdomains will also have empty grid points, allowing the proteins to move about on the HVR and interact (89). Since receptors and accessory proteins are relatively rare structures on the cell surface, the sparsity of receptors and accessory proteins will be reflected in the simulation, so that most of the membrane will be empty, although the number of proteins will be exaggerated for the purposes of computational tractability and sample size. Each node is initialised with two characteristics, an (x, y) coordinate which determines its location in the grid, and either one of the protein species or an empty status.

It is necessary for the modelled receptors and accessory proteins to be able to interact; proteins on the membrane are affected by random movements, caused by Brownian motion. At each time step, a protein is chosen in turn from the population of proteins. A neighbouring (contiguous) grid point is also chosen at random: note that the selection includes the grid point currently being occupied, so that it is possible to generate a non-move (a stayput). Since the grid is to be modelled in a similar manner to a cellular automaton, we have chosen a representation where the neighbourhood consists of nine grid points; those that surround the grid point, and the grid point itself. Each possible move has an equal probability of being chosen. Note that there is no distinction made between the species regarding the speed with which they move; although it is physically possible that this is the case, it is unlikely that differing velocities of protein species will make much difference at the level of detail of the simulation. There is, however, a difference between proteins encapsulated on a HVR and those which are free proteins, that is, those which are anchored in the cell membrane but which do not form part of a microdomain; differing diffusion rates will be dealt with below.

If the chosen grid point is empty, then the protein can move to it, and the previously occupied grid point will be given the empty status: if the selected neighbouring grid point is occupied, then the protein cannot move to it, and so remains in its current grid point; such an event is the simulation's version of a collision, and enforces volume exclusion, so that only one protein can occupy a grid point at any one time.

The random nature of protein movement on the HVR represents the Brownian motion which, as noted, governs protein diffusion on cell membranes. After each movement (or non-movement) has been generated, the simulation time is incremented by $\frac{1}{n}$ where n is the total number of proteins on the cell membrane. An interval of one signifies the time taken for all the proteins to move on the membrane, and represents a simulation's complete time step. HVRs would also be subject to Brownian motion; however, this would add complications to a direct comparison between a simulation with microdomains and one without, and so HVRs are held immobile for the current purposes.

Since the area of the cell membrane being modelled is large relative to the area of the grid point, the simulation should be a reasonably good approximation to a random walk approximation to Brownian motion (89). It should be noted that the grid is toroidal in nature. The diffusion rates used in the simulation are given in table (5.1); an exploration of the Saffman-Delbrück model is given in appendix (5.A).

HVR area H (units in 2nm^2)	Diffusion coefficient
1	1.0
2	0.89635
3	0.82281
4	0.76577
5	0.71917
6	0.67976
7	0.64563
8	0.61552
9	0.58859
10	0.56422

[1] Calculated using the Saffman-Delbrück formula (80)

Table 5.1: Probability of protein mobility

The mobility of a protein inside a microdomain is given by the ratio

$$D = \frac{D_R}{D_{NR}} \qquad (5.1)$$

where D_R is the diffusion rate of an encapsulated protein, and D_{NR} is an unencapsulated protein on the cell membrane (a *free* protein). Both diffusion rates are calculated according to the Saffman-Delbrück model (80). Larger D values correspond to higher rates of diffusion; if D is nonintegral, then the interpretation of D is probabilistic. Proteins outside of HVRs have a diffusion rate of $D = 1$; those inside the microdomains use a calculated diffusion rate depending on the size of the microdomain. If $D < 1$, a random number ψ is generated; if $\psi < D$, then the protein can move, and a random move to one of its neighbouring nodes can occur. For the purposes of the current simulation, friction terms have not been taken into account.

Notice that there may be more receptors and/or microdomains than is biologically reasonable for the area of the cell membrane being simulated; however, the purpose of the simulation is not to realistically model the receptor coverage of a cell membrane, and so this aspect is not relevant to the simulation. The number of receptors and accessory proteins is set to one thousand for each iteration of the simulation, which would be an unusually high distribution for a cell membrane; however, this makes the simulation computationally tractable, since it is more likely that a receptor will encounter a ligand or an accessory protein.

The system is subjected to IL-1β in the following way: the ligand has a fixed probability of striking the membrane. A random number is generated, and if that number is less than the probability of ligand being injected, a random coordinate on the cell membrane is selected. If the coordinate contains a receptor, then a binary complex is formed; otherwise, the ligand is deleted from the simulation. Once the binary complex is formed, it must bind with an accessory protein (by moving into a neighbouring node containing IL-1RAcP) before a ternary complex is formed. Once a ternary complex is formed, a signal transduction event is recorded.

The size of the cell membrane will obviously have an effect on the probability of a bound receptor binding with an accessory protein, and therefore on the

number of signal transduction events. If the simulated cell membrane is smaller, it is more likely that a bound receptor will encounter an accessory protein, and vice versa. The simulation will be iterated over a number of different cell membrane sizes to note its effect on the number of triggered signal events.

Note that, for those simulations which contain HVRs, there are a fixed number of fifty. HVRs each have a size s randomly chosen from $2 \leq s \leq 50$, which is in the range of reported sizes for lipid rafts in the literature (90). HVRs do not change in size or shape for the duration of the simulation. The length of a simulated time step depends on the number of proteins undergoing Brownian motion: to preserve a comparable number of time steps between HVR and non-HVR simulations, HVRs are fixed in place on the cell membrane. Intuitively this would reduce the number of protein-protein interactions, since fewer receptors and accessory proteins would be captured by the microdomains.

5.4 High viscosity regions and protein-protein interactions

To test the hypothesis that HVRs affect protein-protein interaction on the cell membrane, and therefore the number of ternary complexes formed, a number of simulations were performed. One simulation had a number of HVRs, of random sizes, positioned randomly on the membrane: the other has no HVRs, and depends on Brownian motion to bring adjacent proteins into contact on a surface of uniform viscosity. The experiment recorded the number of timesteps required to form a certain number of ternary complexes. The area of the cell membrane was treated as a parameter and varied, since this will also have an effect on protein interaction.

The results of the simulation are shown in Figure (5.2), in this case for a cell membrane area of $A = 500 \times 500$; since the basic unit in the simulation is 4nm^2, this gives a simulated cell membrane of area 1×10^6 nm^2. The simulations which feature HVRs are given in red, and those without are given in blue. As can be seen, those simulations which feature HVRs tend to consistently form ternary complexes more rapidly than those without.

Given computational constraints, the typical number of receptors and accessory proteins has been exaggerated. It is known that very few signal transduction events can elicit a strong response from the cell (93); fewer than ten ligand-occupied receptors are required per cell in order to induce a significant reaction, in comparison with the ten- to one hundred-fold higher occupancy required for most other receptor systems (22). In the simulation, one thousand receptors and accessory proteins have been assigned to the cell membrane, which is much higher than would ordinarily occur; however, the higher distribution of receptors allows a larger sample size. Each experiment was repeated fifty times.

Increasing the area of the cell membrane should affect the number of timesteps taken to form ternary complexes: we would expect the time taken to increase with the area, since receptors would on average have a longer path to travel before encountering an accessory protein. This can be seen in Figure (5.3), where the increase in area does in fact increase the amount of time taken for ternary complexes to form. It is also apparent that HVRs have a positive effect on the formation of ternary complexes. The relative shapes of the generated
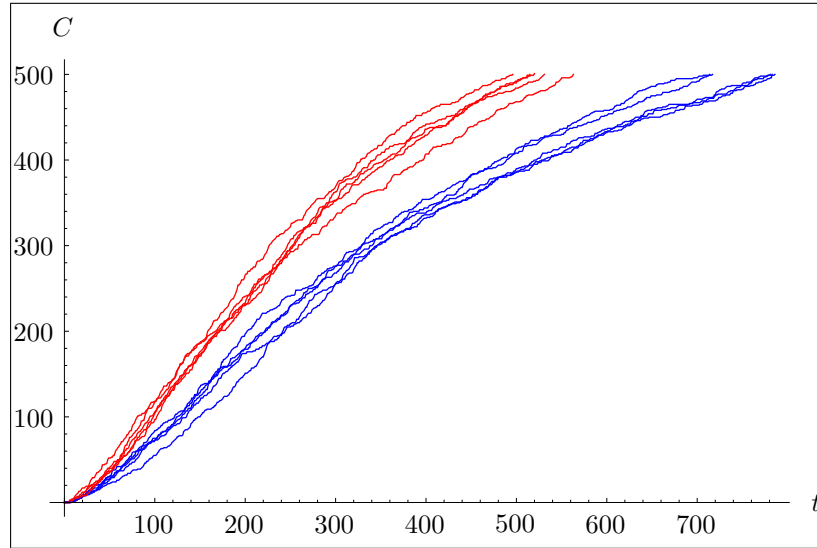
Figure 5.2: Effect of HVRs on ternary complex formation. The graph shows how HVRs tend to create ternary complexes in fewer time steps. The simulations with HVRs present on the membrane, represented in red, produce ternary complexes in less time steps than those without surface HVRs on the membrane, given in blue. The vertical axis, C, shows the number of complexes, and the horizontal axis the number of time-steps, t. The number of HVRs in each simulation is limited to fifty, and the size of each HVR is $2 \leq H \leq 50$, chosen randomly. The simulated cell membrane area is 1×10^6 nm^2, or $A = 500 \times 500$ units.
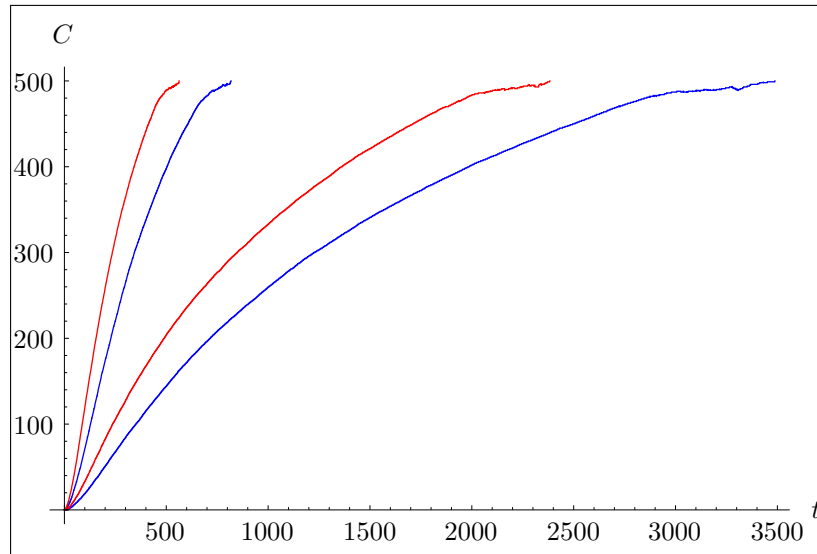
Figure 5.3: Effect of varying the cell membrane used in the simulation. The simulations which feature HVRs are given in red, and those without are given in blue; complex formation rates are averaged over $N = 50$ experimental trials. As can be seen, the larger the cell membrane, the greater number of timesteps taken for ternary complexes to form. The surface area of the cell membranes are 1.44×10^6nm^2, and 4.05×10^6nm^2. Clearly the shapes of the curves generated by the simulations are similar; however, as the horizontal axis shows, the number of timesteps taken to reach the target number of complexes grows with the increase in membrane surface area. Those simulations which feature HVRs consistently take fewer time steps to form the target number of complexes than those which have no HVRs.

curves remain the same given different membrane surface areas, showing that the behaviour of the system is consistent.

The amount of membrane surface covered with HVRs is, to an extent, randomly determined, since the fifty HVRs are assigned a random size H in the range $2 \leq H \leq 50$, but the maximum possible size with this allocation policy on the smallest cell membrane simulated represents ten percent of the total surface area. This is smaller than most estimates of lipid raft coverage cited in the literature, where conservative estimates of membrane coverage range from $24 \pm 2\%$ to $43 \pm 6\%$ (6).

It would be possible to simulate larger cell membranes to observe what effect increasing area had on protein-protein interaction, but it seems reasonable to conclude from figure (5.3) that this would merely increase the timesteps taken to form the ternary complexes. It also seems reasonable to conclude that, given the model outlined above, the presence of HVRs on a cell membrane acts to concentrate protein-protein interactions, and therefore facilitates the formation of ternary complexes in the IL-1β network.

5.5   Estimating the high viscosity region size

According to Simons et al, lipid rafts are estimated to exist in the size range $2 \leq H \leq 50$ (90). It may be illuminating to investigate the effect this range has on the formation of signalling ternaries in the IL-1β network. One way of doing this would be to use the squared area of the lipid raft as a limit, so that the maximum possible size of the HVR is $H \in 4, 9, 25, \cdots, 64$; it may also be instructive to investigate larger areas to observe any effect on the formation of complexes.

The composition of the simulated HVRs will still be randomly placed on the cell membrane, but they will be of uniform area and therefore viscosity. Notice that the largest surface area (100) is larger than the size estimated in the literature (50). It would be interesting to see if the larger surface area of the simulated HVRs limits the formation of signalling ternaries or enhances it, which may reflect on the appropriateness of the range given in the literature.

A limiting factor on such a process would occur when the HVR area grew so large that the viscosity approached zero. In such a case, receptors and other membrane-bound proteins would congregate at the HVR's perimeter. Given the results in Table (5.2), we would expect that the greater the area, the longer time on average would be taken to form signalling ternaries. We would expect from this that very large HVRs would likely be an exceptional occurrence.

It should be noted that the simulation is only a rough guide, since it is unlikely that HVRs form in neat, square regions on the cell membrane. The intention of the experiment is to investigate the relationship between HVR surface area and signalling efficacy. A more reasonable simulation would be to use the area of the HVR as an upper limit, and randomly assign grid points to a HVR.

The experiment has a fixed membrane surface area of $A = 500 \times 500 \times 4$ nm^2. Each simulation iterates for one hundred trials. The number of receptors and accessories remains constant at 1000, and the simulation halts when half of the receptors and accessories are consumed by complex formation. IL-1β is injected into the system whenever a randomly generated number $x > 0.001$; in

HVR size $(2nm)^2$	Formation time	σ
4	2491.42	74.06
9	3928.39	126.59
16	9790.53	367.18
25	25994.04	994.25
36	50000.00	0.00
49	50000.00	0.00
64	50000.00	0.00
81	50000.00	0.00
100	50000.00	0.00

Table 5.2: Effect of HVR area on ternary signalling complex formation. The size of the simulated membrane is $A = 500 \times 500$ units (a unit being $4nm^2$). The number of receptors and accessories are held constant at 1000, and each simulation is repeated for 100 trials. The simulation terminates after 50% of the receptors and accessories are consumed by forming ternary signalling complexes. The simulations successfully form complexes until the HVR size reaches 36, at which point the simulations can no longer form sufficient complexes to terminate; at this point, the simulations always reach their maximum number of timesteps before terminating.

order to save computational runtime, a receptor is picked from the surface of the cell and modified into a signalling binary complex. While this method is clearly not biologically realistic (randomly selecting a grid point and simulating a collision between the membrane and the cytokine would be a more reasonable simulation), it saves the number of clockcycles necessary to run the simulation.

Table (5.2) gives the average time taken to consume 50% of the receptors and accessories by complex formation. Clearly, the smaller area leads to faster complex formation. The average formation time for ternary complexes with four units of square HVR area is relatively rapid; the mean formation time, and the standard deviation, increases until it reaches thirty-six square units. At this point, the system is no longer capable of forming 50% of its receptors and accessories into signalling ternaries (a *signalling half-life*) within the prescribed time limit of 50000 seconds or 500000 iterations of the simulation. The standard deviation in this case obviously falls to zero. Although it is unlikely that nature creates lipid rafts in monotonously neat, square tiles, and therefore the simulation is unlikely to be replicating natural raft formation processes, the simulation does appear to indicate that smaller rafts are more appropriate signalling platforms.

It should be noted that the simulations suggest a smaller area would enhance signalling *in this case*, where it is necessary for a receptor and an accessory to be contiguous. An individual with such a HVR formation strategy would likely have an evolutionary advantage, since the inflammatory response would occur efficiently. However, such a strategy would not be as efficient if more than two membrane-bound proteins were required to form a signalling complex, and so such a strategy would be useful only in the case of systems similar to IL-1β.

Figure (5.4) shows the evolution of the system over time. The paths of the particles on the cellular membrane are preserved, so that the random walk can be observed. The proteins are colour coded, so that receptors are coloured blue, accessories green, binaries red and ternary complexes orange. Areas which have
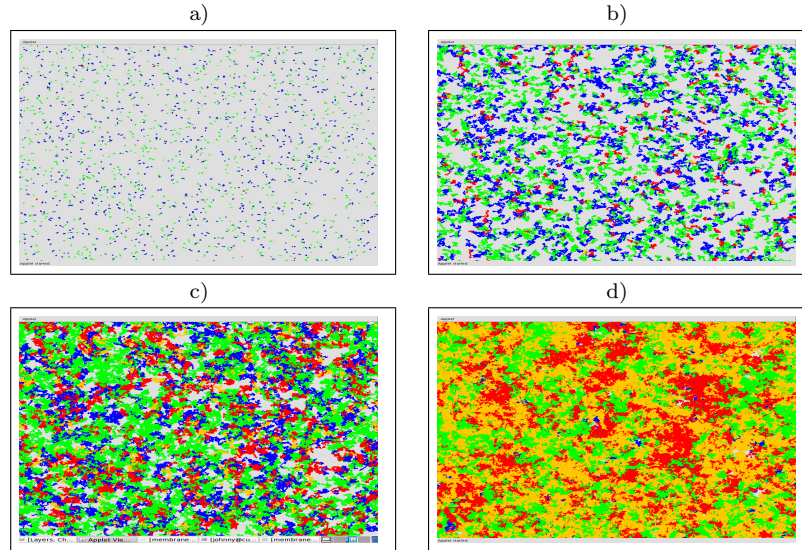
Figure 5.4: Random walk of particles on the cell membrane constrained by HVRs: evolution of the proteins on the cell membrane. The paths of the proteins over the membrane are preserved. Accessory proteins are given in green, receptors in blue, binaries are in red, and ternaries are in orange. Areas of the membrane which have not been visited by a protein are coloured grey. The initial state of the system is given in figure (5.4)(a), where the proteins have covered little of the area of the membrane and few complexes have formed. Figures (5.4)(b) and (5.4)(c) show greater movement and the formation of binary complexes. Figure (5.4)(d) shows a later stage, where most of the receptors have either been consumed by binary complexes or signalling ternary complexes.

not yet been visited by a protein are coloured grey. As would be expected, the numbers of binary and ternary complexes increase with the incidence of ligand and the collisions between binaries and IL-1RAcP, and the number of unbound receptors and accessory proteins decrease. Eventually, as shown in figure (5.4)(d), most proteins are either ternary complexes or binary complexes and accessory proteins which have not yet collided.

5.6   Effects of HVRs on random walks

An assumption that could be made when modelling the cell membrane is that the movements of proteins approximate a random walk. When the viscosity of the membrane is uniform, and the proteins are subject to the noisy environment on and around the cell surface, this would be a reasonable approximation; proteins would be likely to move in a manner described by Brownian motion, subject to the constant collisions from other molecules.

However, the presence on the cell membrane of HVRs would mean that the viscosity would not be uniform. We would expect that the motion of a particle on the cell membrane would be constrained by the presence of HVRs, and their behaviour would vary from unconstrained Brownian motion. If we assume that Brownian motion is a reasonable approximation to dynamics of proteins in a uniform-viscosity model of the cell membrane, is it possible to build a model which compares this with the HVR, nonuniform model?

5.6.1 Random walks with a probable nonmove

We will consider the movement of a particle on a one-dimensional surface. The derivation below will be modified from standard arguments in probability (70), (38). We consider a particle with two degrees of freedom, for example left and right, and include the possibility that the particle does not move.

Let $P(x)$ be the probability of a particle being at a position x at a time n. Let a move to the right be given by p, a move to the left be q, and a non-move be given by r. Then the particle position is given by $(p-q-r)$. The number of possible combinations that are available to reach the same position is given by

$$\frac{n!}{p!q!r!}$$

Then each path occurs with probability

$$p^k q^l r^m$$

The probability that the particle is at $x = (p - q - r)$ at a time n is given by

$$P(x = (p - q - r)) = \frac{n!}{p!q!r!} p^k q^l r^m \tag{5.2}$$

Recall the trinomial relation

$$
\begin{aligned}
(p + q + r)^n &= \sum_{k+l+m=n} \frac{n!}{k!l!m!} p^k q^l r^m \\
&= S(p, q, r)
\end{aligned}
\tag{5.3}
$$

We differentiate w.r.t. p, then multiply by p:

$$
\begin{aligned}
p\frac{\partial S}{\partial p} &= \sum_{k+l+m=n} \frac{n!}{k!l!m!} k \left(p^k q^l r^m \right) \\
&= np \left(p + q + r \right)^{n-1}
\end{aligned}
\tag{5.4}
$$

Since $p + q + r = 1$ we have

$$\sum_{k+l+m=n} \frac{n!}{k!l!m!} k \left(p^k q^l r^m \right) = np \tag{5.5}$$

A similar argument for q and r yields

$$\sum_{k+l+m=n} \frac{n!}{k!l!m!} l \left(p^k q^l r^m \right) = nq \tag{5.6}$$

and

$$\sum_{k+l+m=n} \frac{n!}{k!l!m!} m \left(p^k q^l r^m \right) = nr \tag{5.7}$$

Using these expressions we find

$$< x_n > = \sum_{k+l+m=n} \frac{n!}{k!l!m!} p^k q^l r^m \, (k - l - m)$$
$$= n \, (p - q - r) \tag{5.8}$$

We now need to consider the variance of x_n.

$$< x_n^2 > = \sum_{k+l+m=n} \frac{n!}{k!l!m!} p^k q^l r^m \, (k - l - m)^2 \tag{5.9}$$

Expanding we find

$$\sum_{k+l+m=n} \frac{n!}{k!l!m!} p^k q^l r^m \left(k^2 + l^2 + m^2 - 2kl - 2km + 2lm \right) \tag{5.10}$$

We need to use the trinomial relation to establish the values of k^2, l^2, etc. Differentiating both sides of (5.3) twice, and multiplying by p^2, we obtain

$$\sum_{k+l+m=n} \frac{n!}{k!l!m!} k^2 p^{k-2} q^l r^m$$
$$= n \, (n - 1) \, (n - 2) \, (p + q + r)^{n-2}$$
$$+ \sum_{k+l+m+2=n} \frac{n!}{k!l!m!} k p^k q^l r^m \tag{5.11}$$
$$= n \, (n - 1) \, p^2 \, (p + q + r)^{n-2} + np \, (p + q + r)^{n-1}$$
$$\Rightarrow \sum_{k+l+m=n} \frac{n!}{k!l!m!} k^2 p^k q^l r^m = n \, (n - 1) \, p^2 + np$$

since we have $p + q + r = 1$. A similar argument yields

$$\sum_{k+l+m=n} \frac{n!}{k!l!m!} l^2 p^k q^l r^m = n \, (n - 1) \, q^2 + nq \tag{5.12}$$

and

$$\sum_{k+l+m=n} \frac{n!}{k!l!m!} m^2 p^k q^l r^m = n \, (n - 1) \, r^2 + nr \tag{5.13}$$

We now have expressions involving k^2, l^2 and m^2, and we require the coefficients kl, km, and lm.

Differentiating w.r.t. p, then q, and multiplying appropriately, we find

$$n \, (n - 1) \, pq \, (p + q + r)^{n-2} = n \, (n - 1) \, pq$$
$$\Rightarrow \sum_{k+l+m=n} \frac{n!}{k!l!m!} kl p^k q^l r^m = n \, (n - 1) \, pq \tag{5.14}$$

Table 5.3: Table of coefficients

k^2	$n(n-1)p^2 + np$
l^2	$n(n-1)q^2 + nq$
m^2	$n(n-1)r^2 + nr$
kl	$n(n-1)pq$
km	$n(n-1)pr$
lm	$n(n-1)qr$

Repeating the process for p, then r, and q, then r, yields

$$\sum_{k+l+m=n} \frac{n!}{k!l!m!} kmp^k q^l r^m = n(n-1)pr$$
$$\sum_{k+l+m=n} \frac{n!}{k!l!m!} lmp^k q^l r^m = n(n-1)qr \tag{5.15}$$

We have established a number of identities of coefficients through the differentiation of the trinomial identity, as given in Table (5.3). Combining the results obtained we find

$$< x_n^2 > =$$
$$\sum_{k+l+m=n} \frac{n!}{k!l!m!} p^k q^l r^m \left(k^2 + l^2 + m^2 - 2kl - 2km + 2lm\right)$$
$$= n(n-1)p^2 + np + n(n-1)q^2 + nq + n(n-1)r^2 + nr + \tag{5.16}$$
$$n(n-1)pq + n(n-1)pr + n(n-1)qr$$
$$= n(n-1)\left(p^2 + q^2 + r^2 - 2pq - 2pr + 2qr\right) +$$
$$n(p+q+r)$$

Also we have

$$< x_n >^2 = \left(n(p+q+r)\right)^2 \tag{5.17}$$

The variance is obtained by

$$< x_n^2 > - < x_n >^2$$
$$= n(n-1)(p-q-r)^2 + n - n^2(p-q-r)^2$$
$$= n^2(p-q-r)^2 - n(p-q-r)^2 + n - n^2(p-q-r)^2 \tag{5.18}$$
$$= n\left(1 - (p-q-r)^2\right) = n\left((p+q+r)^2 - (p-q-r)^2\right)$$
$$= 4np(q+r)$$

That is

$$\text{Var}(x_n) = < x_n^2 > - < x_n >^2 = 4np(q + r) \tag{5.19}$$

We therefore have an equation for a particle in one dimension which has three degrees of freedom. This may, of course, sound like a contradiction, since only two directions are available for us to utilise, but we could assign $p = q = $ left, $r = $ right, for example, or $p = $ up, $q = r = $ down, or some other combination.

However, we wish to describe the situation where we have the possibility that the particle does not move. Since equation (5.2) describes the probability of finding a particle in a certain *position*, we can see that setting one of the variables p, q, r to zero would describe the contribution of a non-move to the position of a particle. Letting $p = q = \frac{1}{3}$, $r = 0$ would give us

$$\text{Var}^*(x_n) = \frac{4n}{9}. \tag{5.20}$$

where we have Var* rather than Var to indicate that this is the variance of a random walk with a stayput operation. Equation (5.19) could also be extended to a higher number of degrees of freedom, such that $\text{Var}^*(x_n) = < x_n^2 > - < x_n >^2 = 4np(q + r + s)$, for example.

Since from standard text books we know that the standard deviation is the square root of the variance, we would expect a random walk with two degrees of freedom with a nonmove operation to travel

$$\text{Std}^*(x_n) = \sqrt{\frac{4n}{9}}. \tag{5.21}$$

from the origin. We can extend this analysis to include the number of degrees of freedom which we will simulate. These are given in Table (5.4).

5.6.2 Simulated random walks with a probable nonmove

A typical random walk on a two dimensional lattice is thought to have a root mean square distance which varies asymptotically with the square root of the number of steps of the simulation, irrespective of the number of dimensions: that is, $\sqrt{\mathbf{D^2}} \mapsto \sqrt{n}$ (56), where $\mathbf{D}$ is the distance of the protein from its starting point on the simulated membrane, and t is the number of simulated timesteps. However, it should be noted that the theoretical value $\sqrt{t}$ will only be an estimate or approximation, since we are dealing here with discrete distances on a uniformly-spaced lattice, rather than motion in a continuous space.

A random walk on a lattice can easily be simulated, to give us a basis of comparison when further complexities are introduced. We require a distance measure which acts in a reasonable manner on a lattice, where the protein moves from one discrete grid point to another, rather than continuously. There are a number of metrics which could be used as a distance measure; one such measure would be the Manhattan distance or taxicab metric, given by $g((x_1, y_1), (x_2, y_2)) = |x_1 - x_2| + |y_1 - y_2|$ for all points $P_1(x_1, y_1), P_2(x_2, y_2)$ on the Euclidean plane. However, we shall use the Euclidean distance, as given by $\sqrt{x^2 + y^2}$.

Degrees of freedom	$\text{Var}(x_n)^*$	$\text{Std}(x_n)^*$
3	$\frac{4}{9}n$	$\sqrt{\frac{4}{9}n}$
4	$\frac{1}{2}n$	$\sqrt{\frac{1}{2}n}$
5	$\frac{12}{25}n$	$\sqrt{\frac{12}{25}n}$
6	$\frac{4}{9}n$	$\sqrt{\frac{4}{9}n}$
7	$\frac{20}{49}n$	$\sqrt{\frac{20}{49}n}$
8	$\frac{3}{8}n$	$\sqrt{\frac{3}{8}n}$
9	$\frac{28}{81}n$	$\sqrt{\frac{28}{81}n}$

Table 5.4: Variance and standard deviation of a particle on a random walk with a nonmove operation.

t	$(\sqrt{t})$	$(\sqrt{\mathbf{R_2^2}})$	$(\sqrt{\mathbf{R_4^2}})$	$(\sqrt{\mathbf{R_6^2}})$	$(\sqrt{\mathbf{R_8^2}})$
100	10.00	7.93	8.29	10.01	10.77
200	14.14	11.26	11.75	14.19	15.31
300	17.32	13.78	14.40	17.37	18.74
400	20.00	15.94	16.57	20.12	21.66
500	22.36	17.83	18.52	22.50	24.22
600	24.49	19.55	20.21	24.70	26.60
700	26.45	21.04	21.34	26.67	28.74
800	28.28	22.58	22.87	28.52	30.73
900	30.00	23.91	24.15	30.20	32.48
1000	31.62	25.21	25.54	31.92	34.30

Table 5.5: Brownian motion of a particle on a two-dimensional lattice with uniform viscosity. The first column gives the number of timesteps, the second gives a theoretical measure of average distance travelled; the third column, $\mathbf{R_2^2}$, gives the mean distance for a random walk with two possible degrees of freedom, the fourth, $\mathbf{R_4^2}$, gives the mean distance for a particle with four degrees of freedom, and so on. According to theory, the distance of a particle under Brownian motion approximates $\sqrt{t}$, where t is the number of simulated timesteps. Each simulation was repeated for 100000 trials, and the mean results from the trials are given.

With the appropriate distance metric defined, and the degrees of freedom of particle motion constrained to two, four, six and eight, we can see how accurately a random walk on a lattice approaches $\sqrt{\mathbf{D^2}} \mapsto \sqrt{t}$. A simulation was run for a number of different timesteps, where $t \in \{100, 200, \cdots, 1000\}$, and each simulation repeated for 100000 trials. A single particle was placed at the origin on the simulated membrane, and moved randomly for t timesteps. Note that the simulations took place with nontoroidal conditions on the two-dimensional lattice; the lattice does not have boundaries, and is effectively an infinite Euclidean plane.

The results are shown in Table (5.5), where we compare the averaged behaviour of the particle to the theoretical value, the square root of the total number of timesteps in the simulation. The theoretical value is, of course, derived from a *continuous*, rather than a *discrete*, environment, so can only be a rough guide to particle behaviour on a lattice. The theoretical measure, $\sqrt{t}$, is given in the second column, and the results of the simulations given in the remaining columns.

The third column, $\sqrt{\mathbf{R_2^2}}$, shows the simulated random walk with two degrees of freedom. In this case, the mean distance travelled from the origin is clearly less than the theoretical value $\sqrt{t}$ for each $t \in [100, 200, \cdots, 1000]$. Looking at the columns representing four-, six- and eight-degrees-of-freedom, $\sqrt{\mathbf{R_4^2}}$, $\sqrt{\mathbf{R_6^2}}$, and $\sqrt{\mathbf{R_8^2}}$ respectively, we find that the mean distance travelled increases with the number of degrees of freedom available to the particle. This can be seen to occur between $\sqrt{\mathbf{R_6^2}}$, and $\sqrt{\mathbf{R_8^2}}$.

Similarly, we can investigate the effect of a non-move on a random walk. Tables (5.6 - 5.9) give the results of a simulated random walk for a particle with two, four, six and eight degrees of freedom, respectively. The first two columns in each of the tables gives the time t of the simulation and the theoretical mean distance $\sqrt{t}$, respectively. The third column, Std(t)^*, gives the measure of standard deviation of a random walk with the probability of a nonmove, developed in the previous section. The fourth column gives the result of a simulated random walk with no probability of a nonmove. The fifth column gives the mean distance from the origin travelled by the particle, where it is possible for the particle to stay where it is rather than move, with equal probability. We perform simulations for two degrees of freedom with mean square distance $\sqrt{\mathbf{D_2^2}}$ (given in table (5.6)), four degrees of freedom and mean distance $\sqrt{\mathbf{D_4^2}}$ (table (5.8)), six degrees of freedom and mean distance $\sqrt{\mathbf{D_6^2}}$ (table (5.6)), and eight degrees of freedom and mean distance $\sqrt{\mathbf{D_8^2}}$ (table (5.6)).

Table (5.6) shows that the simulation with a non-move has a lower mean squared distance than simulations without a stayput operation. Both $\sqrt{\mathbf{R_2^2}}$ and $\sqrt{\mathbf{D_2^2}}$ are less than the theoretical measure $\sqrt{t}$. This observation also holds for table (5.7), where we have four degrees of freedom; however, it does not hold for the results presented in table (5.8), where we have $\sqrt{\mathbf{R_6^2}} > \sqrt{t} > \sqrt{\mathbf{D_6^2}}$. Finally, in table (5.9), both the eight degrees of freedom mean squared distance and the eight degrees and a non-move are greater than the theoretical estimate, so that we have $\sqrt{\mathbf{R_6^2}} > \sqrt{\mathbf{D_6^2}} > \sqrt{t}$. For all of the results given, we have $\sqrt{\mathbf{R^2}} > \sqrt{\mathbf{D^2}}$.

The standard deviation measure Std(t)^*, developed in the previous section, is also included in tables (5.6 - 5.9). In all cases, $\text{Std(t)}^* < \sqrt{t}$. For the random walk with two degrees of freedom and a nonmove, Std(t)^* is close to

t	$(\sqrt{t})$	Std(t)^*	$(\sqrt{\mathbf{R_2^2}})$	$(\sqrt{\mathbf{D_2^2}})$
100	10.00	6.66	7.93	6.47
200	14.14	9.42	11.26	9.19
300	17.32	11.54	13.78	11.26
400	20.00	13.33	15.94	12.98
500	22.36	14.09	17.83	14.52
600	24.49	16.32	19.55	15.99
700	26.45	17.63	21.04	17.23
800	28.28	18.85	22.58	18.30
900	30.00	20.00	23.91	19.55
1000	31.62	21.08	25.21	20.47

Table 5.6: Brownian motion of a particle on a lattice with uniform viscosity: comparison between two degrees of freedom, and two degrees of freedom plus a non-move. The first column gives the number of timesteps, the second gives a theoretical measure of average distance travelled; the third column gives the standard deviation of a random walk with a nonmove, as derived in the previous section. The fourth column, $\mathbf{R_2^2}$, gives the mean distance for a random walk with two possible degrees of freedom, the fifth, $\mathbf{D_2^2}$, gives the mean distance for a particle with two degrees of freedom and a stayput. The means are generated from 100000 simulations.

$\sqrt{\mathbf{D^2}}$, although slightly larger than the empirical results. For four degrees of freedom and a nonmove, $\sqrt{\mathbf{D^4}}$, the standard deviation is again close to the empirical results, although in this case we have $\sqrt{\mathbf{D^4}} > \text{Std(t)}^*$. With higher degrees of freedom, six and eight respectively, the standard deviation measure Std(t)^* is consistently smaller than the empirical results, and is a less accurate approximation than is the case for two and four degrees of freedom.

The results show that the higher the number of degrees of freedom, the higher the mean square distance from the origin. Furthermore, at approximately six degrees of freedom, the mean square distance $\sqrt{\mathbf{R^2}}$ becomes larger than the theoretical measure $\sqrt{t}$. It should be emphasised that the theoretical measure $\sqrt{t}$ is *only an approximation* to the case of a random walk on a lattice, and so any discrepancy between a theoretical measure defined on a continuous space and an empirical measure on a discrete lattice should not be considered unduly alarming.

5.6.3 Random walks on nontoroidal plane

It could also be observed at this point that the above simulations take place on a nontoroidal Euclidean plane. What effect would a toroidal structure have on the root mean square distance from the particle's origin? Simulations of four- and eight-neighbourhood lattices with toroidal conditions set on a 500×500 grid are given Table (5.10). The experimental protocol is much the same as the previous simulations, the number of trials for each timestep t is 5000 and averaged over each trial. As with the previous simulation runs, the theoretical estimate is less than the empirically discovered value, but similar to the nontoroidal value. It seems reasonable from these experiments to assume that bounding the lattice has relatively little effect on the dynamics of a particle on a two-dimensional

t	$(\sqrt{t})$	$\mathrm{Std(t)}^*$	$(\sqrt{\mathbf{R_4^2}})$	$(\sqrt{\mathbf{D_4^2}})$
100	10.00	7.07	8.29	7.88
200	14.14	10.00	11.75	11.17
300	17.32	12.24	14.40	13.68
400	20.00	14.14	16.57	15.82
500	22.36	15.81	18.52	17.69
600	24.49	17.32	20.21	19.40
700	26.45	18.70	21.34	20.96
800	28.28	20.00	22.87	22.39
900	30.00	21.21	24.15	23.74
1000	31.62	22.36	25.54	25.05

Table 5.7: Brownian motion of a particle on a two-dimensional lattice with uniform viscosity: comparison between four degrees of freedom, and four degrees of freedom plus a non-move.

t	$(\sqrt{t})$	$\mathrm{Std(t)}^*$	$(\sqrt{\mathbf{R_6^2}})$	$(\sqrt{\mathbf{D_6^2}})$
100	10.00	6.66	10.01	9.26
200	14.14	9.42	14.19	13.15
300	17.32	11.54	17.37	16.16
400	20.00	13.33	20.12	18.57
500	22.36	14.90	22.50	20.77
600	24.49	16.32	24.70	22.75
700	26.45	17.63	26.67	24.64
800	28.28	18.85	28.52	26.25
900	30.00	20.00	30.20	27.90
1000	31.62	21.08	31.92	29.41

Table 5.8: Brownian motion of a particle on a two-dimensional lattice with uniform viscosity: comparison between six degrees of freedom, and six degrees of freedom plus a non-move.

t	$(\sqrt{t})$	$\mathrm{Std(t)}^*$	$(\sqrt{\mathbf{R_8^2}})$	$(\sqrt{\mathbf{D_8^2}})$
100	10.00	5.87	10.77	10.20
200	14.14	8.31	15.31	14.43
300	17.32	10.18	18.74	17.72
400	20.00	11.75	21.65	20.46
500	22.36	13.14	24.22	22.89
600	24.49	14.40	26.60	25.10
700	26.45	15.55	28.74	27.05
800	28.28	16.62	30.73	29.03
900	30.00	17.63	32.48	30.75
1000	31.62	18.59	34.30	32.43

Table 5.9: Brownian motion of a particle on a two-dimensional lattice with uniform viscosity: comparison between eight degrees of freedom, and eight degrees of freedom plus a non-move.

lattice.

This can be tested further by allowing toroidal conditions, and varying the area of the simulated membrane. The results of the experiment are given in Tables (5.10), for the four degrees of freedom model, and (5.11), for the eight degrees of freedom model. Note that these tables show only those results for a 500×500 matrix. The simulations for each HVR size are run for t timesteps, where $t \in \{100, 200, \cdots, 1000\}$, with the size of the HVR H varying over the same range, so that the cell membrane has an area $A = 100 \times 100, 200 \times 200, \cdots, 1000 \times 1000$.

Table 5.10: Results for $A = 500 \times 500$ grid shown. Brownian motion of a particle on a two-dimensional lattice with uniform viscosity. These simulations give the movement of particles under Brownian motion with four and eight degrees of movement. The columns give the length of one side of the membrane, the number of timesteps of the simulation, the theoretical distance of the particle from its starting coordinates, and the empirical mean distance for a particle with four degrees of movement. The four-neighbour simulations give values higher than the predicted theoretical values.

H	t	Theoretical: $(\sqrt{t})$	4 degrees: $(\sqrt{\mathbf{D_4^2}})$
500	100	10.00	25.41
500	200	14.14	24.82
500	300	17.32	24.94
500	400	20.00	25.75
500	500	22.36	25.04
500	600	24.49	25.60
500	700	26.45	25.15
500	800	28.28	25.41
500	900	30.00	25.14
500	1000	31.62	25.12

Table 5.11: Results for $A = 500 \times 500$ lattice shown. Brownian motion of a particle on a two-dimensional lattice with uniform viscosity. These simulations give the movement of particles under Brownian motion with eight degrees of movement. The eight-neighbour simulations give values higher than the predicted theoretical values.

H	t	Theoretical: $(\sqrt{t})$	8 degrees: $(\sqrt{\mathbf{D_8^2}})$
500	100	10.00	29.65
500	200	14.14	29.29
500	300	17.32	29.50
500	400	20.00	29.28
500	500	22.36	28.35
500	600	24.49	29.41
500	700	26.45	29.01
500	800	28.28	28.86
Continued on next page			

t	$\sqrt{t}$	$H = 2 : \sqrt{\mathbf{D_8^2}}$	$H = 15 : \sqrt{\mathbf{D_8^2}}$	$H = 2 : \sigma$	$H = 15 : \sigma$
100	10.00	25.58	26.10	132.34	134.81
200	14.14	35.63	36.55	151.80	157.15
300	17.32	43.11	43.41	166.76	167.08
400	20.00	51.80	49.59	185.10	179.16
500	22.36	58.09	57.91	197.44	196.13
600	24.49	59.22	58.74	190.46	188.72
700	26.45	64.39	63.00	197.40	194.17
800	28.28	68.83	77.43	204.72	229.40
900	30.00	75.96	77.73	218.33	223.33
1000	31.62	77.21	78.29	215.96	220.27

Table 5.12: Brownian motion of a particle on a two-dimensional lattice with varying viscosity. These simulations give the movement of particles under Brownian motion with HVRs of size $H = 2, H = 15$. The size of the cellular membrane is $A = 700 \times 700$ units. The HVRs are assigned to random locations on the surface. The columns give the number of simulation timesteps, the theoretical distance of the particle from its starting coordinates, the empirical mean distance for a particle where there are HVRs of two units in size, and the empirical mean distance for a particle in the vicinity of HVRs composed of fifteen units. The last two columns give the standard deviations (σ) for both experiments, which are considerable. Both experiments give values higher than the predicted theoretical values, and, unlike in previous experiments, both increase with the size of the membrane.

Table 5.11 – continued from previous page

H	t	Theoretical: $(\sqrt{t})$	8 degrees: $(\sqrt{\mathbf{D_8^2}})$
500	900	30.00	29.03
500	1000	31.62	28.86

As can be seen from the tables, once again the empirical mean value is larger than the theoretical value, and increases with the area of the HVR. Furthermore, more degrees of freedom lead to higher root mean square distances from the point of origin. However, the increase in the number of timesteps does not seem to significantly affect the mean distance, $\sqrt{\mathbf{D_4^2}}$ and $\sqrt{\mathbf{D_8^2}}$.

These simulations give us a guideline to Brownian motion on two-dimensional toroidal cellular membranes, but does not take into account higher viscosity regions such as HVRs on the cell surface. This can be achieved with a slight modification of the previous experimental protocol. We iterate over HVRs which vary over size $H \in \{2, 3, \cdots, 15\}$, with the viscosity set accordingly.

The HVRs were randomly assigned on the membrane; the sizes of the HVR are adhered to, rather than treated as an upper limit. The area of the membrane was varied over $A \in \{100 \times 100, 200 \times 200, \cdots, 1000 \times 1000\}$, and the number of simulated timesteps t varied over $t \in \{100, 200, \cdots, 1000\}$. Each set of parameters was iterated over for 5000 trials. Table (5.12) shows the results of running an experiment on a 700×700 membrane, where the HVR size are the extreme ends of the range, namely 2 and 15 units, for comparative purposes.

As can be seen from the table, in comparison with the experiments where there are no high viscosity regions (see Tables (5.10), (5.11)). The RMS distance is much greater than both the theoretical value and the previous experiments. Notice, however, that there is not much difference between the two different HVR sizes H.

It appears that the mere presence of HVRs on the membrane is sufficient to significantly increase the mean distance. The reason for this seems intuitively obvious, that the protein performs a random walk on the membrane until it encounters a HVR; after this point, the probability of it escaping the HVR is considerably less than if it were in a uniform, low viscosity area. It seems reasonable to conclude that the Brownian motion of a protein on a two dimensional lattice is constrained by the presence of HVRs.

5.7   Variable-sized rafts with an upper limit

Having investigated the behaviour of particles in the presence of uniform-sized HVRs, we can now examine a less regulated approach to HVR formation. In the following experiment, HVR sizes will be assigned randomly, up to a certain limit on their size. Units of lipid will be added to the HVR so that they are roughly contiguous. An origin for the HVR is randomly assigned, and the next unit of lipid will be chosen from its neighbourhood; the next point will in turn be assigned from the neighbourhood of the previous point, until the randomly determined area of the HVR has been exhausted.

The experimental protocol is much as before. The proteins and HVRs are distributed randomly across the cell membrane. The membrane is a $A = 500 \times 500$ lattice. The upper limit of the area of the HVR is set. The size of each HVR is randomly determined from this upper limit, that is, a random number r is generated such that $2 \leq r \leq \epsilon$, where ϵ is the upper limit. The HVRs are assigned lipid units contiguously until they reach H. We vary the upper limit ϵ such that $\epsilon \in \{4, 9, 16, 25, 36, 49, 64, 81, 100, 121, 144, 169, 196, 225\}$. Each value of the ϵ parameter is repeated for one hundred trials, and the number of iterations taken to reach the signalling half-life is averaged over the number of trials.

The results of the experiment are given in Table (5.13). Clearly, the most effective upper limits, in the context of the signalling network that we are considering, are four and nine. The next value is an order of magnitude larger. Interestingly, the signalling does not simply increase in proportion with the upper limit ϵ, and in fact the mean time to the signalling half-life gradually *decreases* after $\epsilon = 25$. However, for the purposes of the IL-1β network, the optimal size of HVRs would appear to be rather small.

5.8   Effect of Type-II receptor

Having explored the effects of the lattice and the neighbourhood shape on signalling, and the further effect of HVRs, the Type-II receptor is introduced onto the simulated membrane. The experimental protocol should be familiar from previous sections. The proteins and HVRs are distributed randomly across the cell membrane.

HVR area $H = (2\text{nm})^2$	Average formation time
4	2559.46
9	3679.13
16	40547.04
25	47154.35
36	45891.26
49	39290.99
64	33678.04
81	32895.24
100	29851.71
121	25628.22
144	23922.80
169	21853.35
196	24402.43
225	22034.30

Table 5.13: Effect of HVR area on ternary signalling complex formation. The size of the simulated membrane is $A = 500 \times 500$ units (a unit being 4nm^2). The number of receptors and accessories are held constant at 1000, and each simulation is repeated for one hundred trials. The simulation terminates after 50% of the receptors and accessories are consumed by forming ternary signalling complexes.

The size of the membrane is chosen to be closer to average human cell sizes, although large enough to give significant effects. The membrane size varies over $A = 100 \times 100, 200 \times 200, 300 \times 300$. The upper limit of the area of the HVR is once again restricted, and the size of each HVR is randomly determined up to this upper limit. The HVRs are assigned lipid units contiguously until they reach H elements. We vary the upper limit ϵ such that $\epsilon \in \{4, 9, 16, 25, 36, 49, 64, 81, 100, 121, 144, 169, 196, 225\}$. Each value of the ϵ parameter is repeated for one hundred trials. Each trial has a maximum possible number of iterations $t = 20000$, which represents a more realistic period in terms of human immune response times. All data is collected at whichever timestep the simulation terminated.

Table 5.14: Effect of Type-II receptor on HVR signalling complex formation. Results are given for membrane sizes varying over $A = 100 \times 100$, 200×200, 300×300; the membrane sizes are chosen to be closer to human cell sizes. The average number of complexes formed during the simulation are given. The complexes are: signalling binary $SBIN$, nonsignalling binary $NSBIN$, signalling ternary $STERN$, and nonsignalling ternary $NSTERN$. Each trial was given a maximum $t = 20000$ iterations before termination; this is a more biologically realistic timescale. The number of Type-I and Type-II receptors and receptor accessory proteins were all held constant at $U = 100$. The size of the membrane, and the upper limit of the HVR size, were varied. In this way the accessory is a constrained resource, which both types of receptor have to compete for. Larger HVR sizes form complexes more readily than smaller HVR sizes. As the HVR size increases, the number of nonsignalling ternaries decreases. This is to be expected from the competition for the constrained quantity of available receptor accessory. Simulations were averaged over $N = 100$ trials for each set of parameters.

Membrane: 100×100				
HVR area H $(2\text{nm})^2$	SBIN	NSBIN	STERN	NSTERN
2	53.53	47.04	44.83	51.31
3	55.13	48.61	43.04	49.56
4	57.29	52.21	40.88	45.95
5	59.01	55.43	39.29	42.94
6	60.97	59.52	37.47	38.9
7	63.34	62.38	35.35	36.31
8	66.43	64.99	32.35	33.79
9	69.93	68.50	28.86	30.29
10	74.39	75.31	24.39	23.47
11	73.06	72.71	25.72	26.07
12	72.50	73.06	26.30	25.73
13	72.94	72.69	25.84	26.09
Membrane: 200×200				
2	56.95	52.46	41.28	45.76
3	58.23	52.66	40.28	45.85
4	59.27	55.70	39.23	42.79
5	61.30	58.38	37.32	40.25
6	63.62	61.47	35.24	37.38
7	66.57	65.95	32.33	32.94
8	69.64	69.10	29.26	29.79
9	73.06	73.78	25.83	25.12
10	77.42	77.19	21.48	21.71
Continued on next page				

Table 5.14 – continued from previous page

HVR area H	SBIN	NSBIN	STERN	NSTERN
11	76.27	76.27	22.62	22.62
12	75.33	76.26	23.55	22.62
13	75.36	74.96	23.54	23.95
Membrane: 300×300				
2	60.51	57.35	38.22	41.38
3	61.69	58.52	37.04	40.22
4	62.61	60.12	36.19	38.67
5	63.96	62.56	34.93	36.31
6	65.43	64.65	33.53	34.31
7	68.09	69.09	30.88	29.89
8	72.76	72.58	26.24	26.42
9	76.90	76.95	22.08	22.03
10	80.27	80.56	18.71	18.43
11	79.55	79.49	19.47	19.53
12	79.60	79.55	19.37	19.41
13	77.79	78.13	21.18	20.85

The parameters for the simulations were kept the same, with 100 IL-1β, and 100 Type-I and -II receptors. The receptor accessory was also set to 100 as a constraint on complex formation, so that the two receptors have to compete to form ternary complexes. The upper limit of the HVRs and the size of the membrane were the only parameters allowed to vary.

The results are given in Table (5.14). The size of the membrane is a significant factor here; the larger membrane appears to form signalling ternaries more readily than the smaller membranes, for equal values of HVR area. What is common to all three membrane areas is that HVRs with a larger upper limit more readily form complexes of either kind than HVRs with a smaller upper limit.

As the HVR size increases, the number of nonsignalling ternaries decreases. This is to be expected from the competition for the constrained quantity of available receptor accessory. However, the sequestration of resources, as would be expected from Section (4.7), would arrest further signalling ternary formation in the event of a further IL-1β stimulus.

The effect of HVRs on signalling has intensified the signalling complex formation process, although a higher ratio of Type-II receptors would inhibit sufficient signalling ternaries being formed to initiate signalling transduction.

5.9 Discussion

The classic image of the cell membrane has been modified by recent research. (2), (27), (57), (67). It has been suggested that the plasma membrane is a more complex structure than hitherto assumed, shaped by cytoskeletal interactions. We remain agnostic as to the causes of enhanced protein-protein interactions on the membrane; rather than assuming the existence of structures known as

lipid rafts, we presented a more abstract structure, referred to as high viscosity regions (HVRs).

The efficacy of areas of high viscosity in enabling protein-protein interactions on the cell membrane has been considered in a number of experiments. Using the Saffman-Delbrück model of diffusion in cellular membranes we created a model based on the area of the HVR, where the larger the area, the higher the viscosity. It was found that HVRs facilitate protein-protein interaction, such as the binding of a binary complex to an accessory process, compared to simulated membranes without areas of higher viscosity. From the experiment, it would seem that HVRs facilitate formation of signalling ternary complexes.

Since higher viscosity regions enable more rapid complex formation, and thereby more rapid signal transduction, we investigated the optimal size of the HVR in terms of the IL-1β network. A size of between four and nine units, where each unit is 4 nm^2, was found to be the optimal range for IL-1β signal transduction.

Assuming that Brownian motion is a good approximation to the passage of receptors and accessory proteins on the cell membrane, we compared the passage of a particle on a cell membrane in the presence and the absence of high viscosity regions. This required empirically establishing an average measure of Brownian motion on a two-dimensional lattice, since this is our representation in a cellular automaton environment of the cell membrane. Once this was established, with the appropriate number of degrees of freedom for our simulation, we considered the effect of high viscosity regions on the lattice/cell membrane. The presence of HVRs on the lattice greatly increased the mean distance travelled by the receptor on the lattice. This could be explained by the receptor being captured by a high viscosity region, and remaining in it until the end of the experimental trial.

In summary, high viscosity regions (within a certain range of areas) were found to enhance signalling transduction in the IL-1β network, by enhancing protein-protein interaction on the cellular membrane.

5.A   Appendix: The Saffman-Delbrück model

It might be appropriate at this point to focus briefly on the theory underlying the Saffman-Delbrück equation. Saffman and Delbrück realised that the rotational and translational diffusion of protein and lipid molecules in cellular membranes could be studied theoretically by applying a model of Brownian motion to a hydrodynamic model (80). Taking the membrane as an infinite plane sheet of viscous fluid (a lipid layer) separating infinite regions of a less viscous fluid (water, for example), they took the protein to be a cylinder with axis perpendicular to the plane of the sheet, its dynamics determined by Brownian motion.

In the following, we will employ the same notation as used in the original paper as far as possible. Diffusion of a particle subject to Brownian motion is given by two diffusion coefficients, D_T and D_R, which represent the translational and rotational displacements. Motion in a plane and rotation about a perpendicular axis are given by

$$\bar{r}^2 = 4D_T t$$

and

$$\bar{\theta}^2 = 2D_R t$$

where $\bar{r}^2$ and $\bar{\theta}^2$ are the mean square displacement and angular rotation in time t. The diffusion coefficients can be related to the particle movement by the Einstein relations

$$D_T = kTb_T, \ D_R = kTb_R$$

where k is Boltzmann's constant, T is the absolute temperature and b is the movement, independent of force or torque, defined as the velocity, or angular velocity, produced by steady unit force. For a sphere in an unbounded fluid of viscosity μ it is well known that

$$b_T = \frac{1}{6\pi\mu a}, \ b_R = \frac{1}{8\pi\mu a^3}$$

The ratio of these two mobilities is independent of the viscosity:

$$\frac{b_T}{b_R} = \frac{4}{3}a^2$$

where a denotes the particle radius. However, we need to consider two different types of viscosity, that of the lipid layer (cell membrane) and the surrounding layer, the viscosity of water. If we let μ be the viscosity of the cell membrane and μ' be the viscosity of water, then clearly $\mu \gg \mu'$. A finite translational mobility b_T can be found by taking account of the inertia of the viscous fluid; it is then found that

$$b_T = \frac{1}{4\pi\mu h}\left(\log\frac{4\mu}{\rho U a} + \frac{1}{2} - \gamma\right)$$

where ρ denotes the density of the fluid, U is the translational velocity and γ is Euler's constant.

This model has been supported experimentally (75), and by further modelling work by Hughes et al (45). Peters and Cherry give the lateral and rotational diffusion equations as

$$D_R = \frac{kT}{4\pi a^2 h\eta}$$

and

$$D_L = \frac{kT}{4\pi h\eta} \left(\log \frac{\eta h}{\eta_w a} - \gamma \right)$$

where the protein is modelled as a cylinder of diameter a spanning a membrane of width h. The membrane is treated as a fluid with viscosity η, with η_w the viscosity of the surrounding, less viscous medium, and the equations are accurate when $\eta_w \ll \eta$. The equations can be combined to yield

$$\frac{D_L}{D_R} = a^2 \left(\log \frac{kT}{4\pi h a^2 \eta_w D_R} - \gamma \right)$$

The model will use the third formulation of the Saffman-Delbrück equation, as modified and expanded by Evans and Hochmuth (original paper's notation) (31):

$$D_T = \frac{kT}{4\pi B} \log \left(\frac{B}{vr} \right) \tag{5.22}$$

where k is the Boltzmann constant, T is the absolute temperature (taken in this case as the temperature of the human body), B is the viscosity of the bilayer surface (i.e. the cell membrane), which is set to unity, v is the viscosity of water (taken as 10^{-2} in comparison with the viscosity of the bilipid layer (80)), and r is the radius. Since we are dealing, for computational convenience, with a lipid raft of square or rectangular shape, rather than a circle, the diameter is taken as the square root of the sum of the two dimensions of the lipid raft squared. Notice that we have an expression only for the diffusion coefficient which relates to translational velocity; this is appropriate, since rotational velocity is not being modelled.

Chapter 6

Conclusion: inhibition in the IL-1β network

IL-1β is a pro-inflammatory cytokine essential to the functioning of the immune system (30), (1). The response of inflammatory cytokines proves lethal to millions every year around the globe through endotoxic shock. The study of endotoxic shock led to the discovery of the biochemical mediators known as cytokines, and eventually to the identification of IL-1. Interleukin-1 is a major mediator of the inflammatory response, and thus must be kept under strict control by the immune system.

The IL-1 network exhibits a complexity which has been noted by many researchers (23), (7). It exists in two forms, α and β, which afforded a natural way of drawing a boundary around which part of the network was to be modelled: a choice between the α or β forms. The β form was chosen for investigation since it is known to have a higher potency than the α form (62), (19).

IL-1β requires the formation of a signalling ternary complex in order to trigger signalling transduction; it needs to bind with the signalling (Type-I) receptor, and for this binary complex in turn to be bound by a receptor accessory protein, before signalling transduction can proceed. A variety of control mechanisms which inhibit the formation of this signalling ternary process have evolved. These have been modelled using a variety of techniques.

6.1   Summary of results

A four-dimensional ordinary differential equation model was developed in Chapter 2. The differential equations were developed by applying the Michaelis-Menten model and the related Briggs-Haldane model, favoured in enzyme kinetics for chemical systems which rapidly reach equilibrium or quasi-equilibrium states. An outline of the Michaelis-Menten model was given in Section 2.A, and of Briggs-Haldane in 2.B. The equations described the complex formation which would happen on a cell membrane if it expressed the Type-I and Type-II IL-1β receptors. Four types of complex formation were permissible in the model: signalling binary and ternary complexes, and their nonsignalling counterparts. The amount of unbound ligand, receptors and receptor accessories were given as conservation laws.

Initial analysis of the system of differential equations implied that a reduction and simplification of the model would yield more tractable results. In Section 2.2, the system was reduced to two dimensions and nondimensionalised, where the large disparity between the association and dissociation rates was exploited. The simplified system was shown to be in equilibrium whenever the number of receptors was equal to the ligand. Linear stability analysis gave a number of equilibria for this approximate form of the system, but not too much emphasis was given to this analysis, due to its rather simplified nature. Many elements which had been excluded were thought likely to significantly affect the dynamics of the system.

In Section 2.3, a more complete analysis of the biological equilibria is given. The biological domain, those values for which the variables representing the complexes hold, was shown to be forward invariant and inward pointing under the vector field:

$$\dot{\phi} = (\sigma - \phi)(C_{AP} - S\phi) - \rho_y \phi \tag{6.1}$$

$$\dot{\sigma} = r(1 - \sigma)(L - S\sigma) - \rho_w(\sigma - \phi) \tag{6.2}$$

From standard theorems, it followed from this that there must be at least one equilibrium inside the biological domain. After further analysis, and the application of the Poincaré-Hopf index theorem (this theorem is explored in appendix 2.C), it was determined that there is a unique biological equilibrium.

The central role of the ratios $\frac{C_{AP}}{S}$ and $\frac{L}{S}$ was further accentuated. $\frac{C_{AP}}{S}$ is the ratio of unbound receptor accessory to unbound receptors (of either kind), and $\frac{L}{S}$ is the ratio of unbound ligand to unbound receptors. It was found that, if $\frac{C_{AP}}{S} < 1$, the availability of the receptor accessory protein is less than the availability of both Type-I and Type-II receptors. In this case the receptor accessory is the limiting resource. For low values of $\frac{L}{S}$, it was found that the density of ternary complexes is limited by availability of ligand. For larger values of $\frac{L}{S}$, it was found that there are more binary complexes than ternary complexes, so that ternary formation is affected by the scarcity of the receptor accessory. In the case where $\frac{C_{AP}}{S} > 1$, the availability of the unbound receptors was found to be the limiting resource.

The IL-1β network is composed of elements which occur at very low physiological quantities. The type-I receptor is not abundant, but evokes a powerful response without a high level of receptor occupancy (6). Since IL-1β typically acts at very low concentrations, the population sizes of signalling and nonsignalling complexes will be small, and random fluctuations will have a disproportionate effect. Stochastic modelling techniques such as Markov chain models are useful in such a context. In Chapter 3, Section 3.1 a Markov chain model was developed to investigate the state changes between unbound ligand and the signalling binary, nonsignalling binary, signalling ternary and nonsignalling ternary complexes. The trials started with a relatively low number of total iterations and increased, from where $100 \leq n \leq 5 \times 10^8$, until the probability distribution of each state in the system became apparent: as the number of iterations increased, the system became rapidly attracted to the signalling ternary state.

In Section 3.1.2, the mean sample path of the system was analysed. It was assumed that there would be an effectively infinite number of receptors and receptor accessory proteins, so as not to constrain complex formation. A

simulation was designed which terminated either when a ternary complex was formed, or the maximum number of iterations was reached. Each experimental trial was a sample path of the Markov chain. The number of iterations required to reach a state T was recorded as the result of the trial. The behaviour of the system was observed both with and without the Type-II nonsignalling receptor. It was found that the effect of the Type-II receptor was to slow the formation of the signalling ternary complex.

The long term behaviour of the system was analysed in Section 3.1.3. The stationary distribution was found both analytically and numerically, with the signalling ternary state being found to be approximately equal to one. Further analysis compared the stationary distribution of the system with a system where all the dissociation rates were set to zero. The dissociation rates, and their relevant probabilities, are *extremely* small in comparison to the association rates, but made a fundamental change to the distribution of the two systems. In the first, the signalling ternary was the stationary distribution; however, the system with no defined dissociation had two stationary distributions, the signalling and nonsignalling ternaries. From this analysis, it was concluded that the dissociation probabilities, despite their insignificant size relative to the association probabilities, played an essential role in the dynamics of the IL-1β network. Without the dissociation probabilities, there were two possible final outcomes for the system, the signalling and nonsignalling ternary complexes T and NT; however, with the dissociation probabilities greater than zero, the probability of the Markov process arriving at the signalling ternary complex T was found to be approximately one.

The effects of the interleukin-1 receptor antagonist on the dynamics of the network were examined in Section 3.2.1. The stationary distribution was found analytically, and solving numerically once again the signalling ternary was found to be the stationary distribution, with the state with the second largest probability being the antagonist-Type-I-bound ternary complex.

The effect of the distribution of the ligand on the system was also considered. A parameter q was introduced which determined whether or not the ligand was IL-1β or IL-1Ra; that is, the ligand was considered to be in a superposition that remains undetermined until an association event takes place, whereupon it changes from an unbound ligand U to IL-1β L or receptor antagonist R with transition probabilities $1 - q : U \to L$ and $q : U \to R$, where q is the proportion of IL-1Ra units, and $1 - q$ is the proportion of IL-1β units in the extracellular environment. Simulations were carried out with this expanded system, and the mean sample path of the Markov chain was calculated.

From these experiments, it was concluded that the receptor antagonist increases the average sample path taken to form signalling ternary complexes. IL-1Ra was found to perform a similar role to the type-II receptor in the IL-1β network. Furthermore, both the antagonist and the type-II receptor appear to have a synergistic effect on the network, acting in concert to slow the formation of signalling ternaries and thus signal transduction.

As the probability of the determination of the ligand superposition U becoming IL-1β becomes less, the mean path length to signalling ternary complex formation becomes much greater, and IL-1Ra-bound ternary complex formation takes on average much fewer iterations.

The effects of the receptor antagonist and the nonsignalling receptor, from the results of simulations and experiments in Chapter 3, can be summarised as

follows:

- IL-1Ra without Type-II:

    - slows signalling complex formation: the formation of signalling complexes is noticeably slower for higher values of q,

    - sequesters Type-I receptors: prevents formation of signalling by consuming Type-I receptors, making them unavailable for signalling complex formation,

    - sequesters receptor accessory protein: prevents formation of signalling by consuming receptor accessory proteins, making them unavailable for signalling complex formation.

- IL-1Ra with Type-II:

    - further slows signalling complex formation: a synergistic interaction between the antagonist and the nonsignalling receptor slows signalling complex formation, confirming what was shown in Section 3.2, with increasing q,

    - sequesters both Type-I receptor and receptor accessory protein: antagonistic ternaries consume the receptor accessory protein, therefore impeding formation of signalling ternary complexes.

In Chapter 3, the supply of receptors and receptor antagonists were assumed to be inexhaustible; in Chapter 4, these resources were explicitly constrained. A stochastic system investigated the effects of finite receptors and accessories, following on from the model developed in Chapter 3 and the analysis in Chapter 2, which emphasised the importance of the ratios of ligand and receptor accessories to the total number of receptors.

Experiments were run to determine the effect of the Type-II receptor on signal transduction, then the receptor antagonist, and then both inhibitory mechanisms. In Section 4.7, the range of human-typical parameters were derived from the literature, as guided by the ratios derived in Chapter 2. The lower end of this range was chosen, so as to further explore the effect of constrained resources on signal transduction.

Two effects were found from the presence of the receptor antagonist on signalling transduction. Nonsignalling ternaries consume the receptor accessory, and Type-I-antagonist complexes consume the signalling receptor and the accessory protein, thereby making them unavailable for forming signalling ternary complexes, confirming the results of Chapter 3. Furthermore, antagonist ternaries continued to form after IL-1β has been consumed, sequestering receptors and accessories and making them unavailable to further IL-1β stimulus.

The ongoing consumption of receptors and accessories, inhibiting further signalling ternary complex formation, suggested a further control mechanism. A cell in the vicinity of an infection or tissue damage is likely to be subjected to the emission of cytokines from damaged cells or immune system cells at random intervals. Sequestration of receptors and accessories by elements of the network which do not contribute to signal transduction, could prevent the cell from being able to respond to further IL-1β. IL-1β is a very potent chemical, and the consumption of limited resources could have evolved as a means to limit the physiological response of cells.

The simulations presented so far have taken place on an idealised, featureless cell membrane. In recent years the classical image of the plasma membrane has been challenged. It has been suggested that the plasma membrane is a more complex and compartmentalised structure, driven by a variety of lipid-lipid, lipid-protein and cytoskeletal interactions, than previously thought (2), (27), (57), (67).

Simons and Ikonen were the first to suggest the raft hypothesis (91). Collected data indicated that glycosphigolipids (GSLs) could form small, liquid ordered phase microdomains in phospholipid bilayers (107). These GSL microdomains are further stabilised with cholesterol, sometime reinforced with cholesterol binding proteins such as caveolins. The microdomains may promote compartmentalisation of raft-associated proteins, such as receptors, and associated proteins. These properties suggest that lipid rafts may be fundamental agents in the signal transduction process.

A probabilistic cellular automata model was developed to investigate how higher viscosity regions (HVRs) on the membrane could colocate receptors and accessories, and how that would affect signalling ternary formation. After establishing that HVRs increase complex formation, the Type-II receptor was added to the network.

The size of the membrane was found to be a significant factor. The larger membranes formed signalling ternaries more readily than smaller membranes, for equal values of HVR area. What was found to be common to all three membrane areas was that the larger rafts (HVRs), up to an experimentally-determined upper limit, aided signalling complex formation more than smaller rafts.

As the raft size increased, the number of nonsignalling ternaries decreased. This was expected from the competition for the constrained quantity of available receptor accessory. However, the sequestration of resources, as would be expected from Section 4.7, would arrest further signalling ternary formation in the event of a further IL-1β stimulus. The effect of HVRs on signalling intensified the signalling complex formation process, although a higher ratio of Type-II receptors would inhibit sufficient signalling ternaries being formed to initiate signalling transduction.

6.2   Discussion

Research by its nature generates further intriguing questions to be answered, which in turn generate other avenues for research, in a seemingly infinite regress. In this thesis the author has concentrated on two inhibitory components in a cytokine network replete with them. There are many other control mechanisms at work on IL-1β, as detailed in Section 1.4, any of which would make a suitable focus for a detailed piece of research. It would be relatively easy to expand on the current work merely by adding one or two other inhibitory components to what has been explored here.

There are other research techniques which could have been used: treating the IL-1β network as a reaction-diffusion system would seem to be a worthwhile focus for research, and the author did some initial work, but other research paths opened up, and so the reaction-diffusion path was neglected. This will form the basis of a future research project.

The concept of HVRs (or lipid rafts, if we briefly drop our agnosticism) would make an intriguing basis for further research. From the results presented in Chapter 5, we have an upper limit for the size of a lipid raft in relation to its efficacy as a concentrator of protein-protein interaction, and some results on the motion on the cell membrane which could be compared with experimental observation and data.

The probabilistic cellular automata models could have been expanded to include a third dimension, the extracellular environment directly above the cell membrane; in fact, the author has the code, but ran out of time (and computer clockcycles) before such models could be explored in sufficient depth. The probabilistic cellular automaton in three dimensions is probably the most useful tool presented here for spatial simulation on or near a cellular membrane. Using a suitably modified version of the Gillespie algorithm would be likely to yield good results (34).

This thesis has modelled a number of the inhibitory components of the IL-1β network, and explored their effect on signalling transduction; it would be intriguing to model further components of this complex network, and find what other effects are waiting to be discovered.

Bibliography

[1] G. Acosta-Rodriguez. Interleukins 1β and 6 but not transforming growth factor- are essential for the differentiation of interleukin 17producing human t helper cells. *Nature Immunology*, 8:942–949, 2007.

[2] R. G. Anderson and K. Jacobson. A role for lipid shells in targeting proteins to caveolae, rafts, and other lipid domains. *Science*, 296:1821–1825, 2002.

[3] C. Andrei et al. Phospholipases c and a2 control lysosome-mediated il-1 beta secretion: Implications for inflammatory processes. *Proc Natl Acad Sci U S A*, 101:9745–9750, 2004.

[4] W. Arend. Binding of il-1 alpha, il-1 beta, and il-1 receptor antagonist by soluble il-1 receptors and levels of soluble il-1 receptors in synovial fluids. *Journal of Immunology*, 153:4766–4774, 1994.

[5] W. Arend. The balance between il-1 and il-1ra in disease. *Cytokine and Growth Factor Reviews*, 13:323–340, 2002.

[6] P. E. Auron. The interleukin 1 receptor: Ligand interactions and signal transduction. *Cytokine and Growth Factor Reviews*, 9:221–237, 1988.

[7] O. Bandman et al. Complexity of inflammatory responses in endothelial cells and vascular smooth muscle cells determined by microarray analysis. *Ann N Y Acad Sci*, 975:77–90, 2002.

[8] C. Bensimon et al. A monoclonal antibody recognizing 68- to 75-kilodalton protein(s) associated with the human il-1 receptor. *J Immunol*, 142:2290–2298, 1989.

[9] C. Bensimon et al. Two distinct affinity binding sites for il-1 on human cell lines. *J Immunol*, 143:1168–1174, 1989.

[10] P. Bodel. Studies on the mechanism of endogenous pyrogen production. *Yale J Biol Med*, 43:145–163, 1970.

[11] J. Briggs. *Enzymes*. MIT Press, Cambridge, MA, 1st edition, 1965.

[12] A. Cavalli et al. Localization of sarcolemmal proteins to lipid rafts in the myocardium. *Cell Calcium*, 42:313–322, 2007.

[13] D. P. Cerretti et al. Molecular cloning of the interleukin-1 beta converting enzyme. *Science*, 256:97–100, 1992.

[14] R. Chizzonite et al. Two high-affinity interleukin 1 receptors represent separate gene products. *Proc Natl Acad Sci USA*, 86:8029–8033, 1989.

[15] F. Colotta et al. The type ii decoy receptor: a novel regulatory pathway for interleukin 1. *Immunol Today*, 15:562–566, 1994.

[16] Y. Cui et al. Shedding of the type ii il-1 decoy receptor requires a multi-functional aminopeptidase, aminopeptidase regulator of tnf receptor type 1 shedding. *J Immunol*, 171:6814–6819, 2003.

[17] E. B. Cullinan et al. Il-1 receptor accessory protein is an essential component of the il-1 receptor. *J Immunol*, 161:5614–5620, 1998.

[18] J. Damjanovich et al. Dynamic receptor superstructures at the plasma membrane. *Quarterly Reviews of Biophysics*, 30:67–106, 1997.

[19] J. Davidson et al. A study of the pyrogenic actions of interleukin-1 alpha and interleukin-1 beta: interactions with a steroidal and a non-steroidal anti-inflammatory agent. *Br J Pharmacol*, 100:542–546, 1990.

[20] C. A. Dinarello. Interleukin-1 and interleukin-1 antagonism. *Blood*, 77:1627–1652, 1991.

[21] C. A. Dinarello. The interleukin-1 family: 10 years of discovery. *FASEB J*, 8:1314–1324, 1994.

[22] C. A. Dinarello. Biologic basis for interleukin-1 in disease. *Blood*, 87:2095–2147, 1996.

[23] C. A. Dinarello. Interleukin-1, interleukin-1 receptors and interleukin-1 receptor antagonist. *Int Rev Immunol*, 16:457–499, 1998.

[24] S. K. Dower. Interleukin-1 association and dissociation rates. *Unpublished data*, 2007.

[25] S. K. Dower. Interleukin-1 biacore results. *Personal communication*, 2007.

[26] C. M. Dubois et al. Transforming growth factor beta is a potent inhibitor of interleukin 1 (il-1) receptor expression: proposed mechanism of inhibition of il-1 action. *J Exp Med*, 172:737–744, 1990.

[27] M. Edidin. The state of lipid rafts: from model membranes to cells. *Annu Rev Biophys Biomol Struct*, 32:257283, 2003.

[28] R. Einstein et al. Type i il-1 receptor: ligand specific confirmation differences and the role of glycosylation in ligand binding. *Cytokine*, 8:206–213, 1996.

[29] S. P. Eisenberg et al. Interleukin 1 receptor antagonist is a member of the interleukin 1 gene family: evolution of a cytokine control mechanism. *Proc Natl Acad Sci U S A*, 88:5232–5236, 1991.

[30] A. Enk et al. An essential role for langerhans cell-derived il-1 beta in the initiation of primary immune responses in skin. *Immunology*, 150:3698–3704, 1993.

[31] E. Evans and R. M. Hochmuth. Mechano-chemical properties of membranes. *Current Topics in Membranes and Transport*, 88:1–62, 1978.

[32] K. A. Fitzgerald and L. A. O'Neill. The role of the interleukin-1/toll-like receptor superfamily in inflammation and host defence. *Microbes Infect*, 2:933–943, 2000.

[33] N. J. Gay and F. J. Keith. Drosophila toll and il-1 receptor. *Nature*, 351:355–356, 1991.

[34] D. Gillespie. Exact stochastic simulation of coupled chemical reactions. *The Journal of Physical Chemistry*, 81:23402361, 1977.

[35] R. A. Goldsby et al. *Kuby immunology*. W H Freeman, New York, 4th edition, 2000.

[36] S. A. Greenfeder et al. Molecular cloning and characterization of a second subunit of the interleukin 1 receptor complex. *J Biol Chem*, 270:13757–13765, 1995.

[37] S. A. Greenfeder et al. Molecular cloning and characterization of a second subunit of the interleukin 1 receptor complex. *J Biol Chem*, 270:13757–65, 1995.

[38] G. Grimmett and D. Stirzaker. *Probability and random processes*. Oxford University Press, Oxford, 2001.

[39] Y. Gu et al. Interleukin-1β converting enzyme requires oligomerization for activity of processed forms in vivo. *EMBO J*, 14:1923–1931, 1995.

[40] D. J. Hazuda et al. The kinetics of interleukin 1 secretion from activated monocytes: Differences between interleukin 1 alpha and interleukin 1 beta. *J Biol Chem*, 263:8473–8479, 1988.

[41] D. K. Heidary et al. Long-range coupling between separate docking sites in interleukin-1β. *Journal of Molecular Biology*, 353:1187–1198, 2005.

[42] J. Hofbauer and K. Sigmund. *Evolutionary Games and Population Dynamics*. Cambridge University Press, 1998.

[43] R. Horuk et al. A biochemical and kinetic analysis of the interleukin-1 receptor: Evidence for differences in molecular properties of il-1 receptors. *J Biol Chem*, 262:16275–16278, 1987.

[44] J. Huang et al. Recruitment of irak to the interleukin 1 receptor complex requires interleukin 1 receptor accessory protein. *Proc Natl Acad Sci USA*, 94:12829–12832, 1997.

[45] B. D. Hughes et al. The translational and rotational drag on a cylinder moving in a membrane. *J Fluid Mechs*, 110:349–372, 1981.

[46] M. Irmler et al. Granzyme a is an interleukin-1α -converting enzyme. *J Exp Med*, 181:1917–1922, 1995.

[47] F. M. J et al. Human pro-il-1 beta gene expression in monocytic cells is regulated by two distinct pathways. *J Immunol*, 140:2267–2273, 1988.

[48] N. Jarrous and R. Kaempfer. Induction of human interleukin-1 gene expression by retinoic acid and its regulation at processing of precursor transcripts. *J Biol Chem*, 269:23141–23149, 1994.

[49] L. E. Jensen. Il-1 signaling cascade in liver cells and the involvement of a soluble form of the il-1 receptor accessory protein. *J Immunol*, 164:5277–5286, 2000.

[50] S. A. Jobling et al. Biological activity and receptor binding of human prointerleukin-1β and sub-peptides. *J Biol Chem*, 263:16372–16389, 1988.

[51] D. M. Jurič and M. Čarman Kržan. Interleukin-1β, but not il-1α, mediates nerve growth factor secretion from rat astrocytes via type i il-1 receptor. *Int J Dev Neurosci*, 19:675–683, 2001.

[52] M. J. Karnovsky et al. The concept of lipid domains in membranes. *J Cell Biol*, 94:1–6, 1982.

[53] E. Klipp et al. *Systems Biology in Practice: Concepts, Implementation and Application*. Wiley-VCH, Berlin, 2005.

[54] J. Knop et al. The type ii il-1 receptor interacts with the il-1 receptor accessory protein: a novel mechanism of regulation of il-1 responsiveness. *J Immunol*, 161:6871–6877, 1998.

[55] C. Kollewe. The first two n-terminal immunoglobulin-like domains of soluble human il-1 receptor type ii are sufficient to bind and neutralize il-1beta. *FEBS Lett*, 487:189–193, 2000.

[56] J. Korak. Random walks on the menger sponge. *Chemical Physics Letters*, 275:199–202, 1998.

[57] A. Kusumi and I. Koyama-Honda. Molecular dynamics and interactions for creation of stimulation-induced stabilized rafts from small unstable steady-state rafts. *Traffic*, 5:213230, 2004.

[58] D. Lang et al. The type ii il-1 receptor interacts with the il-1 receptor accessory protein: A novel mechanism of regulation of il-1 responsiveness. *J Immunol*, 161:6871–6877, 1998.

[59] D. Malinowsky. Interleukin-1 receptor accessory protein interacts with the type ii interleukin-1 receptor. *FEBS Lett*, 429:299–302, 1998.

[60] C. J. March et al. Cloning, sequence and expression of two distinct human interleukin-1 complementary dnas. *Nature*, 315:641–647, 1985.

[61] K. Matsushima et al. Properties of a specific il-1 receptor on human ebv-transformed b lymphocytes: identity of the receptor for il-1a and il-1β. *J Immunol*, 136:4496–4502, 1986.

[62] S. G. Matta et al. Interleukin-1 alpha and interleukin-1 beta stimulate adrenocorticotropin secretion in the rat through a similar hypothalamic receptor(s): effects of interleukin-1 receptor antagonist protein. *Neuroendocrinology*, 57:14–22, 1993.

[63] C. J. McMahan et al. A novel il-1 receptor, cloned from b cells by mammalian expression, is expressed in many cell types. *EMBO J*, 10:2821–2832, 1991.

[64] L. C. Miller et al. Live borrelia burgdorferi preferentially activate il-1β gene expression and protein synthesis over the interleukin-1 receptor antagonist. *J Clin Invest*, 90:906–912, 1992.

[65] J. Milnor. *Topology from the Differentiable Viewpoint*. University of Virginia Press, 1965.

[66] S. Munro. Lipid rafts: Elusive or illusive? *Cell*, 115:377–388, 2003.

[67] K. Murase et al. Ultrafine membrane compartments for molecular diffusion as revealed by single molecule techniques. *Biophys J*, 86:4075–4093, 2004.

[68] P. A. Murphy et al. Synthesis of endogenous pyrogen by rabbit leukocytes. *J Exp Med*, 137:1263–1274, 1974.

[69] S. Nakae et al. Interleukin-1 beta, but not interleukin-1 alpha, is required for t-cell-dependent antibody production. *Immunology*, 104:402–409, 2001.

[70] A. Nakano. http://cacs.usc.edu/education/phys516.html.

[71] D. Neumann et al. The membrane form of the type ii il-1 receptor accounts for inhibitory function. *J Immunol*, 165:3350–3357, 2000.

[72] D. V. Nicolau et al. Identifying optimal lipid raft characteristics required to promote nanoscale protein-protein interactions on the plasma membrane. *Mol Cell Biol*, 26:313–323, 2006.

[73] A. J. O'Neill and C. Dinarello. The il-1 receptor/toll-like receptor superfamily: crucial receptors for inflammation and host defense. *Immunology Today*, 21:206–209, 2000.

[74] S. Orlando et al. Selectivity release of the type ii decoy il-1 receptor. *Cytokine*, 12:1001–1006, 2000.

[75] R. Peters and R. J. Cherry. Lateral and rotational diffusion of bacteriorhodopsin in lipid bilayers: Experimental test of the saffman-delbruck equations. *Proc Natl Acad Sci*, 79:4317–4321, 1982.

[76] S. Poole and R. E. Gaines Das. The international standards for interleukin 1α and interleukin 1β: Evaluation in an international collaborative study. *J Immunol Methods*, 142:1–13, 1991.

[77] A. P. Pralle et al. Sphingolipid-cholesterol rafts diffuse as small entities in the plasma membrane of mammalian cells. *J Cell Biol*, 148:997–1008, 2000.

[78] I. A. Prior et al. Direct visualization of ras proteins in spatially distinct cell surface microdomains. *J Cell Biol*, 160:165–170, 2003.

[79] J. Sadouk. Human synovial fibroblasts coexpress il-1 receptor type i and type ii mrna : the increased level of the il-1 receptor in osteoarthritic cells is related to an increased level of the type i receptor. *Lab Investigation*, 73:347–355, 1995.

[80] P. G. Saffman and M. Delbruck. Brownian motion in biological membranes. *Proc Natl Acad Sci USA*, 72:3111–3113, 1975.

[81] R. Schindler et al. Dissociation between interleukin-1β mrna and protein synthesis in human peripheral blood mononuclear cells. *J Biol Chem*, 265:10232–10237, 1990.

[82] R. Schindler et al. Il-1 induces il-1: Iv: Ifn-γ suppresses il-i but not lipopolysaccharide-induced transcription of il-1. *J Immunol*, 144:2216–2222, 1990.

[83] R. Schindler et al. Recombinant c5a stimulates transcription rather than translation of interleukin-1 (il-1) and tumor necrosis factor: translational signal provided by lipopolysaccharide or il-1 itself. *Blood*, 76:1631–1638, 1990.

[84] U. Schonbeck et al. Generation of biologically active il-1 beta by matrix metalloproteinases: a novel caspase-1-independent pathway of il-1 beta processing. *J Immunol*, 161:3340–3346, 1998.

[85] K. Schotanus et al. Domains of rat interleukin 1 beta involved in type i receptor binding. *Endocrinology*, 36:332–339, 1995.

[86] I. Segel. *Enzyme kinetics*. John Wiley and Sons, Chichester, 1st edition, 1975.

[87] E. Serkkola and M. Hurme. Synergism between protein-kinase c and camp-dependent pathways in the expression of the interleukin-1β gene is mediated via the activator-protein-i (ap-1) enhancer activity. *Eur J Biochem*, 213:243–249, 1993.

[88] L. Shapiro and C. A. Dinarello. Osmotic regulation of cytokine synthesis in vitro. *Proc Natl Acad Sci USA*, 92:12230–12234, 1995.

[89] P. Sharma et al. Nanoscale organization of multiple gpi-anchored proteins in living cell membranes. *Cell*, 116:577–589, 2004.

[90] K. Simons and R. Ehehaltg. Cholesterol, lipid rafts, and disease. *J Clin Invest*, 110:597–603, 2002.

[91] K. Simons and E. Ikonen. Functional rafts in cell membranes. *Nature*, 387:569–572, 1997.

[92] J. E. Sims. Cloning the interleukin 1 receptor from human t cells. *Proc Natl Acad Sci USA*, 86:89468950, 1989.

[93] J. E. Sims and S. K. Dower. Interleukin-1 receptors. *Eur Cytokine Netw*, 5:539–546, 1994.

[94] S. J. Singer and G. L. Nicolson. The fluid mosaic model of the structure of cell membranes: Cell membranes are viewed as two-dimensional solutions oriented globular proteins and lipids. *Science*, 175:720–731, 1972.

[95] D. Smith et al. The soluble form of il-1 receptor accessory protein enhances the ability of soluble type ii il-1 receptor to inhibit il-1 action. *Immunity*, 18:87–96, 2003.

[96] G. Sowa et al. Distinction between signaling mechanisms in lipid rafts versus caveolae. *PNAS*, 98:14072–14077, 2001.

[97] E. Spanier. *Algebraic Topology*. McGraw-Hill, 1966.

[98] M. Y. Stoeckle and L. Guan. High-resolution analysis of gro-α mrna poly (a) shortening: regulation by interleukin-1β. *Nucl Acid Res*, 21:1613–1617, 1993.

[99] J. A. Symons et al. Soluble type ii interleukin 1 (il-1) receptor binds and blocks processing of il-1 beta precursor and loses affinity for il-1 receptor antagonist. *Proc Natl Acad Sci USA*, 92:1714–1718, 1995.

[100] J. Tron. Flow cytometric measurement of fluorescence resonance energy transfer on cell surfaces: Quantitative evaluation of the transfer efficiency on a cell-by-cell basis. *Biophysical Journal*, 45:939–946, 1984.

[101] E. Vannier and C. A. Dinarello. Histamine enhances interleukin (il)-1-induced il-1-gene expression and protein synthesis via h2 receptors in peripheral blood mononuclear cells: comparison with il-1 receptor antagonist. *J Clin Invest*, 92:281–287, 1993.

[102] G. P. Vigers et al. Crystal structure of the type-i interleukin-1 receptor complexed with interleukin-1beta. *Nature*, 386:190–194, 1997.

[103] N. P. Walker et al. Crystal structure of the cysteine protease interleukin-1 beta-converting enzyme: a (p20/p10)2 homodimer. *Cell*, 78:343–352, 1994.

[104] H. Wesche. Effects of il-1 receptor accessory protein on il-1 binding. *FEBS Lett*, 429:303–306, 1998.

[105] H. Wesche et al. The interleukin-1 receptor accessory protein (il-1racp) is essential for il-1-induced activation of interleukin-1 receptor-associated kinase (irak) and stress-activated protein kinases (sap kinases). *J Biol Chem*, 272:7727–7731, 1997.

[106] K. P. Wilson et al. Structure and mechanism of interleukin-lβ converting enzyme. *Nature*, 370:270–275, 1994.

[107] M. Zeyda and T. Stulnig. Lipid rafts & co: An integrated model of membrane organization in t cell activation progress. *Lipid Research*, 45:187–202, 2006.